Radiation-Induced Paramagnetic Defects in Coesite and Stishovite, High Pressure Phases of SiO_2

by Kazutoshi Ogoh

Ph. D. Thesis 1996

Osaka University
Toyonaka, Osaka, JAPAN

Abstract

Several radiation-induced defects in coesite and stishovite, which are high pressure phases of silicon dioxide (SiO_2), have been identified by electron spin resonance (ESR) and thermoluminescence (TL) in this thesis. Silicon dioxide is one of the major materials that constitute terrestrial planets. Radiation-induced defects in quartz and amorphous SiO_2 have already been studied by ESR and TL, and used for dating of geological and archaeological samples. Defects in the materials have been matters of interest especially in amorphous SiO_2 formed on Si wafer in the process of semiconductor.

Coesite and stishovite can be synthesized not only from silica glass and quartz but also from feldspar under high pressure. These high pressure phase materials were found around meteor impact craters in nature, and thought to have been transformed from quartz in sandstone at the impact moment. Since the mineralization, lattice defects created by natural radiation should have been accumulated in the minerals. The age (T) of mineralization, therefore the age of the meteor impact, will be obtained by ESR or TL dating method. If we observe ESR lines characteristic for coesite and stishovite in some samples after irradiation, we can obtain how high pressure the samples have undergone.

This thesis is the first study on radiation-induced paramagnetic defects in synthetic coesite and stishovite. I have characterized the defects using ESR and proposed some models for them. General introductions are written in Chapter 1. E' type centers are described in Chapter 2. Oxygen hole centers related with aluminum impurities are discussed in Chapter 3. Atomic hydrogen centers, H^0, in both materials are dealt in Chapter 4 with both ESR and TL studies. The characteristics of all identified centers with their ESR parameters (g-factor and hyperfine A value) are summarized in Chapter 5. Re-constructed natural radiation data and a dating study on natural quartz from a caldera are written in Appendix A and B, respectively.

Table of Contents

1. Introduction

1-1.General Introduction

(1) Purpose

Silicon dioxide is one of the major materials that constitute terrestrial planets. High pressure phases of SiO_2, coesite and stishovite, were found around meteor impact craters in nature. They can be indicators of pressure at the meteor impact moments. Natural radiation creates paramagnetic defects in coesite and stishovite from the mineralization. The age (T) of the meteor impact craters will be obtained, if the accumulated natural radiation dose (the radiation-induced defects) are estimated by electron spin resonance (ESR) or thermoluminescence (TL). This method will be applied not only for the craters on the earth but also on other planets including satellites in the next century. Several radiation-induced paramagnetic defects in synthetic coesite and stishovite are identified by ESR and TL first in this thesis. It will be possible to study the shock process that terrestrial planets and satellites have undergone using ESR of the defects.

(2) Electron Spin Resonance (ESR) and Paramagnetic Defects in Solids

Electron spin resonance (ESR) or electron paramagnetic resonance (EPR) is a physical method of observing resonance absorption of microwave by unpaired electron spins in a magnetic field. An electron has a magnetic moment due to its spin $s = 1/2$. The tiny electron spin magnets form magnetically neutral pairs in atoms and molecules. No net magnetic is present due to the neutralizing effects of the pairing of electron spins in most materials. A few specific atoms and ions that have parallel spins are exceptions (atoms and molecules in a triplet state, and transition metal and rare earth ions with d and f electrons, respectively).

Natural or artificial radiation ionizes atoms or molecules, i. e., breaks the pair of electrons. When the ionized electron is trapped by some other atoms, an electron-excess atom and an electron-deficient atom are formed: the former and the latter, both with an unpaired electron, are called "trapped electron" and "trapped hole" centers, respectively. They have net magnetic moment, μ_e due to the unpaired electron spins.

When a crystalline solid is irradiated, sometimes atoms are ejected from the lattice position, forming vacancies and interstitials that are intrinsic point defects in the solid.

Impurity atoms also exist in a lot of solids. If radiation-induced unpaired electrons or holes are trapped by these point defects, they are detectable with ESR.

Unpaired spins of the electron trapped or hole trapped centers tend to align parallel to the direction of an external static magnetic field. The direction of the magnetic moment due to the electron spin which is initially random, becomes either the same as or opposite to that of the external magnetic field. These two spin states are energetically different and called "up spin" and "down spin" states. The electron spins excited from the lower level to the higher level by the absorption of the microwave quanta flop to the lower level by the lattice vibration in a time called the "spin-lattice relaxation time" (T_1). Flopping of the spins also occurs due to the interaction among spins and this flopping time is called the "spin-spin relaxation time" (T_2). If the microwave power is so high as to pump out the spins in the lower level or the relaxation time is too long for the population to be restored, a decrease in the signal intensity is observed. This is called saturation.

The magnetic properties of unpaired electrons are expressed by the following parameters:

Spin angular momentum, $S(\mathbf{h}/2\pi)$ (**h**: Planck constant)

Spin quantum number, S : $S = 1/2$ for an electron.

Magnetic quantum number, M : $M = +1/2$ and $M = -1/2$ are allowed.

Bohr magneton, β : the basic unit of a small magnet for an electron spin.

Magnetic moment, μ_e : $\mu_e = -g\,\beta S$

Spectroscopic splitting factor, g : $g = 2.0023$ for a free electron.

The energy yielding different spin states under the external magnetic field H is known as the "Zeeman effect" and depends on H and the magnetic moment ($g\beta M$) of the electron. The Zeeman energy, $E_z = -\mu_e H$, is

$$E_z = g\beta HM. \qquad (1-1)$$

The direction of the spin is changed by absorption of microwaves when the energy difference ($\Delta E = g\beta H$) is equal to the quantum energy of an electromagnetic wave, $h\nu$. Here ν is the frequency of the microwave. This absorption is ESR.

In solids, the g-factor of most species do deviate slightly from that of the free electron (g_e) due to the contribution of orbital angular momentum via the magnetic spin-orbit

interaction (λLS). A multi-spin system such as some paramagnetic ions or an exchange coupled pair of spins has a total quantum number larger than 1 ($S \geq 1$). In this case, M takes $2S+1$ values from $S, S-1, \bullet\bullet\bullet, -S+1, S$.

Unpaired electrons in different environments have slightly different g-factors, resulting in the appearance of signals for different centers at different magnetic field strengths. Classically, the slight g-factor change due to the environment might be ascribed to the change of the effective negative charge by spread of the electron wave function. The shift of g-factor occurs indirectly through the spin-orbital magnetic interaction (λLS).

The g-factor is independent of field direction only in isotropic systems. Minerals generate a crystalline magnetic field, which is superimposed on the external magnetic field. If this field is non-cubic, the observed g-factor depends on the orientation of the crystal field with respect to the external field. When measuring powders, one, two and three lines appear with a cubic, axial and rhombic field, respectively.

The resonance condition is represented by

$$g\beta H_0 = h\nu, \qquad (1-2)$$

where H_0 is the resonance magnetic field. One can obtain the resonance absorption by sweeping the magnetic field H, while maintaining the frequency ν constant. For electron spins with $g = 2.0$, the magnetic field H_0 is 339 mT and 1250 mT when the frequency ν is 9.5 GHz (X-band) and 35 GHz (Q-band), respectively. Since a DC-amplification of the ESR signal is not desirable of signal-to-noise ratio, the DC ESR signal is transformed into first derivative line by modulation of magnetic field H with a small additional oscillating magnetic field H_m.

No ESR occurs as long as electrons are paired, the magnetic moments negate each other (diamagnetic substances). However, elements having electron orbits with equal energies show a coupling of the spins. A non-cubic crystalline field causes an initial splitting of the spin levels (which is independent of the orientation), leading to a splitting of the ESR line (fine structure).

Magnetic interaction between an electron spin and a nuclear spin causes another weak splitting of the spin levels, resulting in the hyperfine structure in the ESR. There are $2I+1$ energy levels for each values of M for nuclear spin I in general. In the case that ions which show hyperfine structure interact with another nuclear spin of its surrounding atoms, the hyperfine structure will split again (superhyperfine structure).

Because of the effects above, the ESR behavior of a particular center in a mineral in an external magnetic field is described by the so-called spin-Hamiltonian H_S, which has the general form,

$$H_s = g\beta H + VS + ASI + TSI^* \qquad (1-3)$$

where S is the spin operator, V is the zero-field splitting (fine structure) constant, A is the hyperfine constant and T is the superhyperfine constant. I denotes the nuclear spin moments of the center and its neighbor (I^*). Both g and A are tensors depending on the symmetry of the crystal field.

(3) ESR and TL Dating and Dosimetry Method Using Radiation Induced Defects in Solids

Unpaired electrons and holes are created by natural radiation and trapped by lattice defects in minerals, and observed with electron spin resonance (ESR). Microwave absorption is caused by transfer of electron spins between the energy levels split by Zeeman effect in static magnetic field. These trapped electrons and holes are released from traps by laboratory heating, and recombine emitting light, the process is called thermoluminescence (TL). The accumulated dose from natural radiation given to a specific sample is estimated by relative ESR or TL intensity, and by the signal enhancement with artificial γ-ray irradiation [1-1].

Defects, both in synthetic crystalline quartz and in amorphous silica glass have been studied extensively because of the technological importance of SiO_2 in electronics, optics and telecommunications. ESR and TL dating using quartz has contributed to various fields in earth sciences, such as structural geology, tepherochronology and archaeology.

The total dose of radiation (TD) called an accumulated dose (AD) is obtained from proportional relation between ESR signal or TL peak intensity and radiation dose. If the initial intensity, I_0, is enhanced to the intensity of $I(Q)$, by the addition of an artificial radiation dose of Q Gy, the proportionality relation is

$$I(Q)/I_0 = (TD + Q)/TD \qquad (1-4)$$

or

$$I(Q) = I_0(1 + Q/TD). \qquad (1-5)$$

A linear extrapolation of the signal intensity to the zero ordinate gives the TD as is

schematically shown in Fig. 1-1(a). If the creation ratio of defects get near saturation, the growth curve is fitted to a saturation curve as

$$I(Q) = I_{\infty}[1 - \exp\{-a(Q + TD)\}]. \qquad (1\text{-}6)$$

The ESR age, T [y], can be obtained from the TD [Gy] by assessing the average annual dose, D [Gy], as

$$T[\mathrm{y}] = TD[\mathrm{Gy}] / D[\mathrm{Gy/y}]. \qquad (1\text{-}7)$$

The experimentally obtained TD depends on γ rays from ^{60}Co which is used for the artificial irradiation in general. Hence, the experimentally obtained TD should be expressed as an "equivalent dose (ED)" exactly. The annual dose, D, also depends on kinds of radiation. A given dosage from α particles is less effective in creating defects than the same dosage from β particles or γ rays. The degree of ineffectiveness of α particles is expressed as a k-value. The actual annual dose should be multiplied by the k-value to get the effective annual dose for α particles, and k-value is typically in the range from 0.1 to 0.2. The equation (1-7) should be refined as

$$T[\mathrm{y}] = ED[\mathrm{Gy}] / (kD_{\alpha} + D_{\beta} + D_{\gamma})[\mathrm{Gy/y}]. \qquad (1\text{-}8)$$

where D_{α}, D_{β} and D_{γ} are annual doses from α, β and γ rays, respectively. Natural radiation dose from uranium and thorium series are described in Appendix A. An ESR dating study using impurity centers in quartz is described in Appendix B for example.

1-2.SiO_2 Polymorphs

(1) Phase Diagram

Silicates constitute the commonest class of minerals. The silicon atom, Si with *sp* hybrid orbitals usually forms an SiO_4 tetrahedron with four oxygen atoms with *p* orbitals at the crust of the earth. The SiO_4 tetrahedron is either isolated or joined with one or more oxygen atoms forming a one-, two- or three-dimensional net work. A special type of silicate is silica (SiO_2) where each oxygen atom is bonded with two (or three) silicon atoms to form three-dimensional net work in crystalline form. The silica (SiO_2) appears as half-ionic and half-covalent crystalline polymorphs of α-quartz, β-quartz, tridymite, cristobalite, coesite and stishovite or amorphous.

Alpha-quartz with a trigonal structure is stable at atmospheric pressure and temperature up to 573 °C, as shown in Fig. 1-1. It changes into β-quartz which is stable between 570 °C and 870 °C with minor atomic movements involving no breakage of Si-O bonds [1-1, 2]. Trydimite and cristobalite are produced by heating at 870 °C and 1470 °C, respectively. Coesite and stishovite are high pressure phases of SiO_2. The former is the phase above 2 GPa, and the latter is that above 8 GPa at room temperature, respectively. These are found in sandstones at meteor impact craters in nature, and thought to have transformed from quartz in sandstone at the meteor impact moment.

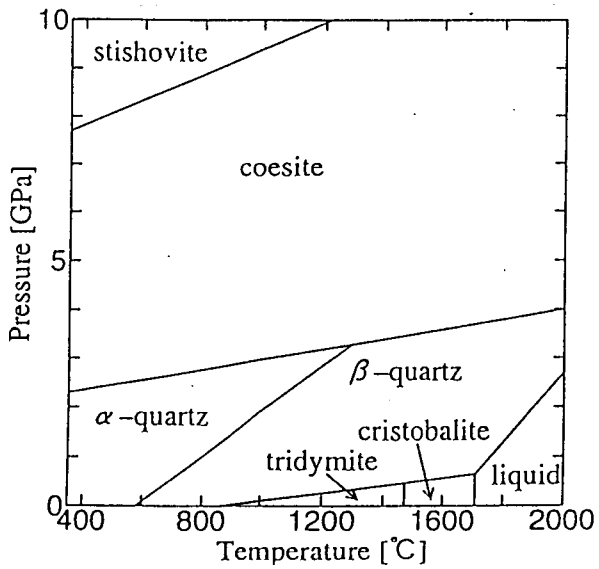

Fig. 1-1 T-P phase diagram of SiO_2 polymorphs modified after [1-3] . Coesite and stishovite are high pressure phases above 2 GPa and 8 GPa at room temperature, respectively. Heating above 1000 °C is necessary for synthesis of the minerals.

(2) Crystal Structures of Alpha-Quartz, Coesite and Stishovite

(a) Alpha-quartz

Alpha-quartz has a hexagonal lattice which contains 3 silicon atoms and 6 oxygen atoms in the coordination unit [1-3, 4]. A schematic structure of α-quartz is shown in Fig. 1-2. The unit cell parameters are a = 4.9134 Å and c= 5.4152 Å [1-1, 3, 4]. Each silicon atom has four oxygen neighbors, approximately tetrahedrally positioned. Each tetrahedron bonded together sharing all four oxygen atoms with next ones. One oxygen atom has two bonds whose lengths are 1.611 Å (long bond) and 1.607 Å (short bond). One silicon has two long bonds and two short bonds. The density of α-quartz is 2.649 g/cm^3.

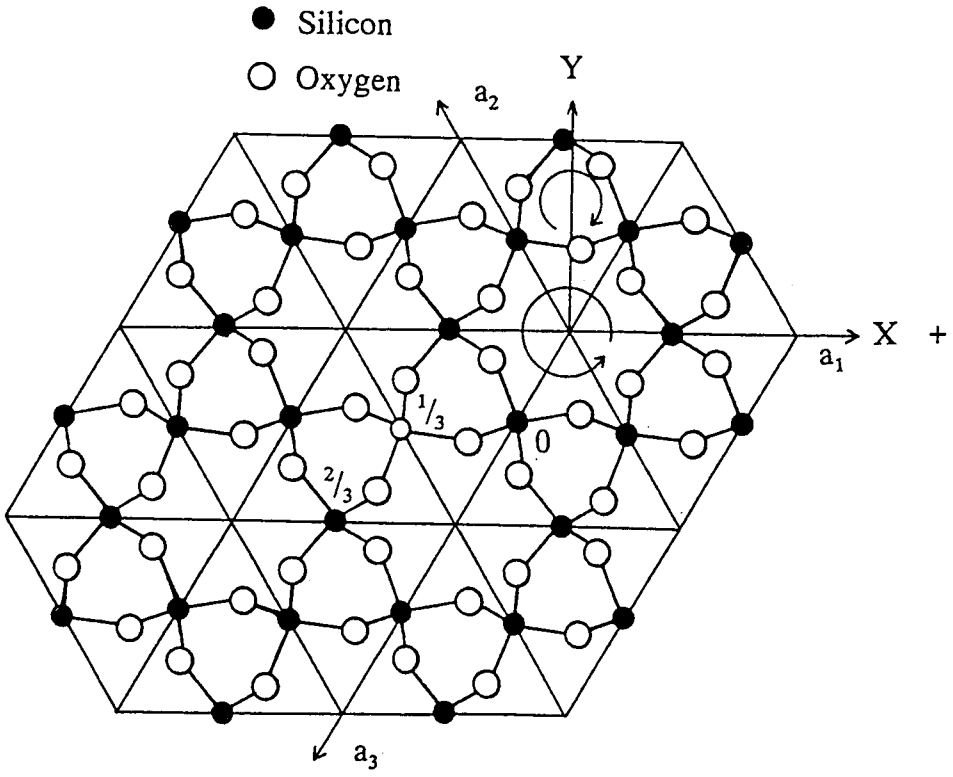

Fig. 1-2 Projection of right α-quartz atomic positions onto the plane perpendicular to c axis, showing twofold axes a_i (i = 1, 2, 3), partially modified after [1-5]. a = 4.9134 Å and c = 5.4142 Å at room temperature.

(b) Coesite

Coesite has a monoclinic lattice which contains 16 silicon atoms and 32 oxygen atoms in the coordination unit [1-3, 4]. A schematic structure of coesite is shown in Fig. 1-3. The unit cell parameters are a = b = 7.17 Å, c = 12.38 Å and $\gamma = 120°$ [1-3, 4]. The structure is made of silicon-oxygen tetrahedra in an arrangement showing some resemblance to the alumina-silica framework of feldspars. The bond lengths vary from 1.590 Å to 1.641 Å. The density of coesite is 2.915 g/cm^3.

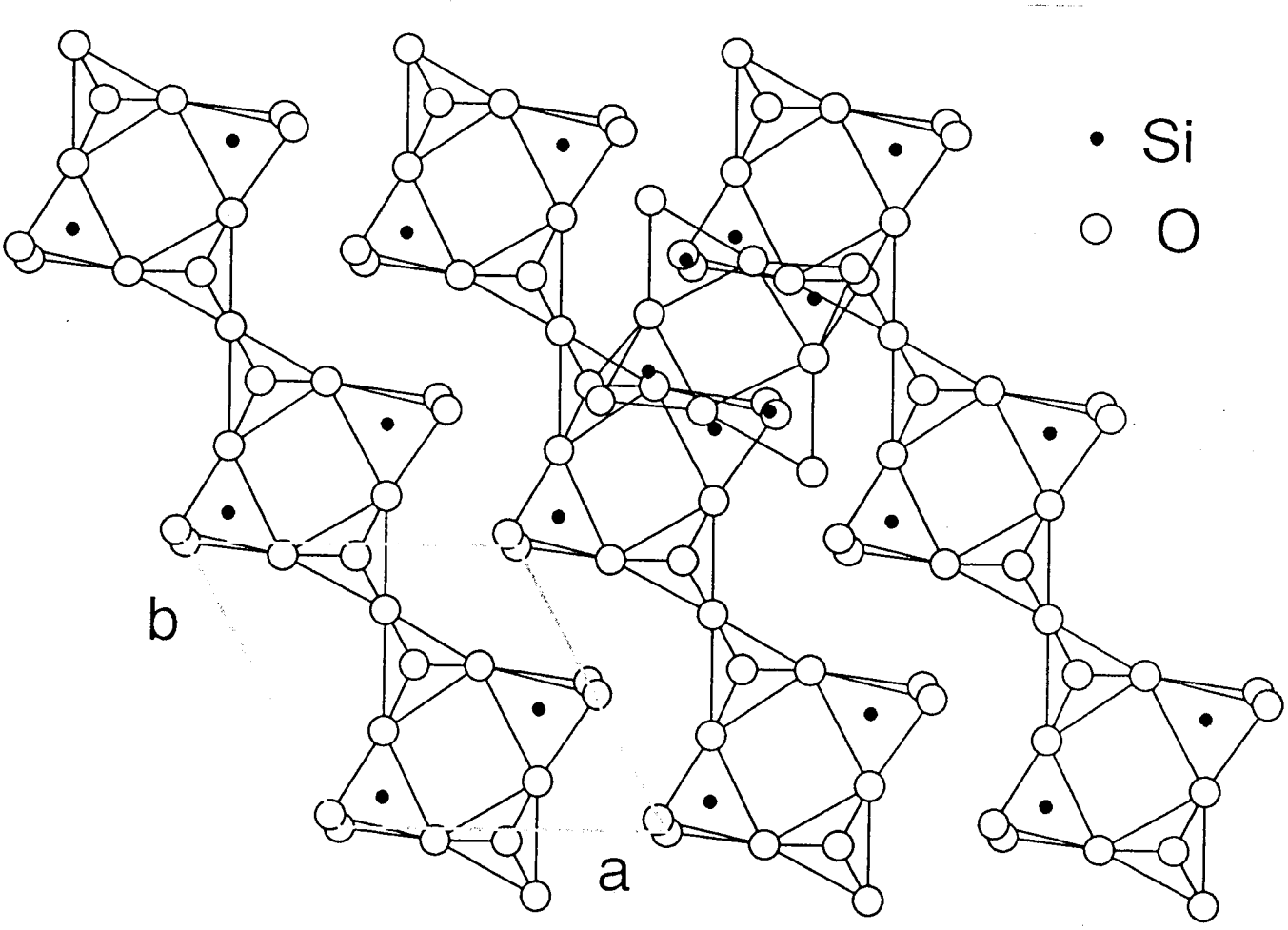

Fig. 1-3 A part of crystal structure of coesite on to [001], partially modified after [1-6]. a = b = 7.17 Å, c = 12.38 Å and $\gamma = 120°$ at room temperature [1-3, 4].

(c) Stishovite

Stishovite is an octahedrally coordinated phase of SiO_2. Each silicon atom has 4 oxygen nearest neighbors and 2 oxygen second nearest neighbors. The short Si-O bond is 1.757 Å length and the long one is 1.810 Å length. The density of stishovite is 4.287 g/cm^3. The structure has a tetragonal lattice which contains 2 silicon atoms and 4 oxygen atoms in the coordination unit [1-3, 4]. A schematic structure of stishovite is shown in Fig. 1-4. The unit cell parameters are a = 4.179 Å and c = 2.665 Å [1-3, 4].

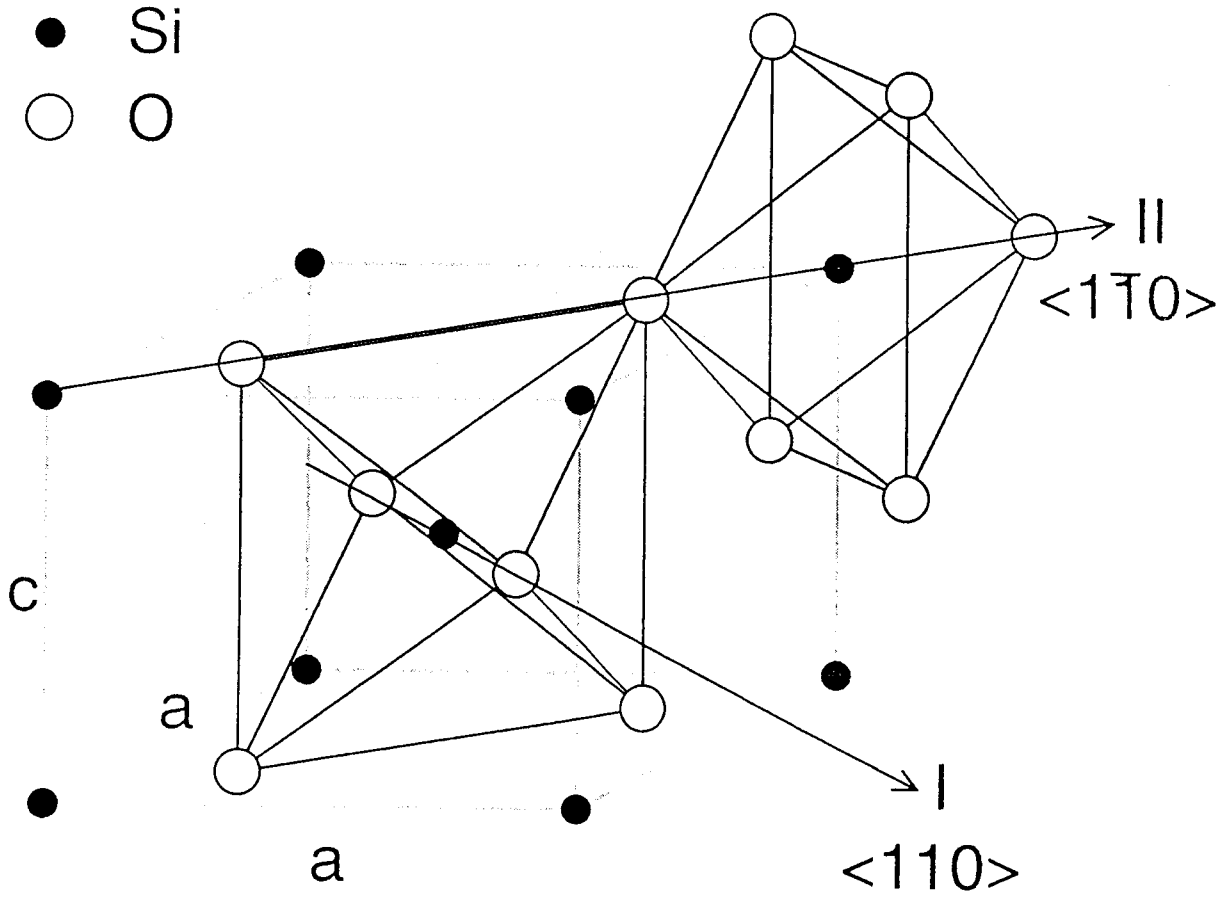

Fig. 1-4 A part of crystal structure of stishovite, partially modified from [1-7]. a = 4.179 Å and c = 2.665 Å at room temperature [1-3, 4].

1-3. Well Known Defects in Quartz and Amorphous SiO_2

Defects in coesite and stishovite are identified in this thesis on an analogy of defects in quartz and amorphous SiO_2. Previous notations of the well known defects in quartz and amorphous SiO_2 are summarized below (modified after [1-1]) for discussion in following chapters. Detail of each defect is written in the related chapter.

Normal Lattice	: $[SiO_4]^0$,	SiO_4^{4-}	or	≡Si-O-Si≡
Intrinsic Defects				
(a) E'_1 center	: $[SiO_3]^+$,	SiO_3^{3-}	or	≡Si • Si≡
(b) peroxy center	: $[SiO_5]^-$,	SiO_5^{5-}	or	≡Si-O(-O •)-Si≡
(c) NBOHC	: $[SiO_4]^+$,	SiO_4^{3-}	or	≡Si-O •
(d) OHC (O_3^- ?)	:			O-O-O •
(e) oxygen vacancies	: $[SiO_3]^{2+}$,	SiO_3^{2-}	or	$[V_{\cdot}]^{2+}$
	$[SiO_3]^0$,	SiO_3^{4-}	or	$[V_{\cdot}2e^-]^0$

Impurity-Related Defects

(a) Al center : Al-related oxygen hole center

$[AlO_4]^0$, $[Al^{3+}h^+]^0$, AlO_4^{4-} or ≡Al-O •

(b) Ge center : Ge-related electron center

$[GeO_4/Li^+]_C^0$, $[Ge^{4+}e^-/Li^+]_C^0$, $GeLiO_4^{4-}$ or (≡Ge-O-)----Li+

(d) Ti center : Ti-related electron center

$[TiO_4/Li^+]_C^0$, $[Ti^{4+}e^-/Li^+]_C^0$, $TiLiO_4^{4-}$ or (≡Ti-O-)----Li+

(e) H^0 center : Atomic Hydrogen center

(f) Other centers

References

1-1 M. Ikeya: New Applications of Electron Spin Resonance (World Scientific, Singapore, 1993).

1-2 F. R. S. Deer, R. A. Howie and J. Zussman: An Introduction to the Rock-Forming Minerals (Longman, Essex 1966).

1-3 D. T. Griffen: Silicate Crystal Chemistry (Oxford University Press, New York, USA, 1992)

1-4 Y. P. Li and W. Y. Ching: Phys. Rev. **B 31** (1985) 2172.

1-5 J. A. Weil: Phys. Chem. Minerals. **10** (1984) 149.

1-6 T. Zoltai and M. J. Buerger: Zeits. Krist. **111** (1959) 129.

1-7 W. H. Baur and A. A. Khan: Acta Cryst. **B 27** (1971) 2133.

2. E' Centers (Oxygen Vacancy Centers Trapping an Unpaired Electron)

2-1. Introduction of E' Centers

Oxygen vacancy centers which trap an electron and two electrons in quartz and quartz glass are called as E' centers and E" centers, respectively [2-1, 2]. Six types of E' and E" centers have been identified: E'_1, E'_2, E'_4, E''_1, E''_2 and E''_3. Little is known about precursors of these defects [2-2]. Similar defects have been observed in other silicates. Newly found E' centers in coesite and stishovite are described in this chapter after introduction of E' and E" centers in quartz.

The best known type is E'_1 center, where an electron is trapped at an oxygen vacancy. The form is $[O_3Si{\bullet}SiO_3]^+$. The E'_1 center was first found in neutron irradiated quartz [2-1], and was characterized in detail by ESR [2-3]. The spectrum shows a strong central line with an anisotropic g-factor of almost axial symmetry, $g_1 = 2.00179$, $g_2 = 2.0053$ and $g_3 = 2.0030$ [2-4], and three hyperfine structures (hfs) with splitting parameter of 40, 0.9 and 0.8 mT when the magnetic field is parallel to the crystal c-axis. The hfs of 40 mT is due to hyperfine (hf) interaction with ^{29}Si [2-3]. This idea was supported by the study investigating E' center in ^{29}Si enriched quartz glasses [2-5].

A model that is consistent with the large hf interaction of 40 mT was proposed [2-6], as shown in Fig. 2-1. The trapped unpaired electron is in a single sp_3 orbital oriented along a bond direction into the vacancy, according to the model. The silicon having the electron relaxes toward the oxygen vacancy while the other silicon, in opposite side, having positive charge mainly relaxes away into the basal plane of its three oxygen neighbors as shown in Fig. 2-1(b). This model agrees well with the obtained spin Hamiltonian parameters [2-3], but dose not explain the weak hfs.

Griscom studied E' center in fuzed silica and concluded that the two weak hfs might be due to protons but not silicons [2-7]. Jani *et al.* showed that the weak hfs are associated with ^{29}Si by an ENDOR study and proposed a divacancy model where another oxygen atom between Si(0) and Si(4) in Fig. 2-1 is also missing [2-4].

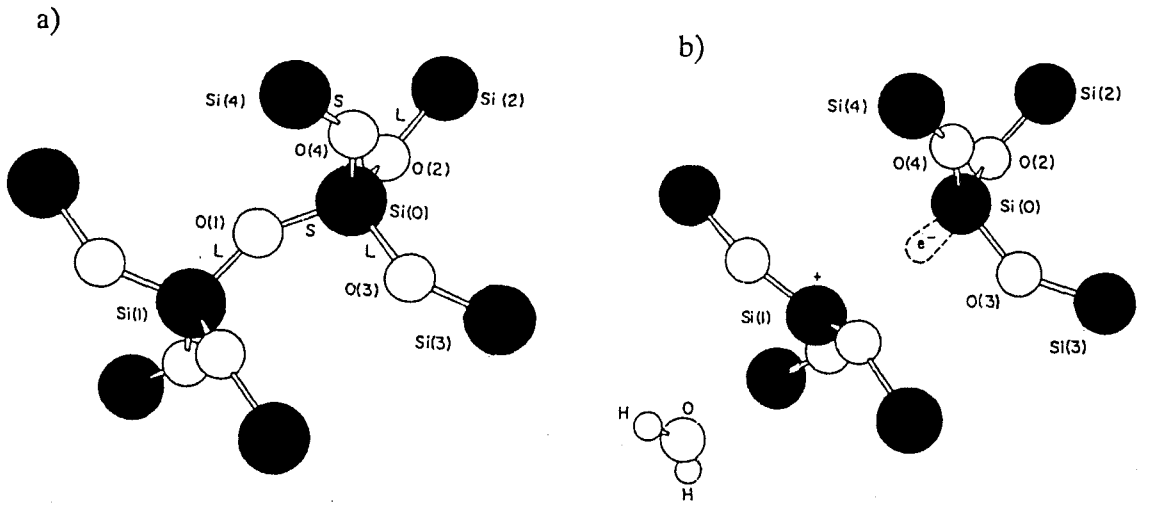

Fig. 2-1 a) A part of atomic dispositions of quartz. b) Minimum energy planar configuration of E'_1 center after [2-8].

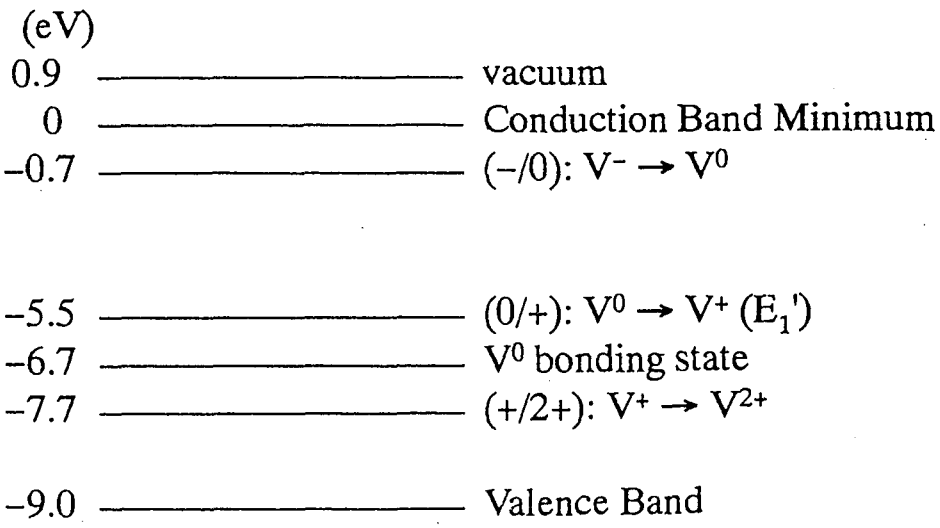

Fig. 2-2 Theoretically calculated energy levels, relative to conduction band minimum, of defect associated with an oxygen vacancy in quartz after [2-8]. V^0, V^+ and V^{2+} denote oxygen vacancies with two, one and no electrons, respectively.

The structure of E'_1 center was simulated theoretically and concluded that the unpaired electron can not be localized at the oxygen vacancy between Si(0) and Si(1) in Fig. 2-1 in the electric structure of minimum energy [2-8]. The energy level for formation of an E'_1 center from a neutral oxygen vacancy (0/+) was also calculated to be - 5.5 eV under the lowest energy level of conduction band according to the one silicon trapping model. The changing level of the bonding state of a neutral oxygen vacancy and that for changing negatively charged state to neutral (0/-) and from single to double positively charged state (+/2+) were also calculated to be - 6.7, - 0.7 and - 7.7 eV respectively as shown in Fig. 2-2.

The formation process of E'_1 center is a significant issue remained. It is created by fast neutron irradiation [2-1, 9] as well as by electron irradiation [2-4] and by γ-ray irradiation at a heavy dose [2-10] with attendant heating at 300 °C. Semi-quantative analysis for correlation between decay of aluminum hole centers $[AlO_4]^0$ and formation of E'_1 centers suggested that holes released from the aluminum hole centers $[AlO_4]^0$ are trapped at neutral oxygen vacancies with two electrons to form E'_1 centers when the sample is heated at from 200 to 300 °C.

Other states of oxygen vacancy trapping an electron (E'_2 and E'_4) were investigated [2-11, 12]. An hfs caused by a hydrogen atom was found. E'' type centers with two electrons ($S = 1$) have been also observed [2-13].

2-2.E' Center in Stishovite

(1) Abstract

X- and Q-band ESR studies were performed on E' center in stishovite synthesized from high-purity SiO_2 glass, followed by γ-ray irradiation using a source of ^{60}Co at room temperature. The E' center has an anisotropic g-factor of orthorhombic symmetry, g_x = 2.0055, g_y = 2.0044 and g_z = 2.0023, an axial hyperfine structure due to ^{29}Si (I = 1/2), A_x = A_y = 1.2 mT and A_z = 8.5 mT, and an almost isotropic superhyperfine structure due to the second-nearest ^{29}Si, A_{shf} = 1.2 mT.

(2) Experimental Procedure

(a) High Pressure Synthesis

Uniaxial split-sphere apparatuses at the Institute for Study of Earth's Interior Okayama University (USSA-5000 and USSA-1000) were used to synthesize stishovite (and coesite). Octahedral MgO medium for high pressure synthesis is shown in Fig. 2-3.

Polycrystalline cluster samples were synthesized at 1200 °C, 13 GPa for 20 or 40 min for stishovite with Pt foil heater. The starting materials were high purity SiO_2 glass used for ESR sample tube and natural quartz including Al and Ti impurities. The used metal foil heaters were taken away carefully from the samples with a diamond file. Crystalline phase of stishovite was confirmed by X-ray diffraction study, and used for ESR studies without grinding.

(b) Artificial γ-ray Irradiation and ESR Measurement

A ^{60}Co-γ-ray source was used to irradiate samples at 3 kGy and 6 kGy at a dose rate of 100 Gy/hour at room temperature. The γ-ray energies of ^{60}Co are 1.173 MeV and 1.333 MeV (both are 100 %). ESR spectra were observed with commercial X- and Q-band ESR spectrometers (JEOL-RE-1X and 2X) at room temperature using 100 kHz field modulation. ESR parameters experimentally obtained, through the analysis of powder spectra, were used to reconstruct the spectra by computer simulation.

The experimental procedures described in (a) and (b) are almost the same throughout this work.

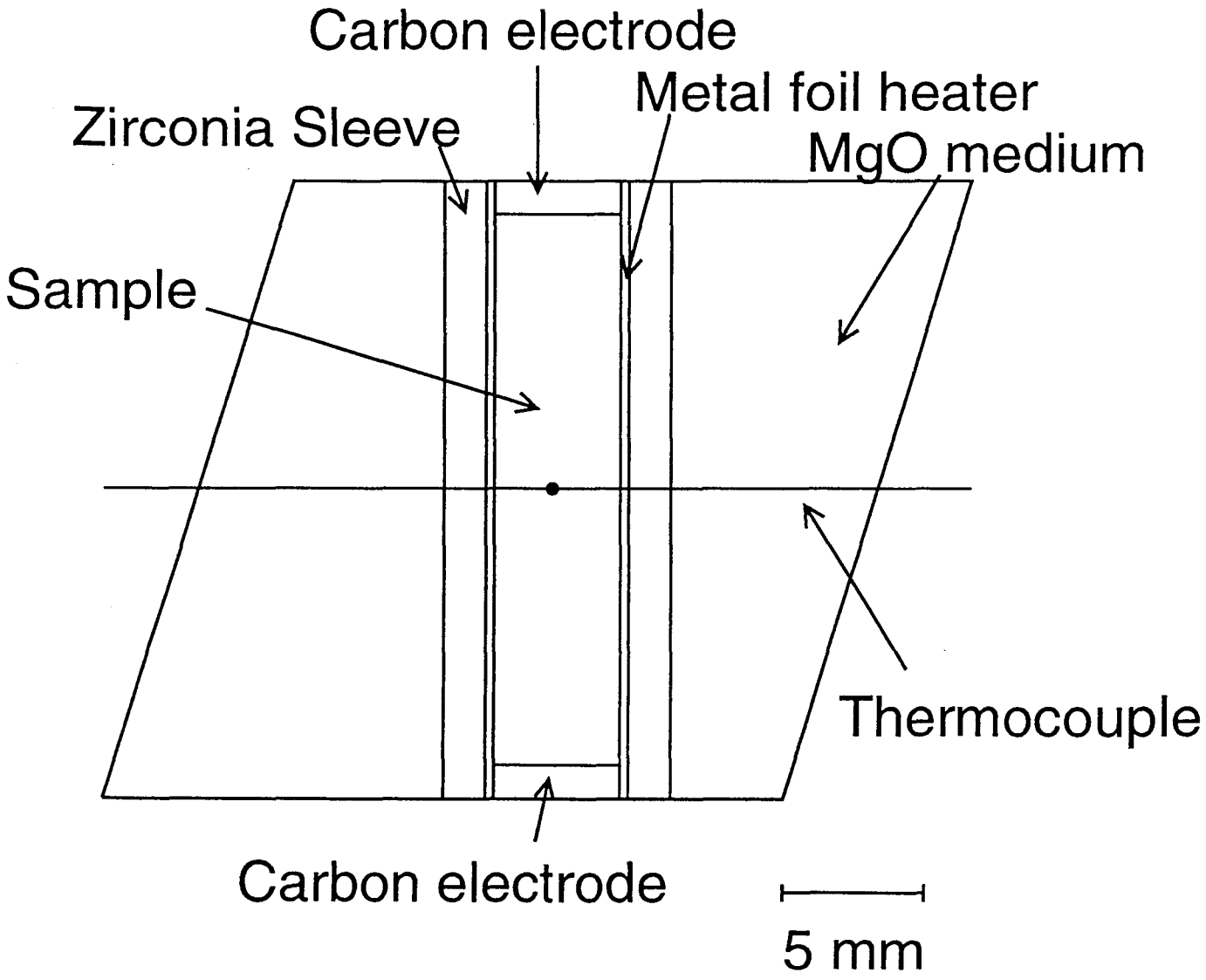

Fig. 2-3 Schematic picture of a cross section of an octahedral MgO specimen used for synthesis of stishovite and coesite. The diameter of the cylindrical metal foil, which raw SiO_2 glass or quartz occupy, is 3.5 mm for stishovite and 4.5 mm for coesite.

(3) Results

Observed X- and Q-band ESR powder spectra of stishovite are shown in Fig. 2-4 (a) and Fig. 2-5 (a), respectively. Simulated spectra for X- and Q-band studies are also shown in Fig. 2-4 (b) and Fig. 2-5 (b), respectively. The observed spectra are not simple differential spectra, because they are powder spectra.

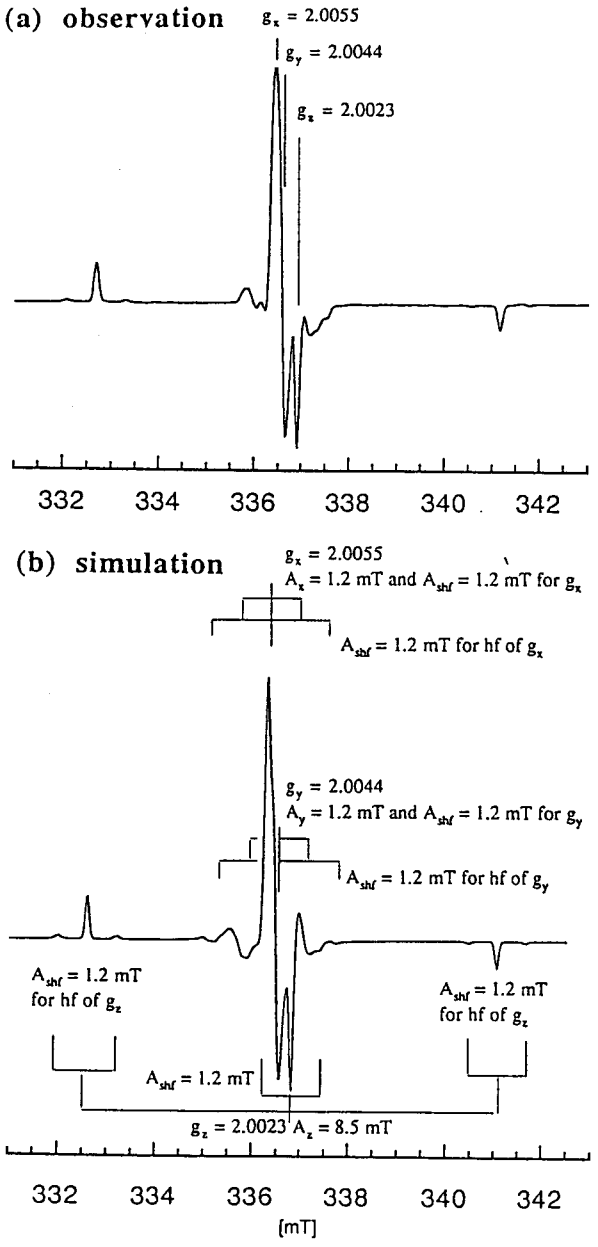

Fig. 2-4 X-band ESR spectra of γ-ray irradiated stishovite. (a) Observation, (b) simulation.

The observed spectra are ascribed to an electron trapped by an oxygen vacancy center with an anisotropic g-factor of orthorhombic symmetry, $g_X = 2.0055$, $g_Y = 2.0044$ and $g_Z = 2.0023$ and an anisotropic hyperfine structure of axial symmetry, $A_X = A_Y = 1.2$ mT and $A_Z = 8.5$ mT. The hyperfine constants in the Q-band spectrum appear slightly smaller than those in the X-band one, as shown in Fig. 2-5 (a), probably because of a small error in the magnetic field setting for Q-band observation.

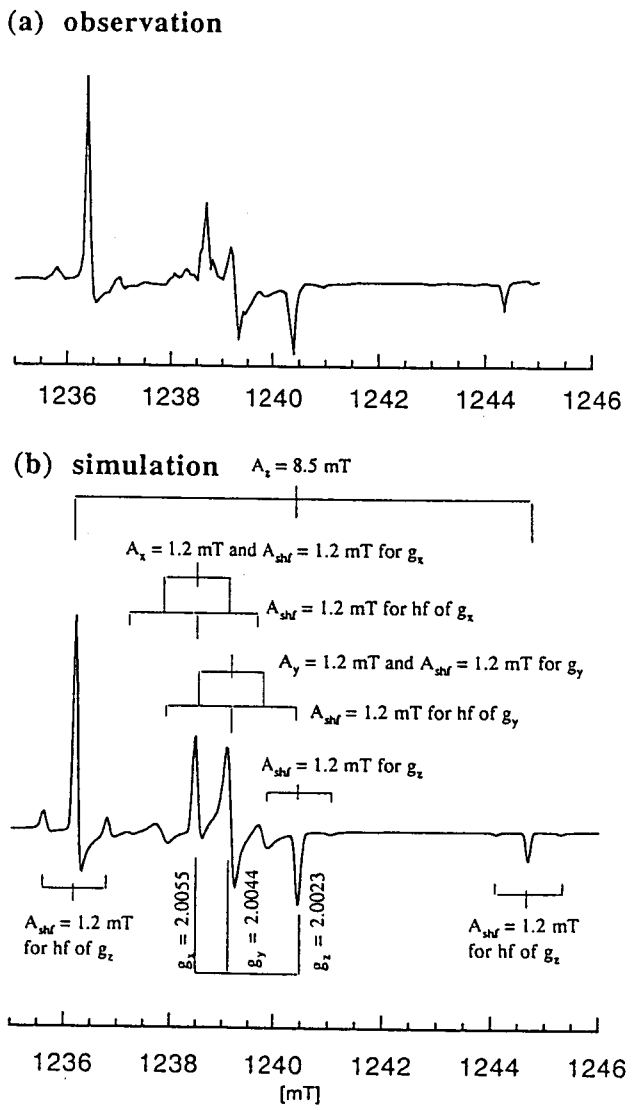

Fig. 2-5 Q-band ESR spectra of γ-ray irradiated stishovite. (a) Observation, (b) simulation.

The ESR spectra with the axial hyperfine structure can be calculated as,

$$H(m_I,\theta)=\frac{h\nu_0}{g\beta}+\left(\frac{K}{g\beta}\right)m_I-\frac{A_\perp^2}{4g\beta h\nu_0}\left(\frac{A_{//}^2+K^2}{K^2}\right)\left[I(I+1)-m_I^2\right]$$

$$-\frac{1}{2g\beta h\nu_0}\left(\frac{A_{//}^2-A_\perp^2}{K}\right)\left(\frac{g_{//}g_\perp}{g^2}\right)^2\sin^2\theta\cos^2\theta m_I^2 \qquad (2\text{-}1),$$

with $g^2=g_{//}^2\cos^2\theta+g_\perp^2\sin^2\theta$, $K^2=(A_{//}^2g_{//}^2\cos^2\theta+A_\perp^2g_\perp^2\sin^2\theta)/g^2$,

$g_{//}=g_z$, $g_\perp=\sqrt{(g_x^2\sin^2\phi+g_y^2\cos^2\phi)}$ and $A_\perp^2g_\perp^2=(A_x^2g_x^2\sin^2\phi+A_y^2g_y^2\cos^2\phi)$,

where θ and ϕ are the angles between the applied magnetic field and the z axis (for θ) and the x axis (for ϕ) on the x-y plane of the defect and ν_0 is the applied microwave frequency. No parameter was changed in the simulation for X- and Q-band spectra, except for microwave frequency and magnetic field.

The magnetic field shifts of g_x and g_y from g_z in the Q-band (ν_0 = 35 GHz) spectrum are about 3.5 times those in the X-band (ν_0 = 9.5 GHz) one, while the hyperfine splitting is considerably axial, $A_x = A_y \ll A_z$, but independent of ν_0. The intensity of the hyperfine-split line at low magnetic field for g_z is calculated to be much larger in the Q-band spectrum than in the X-band one. This is because the powder spectrum averaged over all angles shows a broad signal and the signal overlaps more at low field than at high field owing to the anisotropic g-factor, $g_x \approx g_y > g_z$.

A superhyperfine structure of A_{shf} = 1.2 mT is found first in the Q-band spectrum as a doublet appearing on both sides of an intense hyperfine line of g_z at low field. Not only the hyperfine lines of g_x and g_y with $A_x = A_y$ = 1.2 mT but also all non-split lines are found to have small doublets and to form the finer structures appearing in observed spectra because of the superhyperfine interaction due to ^{29}Si at the second-nearest site, as shown in Fig. 2-5. A small disagreement between simulation and observation suggests the existence of much finer structure or anisotropy of superhyperfine structure. The obtained and confirmed ESR parameters are listed in Table 2-1.

Table 2-1. ESR parameters for E' centers in stishovite and quartz.

Mineral	Signal	g_x (A_x mT)	g_y (A_y mT)	g_z (A_z mT)	Comment	Ref.
stishovite	E' center	2.0055 (1.2)	2.0044 (1.2)	2.0023 (8.5)	^{29}Si	present
					A_{shf} = 1.2 mT	work
quartz	E'_1 center	2.00179 (45.3)	2.00053 (39.1)	2.00030 (39.1)	^{29}Si	2-4
	E'_2 center	$g_{\parallel}$ =2.0022	$g_{\perp}$ = 2.0006	(41.2)	^{29}Si	2-14

Hyperfine structure of E' center is very axial in stishovite, and split constants are much smaller than those of E' centers in quartz.

All the doublet signals have similar microwave power dependence, as shown in Fig. 2-6. However the hyperfine lines of g_x and g_y seem to have two steps in microwave power dependence at low magnetic field in X-band spectra, as shown in Fig. 2-6, due to overlap of an ESR line of the nonbonding oxygen hole center (NBOHC).

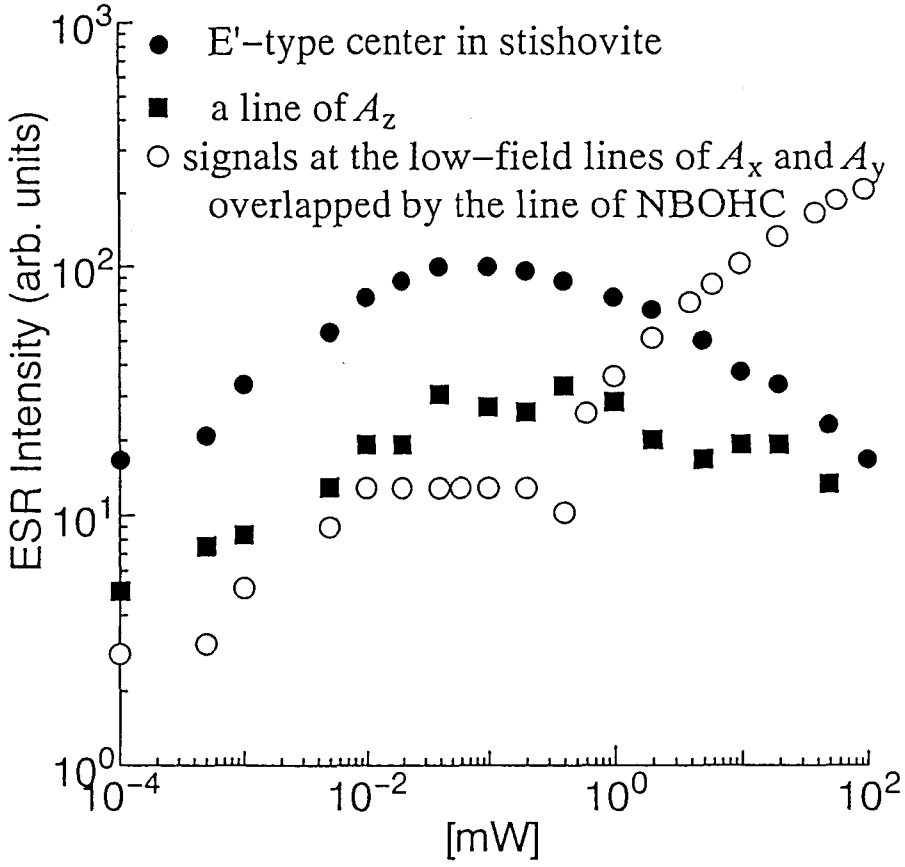

Fig. 2-6 Microwave power dependence of E' center in stishovite and hyperfine (hf) lines. The low-field hf lines of g_x and g_y appear to have two steps, because nonbonding oxygen hole center (NBOHC) overlap them in X-band study.

(4) Discussion

All of the doublets are concluded to be hyperfine and superhyperfine structures due to ^{29}Si (natural abundance of 4.7 %) for the E' center in stishovite, because of similarity of the g-factors and microwave dependence data. Why the hyperfine constants, $A_x = A_y =$ 1.2 mT and $A_z = 8.5$ mT, due to ^{29}Si of the E' center, are smaller in stishovite than those, $A \approx$ 40 mT, in quartz [2-4, 14, 15].

Strong hyperfine interaction occurs due to noticeable lattice relaxation in quartz, the lattice of which contains considerable space and is flexible enough to relax [2-8], as shown in Fig. 2-1. It is possible that silicons surrounding the E' center in stishovite do not relax and the unpaired electron does not interact with the ^{29}Si nucleus as much as in quartz, as shown in Fig. 2-7.

It is necessary to supplement d-type polarization functions with a split-valence s, p basis to construct the stishovite lattice, which is an octahedrally coordinated phase of SiO_2 [2-16]. However the unpaired electron at oxygen vacancy center may be considered to belong to nonbonding sp hybrid orbitals of surrounding silicons for simplicity. The association of the spin with the sp hybrid is based on a comparison of the hyperfine interaction with the expected for atomic $3s$ and $3p$ electrons.

The hyperfine structure is almost axial. The most available orbitals with an anisotropic hyperfine structure are the $3p$ orbitals. The interaction between the nucleus and an unpaired electron in a single p orbital is

$$A_p = (-5/2)g_e\beta_e g_n\beta_n\langle r^{-3}\rangle l_i S_i I_i \quad (2 - 2),$$

where $l_z = -2/3$, $l_x = -1/3$, $l_y = -1/3$ for the orbital p_z. The value of $|A_{3p}/g_e\beta_e|$ is 3.08 mT and the value of $\langle r^{-3}\rangle$ substituted in this formula will be that for a neutral ^{29}Si atom, $\langle r^{-3}\rangle =$ 2.027 a.u. = 12.51 Å^{-3} [2-17]. The anisotropic part of the hyperfine structure is taken to be $|A_{3p}| = \{A_z-(A_x+A_y)/2\}/3$, calculated as 2.4 mT. This suggests that the unpaired electron is in an orbital of 79 % atomic $3p$ character, which is larger than the value of 63 % in quartz [2-3].

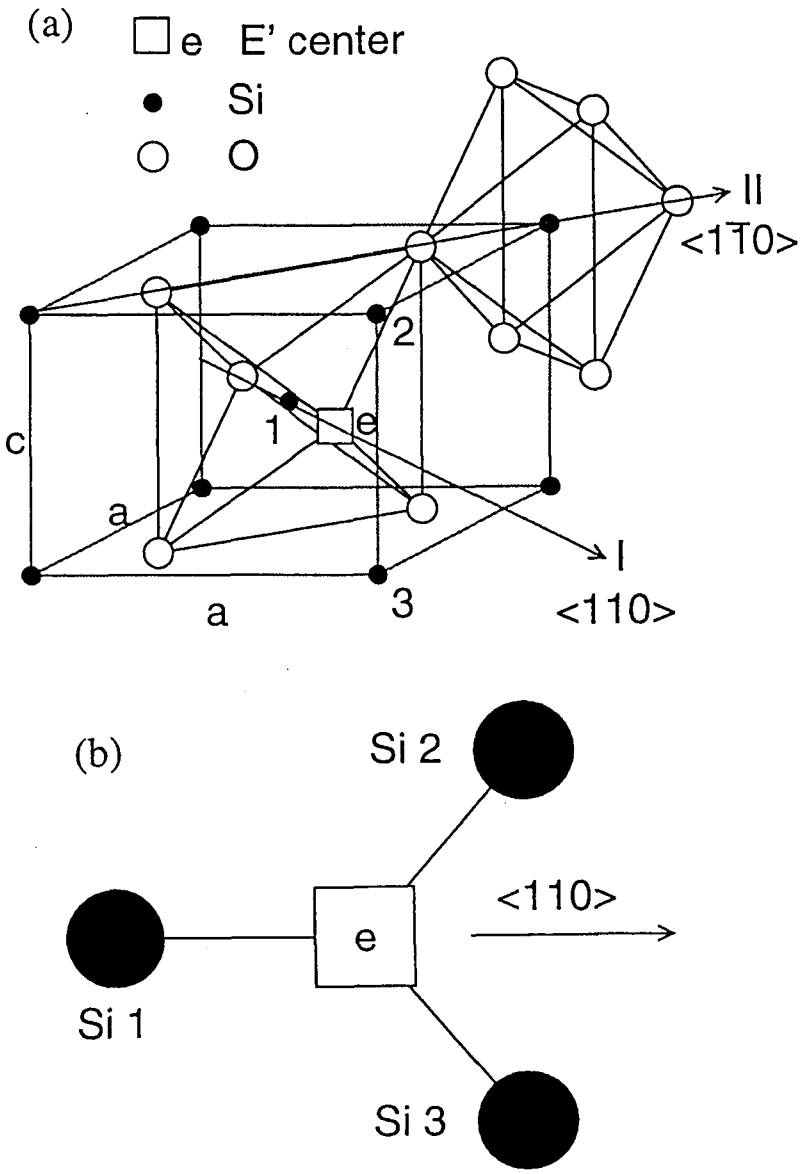

Fig. 2-7 (a) A schematic model for the E' center in stishovite with no lattice relaxation. (b) The unpaired electron in oxygen vacancy and nearest-neighbor silicons. The g_z direction will be parallel to <110> in stishovite lattice. The directions of g_x and g_y should be refined by energy calculation.

The isotropic hyperfine interaction energy of an s electron is

$$A_s = (8\pi/3)g_e\beta_e g_n\beta_n|\Psi_0|^2 S\bullet I \quad (2 - 3),$$

where $|\Psi_0|^2$ is the density of the wave function at the nucleus and $g_n\beta_n I$ is the nuclear moment. The value of $|A_s/g_e\beta_e|$ is 121.8 mT and $|\Psi_{3s}|^2$ is 3.827 a.u. = 25.71 Å^{-3} for a neutral ^{29}Si atom [2-17]. The isotropic part of the hyperfine structure is taken to be the average value: $A = (A_x+A_y+A_z)/3$, calculated as 3.6 mT. This suggests that the unpaired electron is in an orbital of 3.0 % atomic $3s$ character, which is much smaller than the value of 24 % in quartz [2-3].

Three silicons exist at the nearest-neighbor positions of the E' center in stishovite, as shown in Fig. 2-7 (b). The unpaired electron exists 79 % in the orbital of $3p$ character according to the hyperfine data. It can be assumed that the ground-state wave function is dominated by a linear combination of the p orbitals of the three silicons, as shown in Fig. 2-7 (b). The unpaired electron will feel an almost axial field, the principal direction of which is <110>. The direction of $g_z = g_e = 2.0023$ can be considered to be parallel to the <110> direction.

2-3.E' Centers in Coesite

(1) Abstract

X-band ESR studies were performed on E' centers in coesite synthesized from high-purity SiO_2 glass, followed by γ-ray irradiation using a source of ^{60}Co at room temperature. The E' centers have anisotropic g-factors of axial symmetry ($g_{\parallel} = 1.9993$ and $g_{\perp} = 2.0027$), and of orthorhombic symmetry ($g_x = 2.0055$, $g_y = 2.0044$ and $g_z = 2.0023$). The former has an axial hyperfine structure due to ^{29}Si ($I = 1/2$), $A_{\parallel} = 8.1$ mT and $A_{\perp} = 1.2$ mT.

(2) Experimental and Results

Polycrystalline cluster samples were synthesized at 1000 °C, 8 GPa for 20 or 30 min for coesite with Pt foil heater. Crystalline phase of coesite was confirmed by X-ray diffraction study, and used for ESR studies without grinding.

A ^{60}Co-γ-ray source was used to irradiate samples at 3 kGy and 6 kGy at a dose rate of 100 Gy/hour at room temperature. ESR spectra were observed with commercial X-band ESR spectrometer (JEOL-RE-1X) at room temperature with 100 kHz field modulation. ESR parameters experimentally obtained.

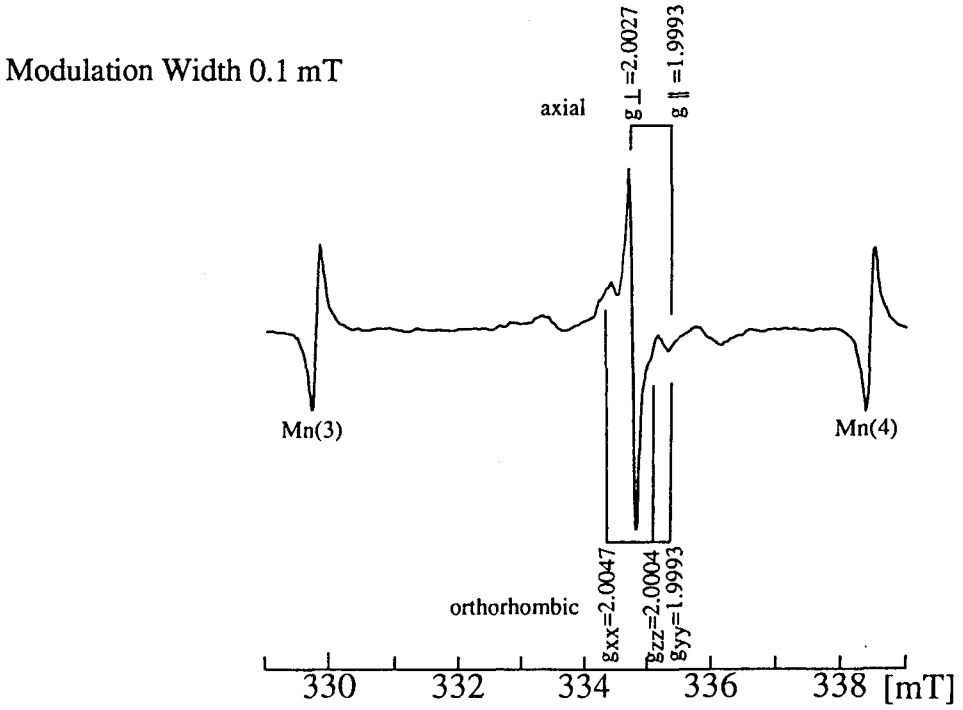

Fig. 2-8 ESR spectrum in coesite observed at room temperature after γ-ray irradiation of 3 kGy.

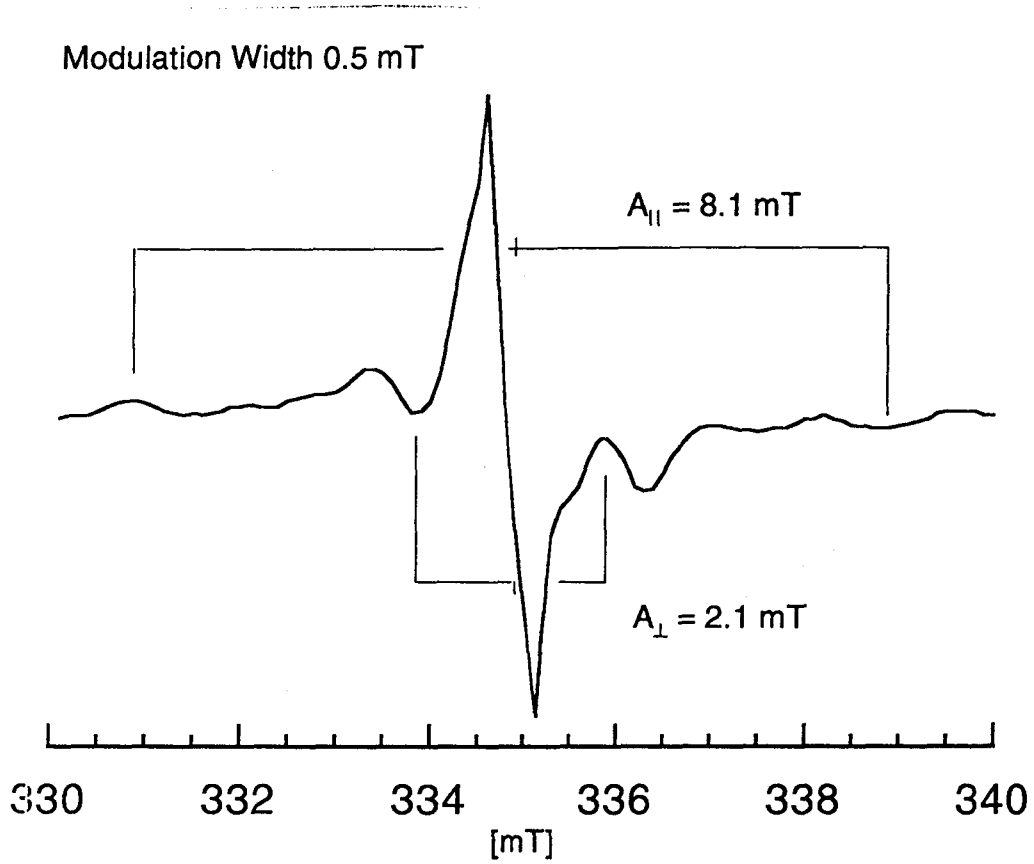

Fig. 2-9 Doublet signals associated with central large ESR line was observed with apparent split parameters of $A_{||}$ = 8.1 mT and $A_{\perp}$ = 2.1 mT in γ-ray irradiated coesite. This situation is very similar to that of hfs of E' center in stishovite.

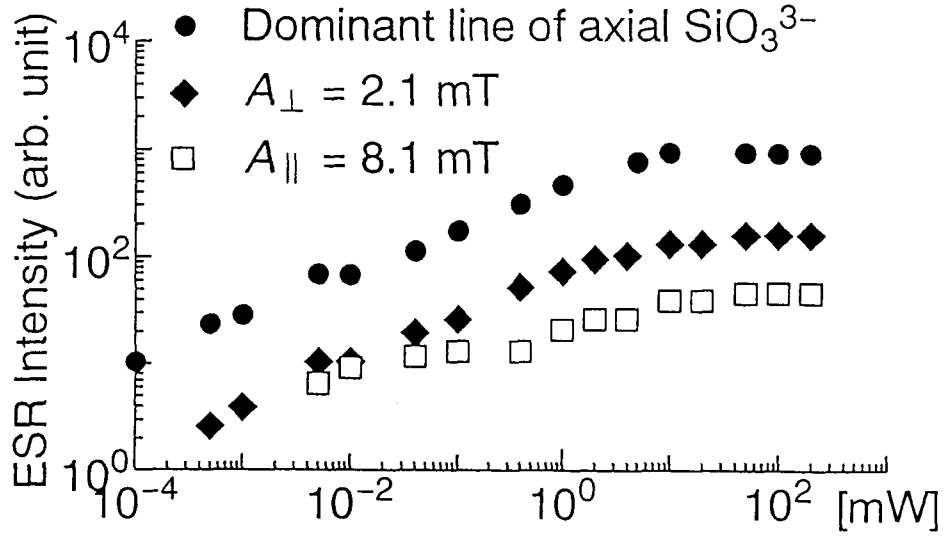

Fig. 2-10 The doublets with apparent hf splitting parameters of $A_{||}$ = 8.1 mT and $A_{\perp}$ = 2.1 mT show almost similar microwave power dependence of the central large axial ESR line. The orthorhombic line shows different microwave power dependence.

ESR spectra of irradiated coesite at room temperature are shown in Fig. 2-8 and Fig. 2-9. Doublet lines like an axial hf structure associated with the central large signal was observed with apparent split parameters of $A_{\parallel} = 8.1$ mT and $A_{\perp} = 2.1$ mT, as shown in Fig. 2-9. The doublet lines show almost similar microwave dependence , as shown in Fig. 2-10.

(3) Discussion

Two types of signals, orthorhombic and axial ones, were identified and compared with the signal of SiO_3^{3-} radical observed in zircon ($ZrSiO_4$) [2-18]. The $g_{\parallel}$ of the axial signal is same as g_y. The similarity of g-factors suggests to attribute the signals to oxygen vacancy defects. The part of orthorhombic signal at $g_z = 2.0004$ was more clearly observed at 77 K. ESR parameters of the defects in synthetic coesite are listed in Table 2-2 together with related centers in quartz, zircon and amorphous SiO_2.

Table 2-2. ESR parameters for E' centers in coesite and related radicals.

Mineral	Signal	g-factor			Saturation Power		Ref.
coesite	orthorhombic	$g_1 = 2.0004$	$g_2 = 1.9993$	$g_3 = 2.0047$	0.04	mW	present
	axial	$g_{\perp} = 2.0027$	$g_{\parallel} = 1.9993$		20	mW	work
zircon	SiO_3^{3-}	$g_z = 2.0004$	$g_y = 1.9993$	$g_x = 2.0047$	?		2-18
quartz	E'_1 center	$g_1 = 2.00179$	$g_2 = 2.00053$	$g_3 = 2.00030$	0.01	mW	2-4
stishovite	E' center	$g_x = 2.0055$	$g_y = 2.0044$	$g_z = 2.0023$	0.06	mW	present

Two oxygen sites exist in the SiO_4 tetrahedral linkage of coesite as shown in Fig. 2-11, though each of quartz and stishovite have only one oxygen site in own structure, as shown in Fig. 2-1 and Fig. 2-7, respectively. The two types of signal, axial and orthorhombic, may be related with the two sites I and II in coesite.

Doublet lines associated with the large axial line were found in X-band observation. The doublet with apparent $A_{\parallel} = 8.1$ mT is very similar to the hyperfine (hf) split g_z line, A_z, of E' center in stishovite, though g-factor of that is almost 2.0027 not 1.9993. Other doublet with apparent $A_{\perp} = 2.1$ mT has also the same g-factor of 2.0027. Lattice relaxation of the E' center in coesite will be as small as that in stishovite, on the assumption that these doublets are axial hf lines of the E' center due to nuclear spin $I = 1/2$ of ^{29}Si in coesite.

Then the anisotropic part of the hfs is taken to be $|A_{3p}| = \{A_z-(A_x+A_y)/2\}/3$, calculated as 2.0 mT. This suggests that the unpaired electron is in an orbital of 65 % atomic $3p$ character, which is almost the same as the value of 63 % in quartz [2-3]. The isotropic part of the hfs is taken to be the average value: $A = (A_x+A_y+A_z)/3$, calculated as 4.1 mT. This suggests that the unpaired electron is in an orbital of 3.4 % atomic $3s$ character, which is much smaller than the value of 24 % in quartz [2-3]. Hyperfine structure of the orthorhombic center has not been found yet. Q-band observation is necessary to determine the structures of the defects.

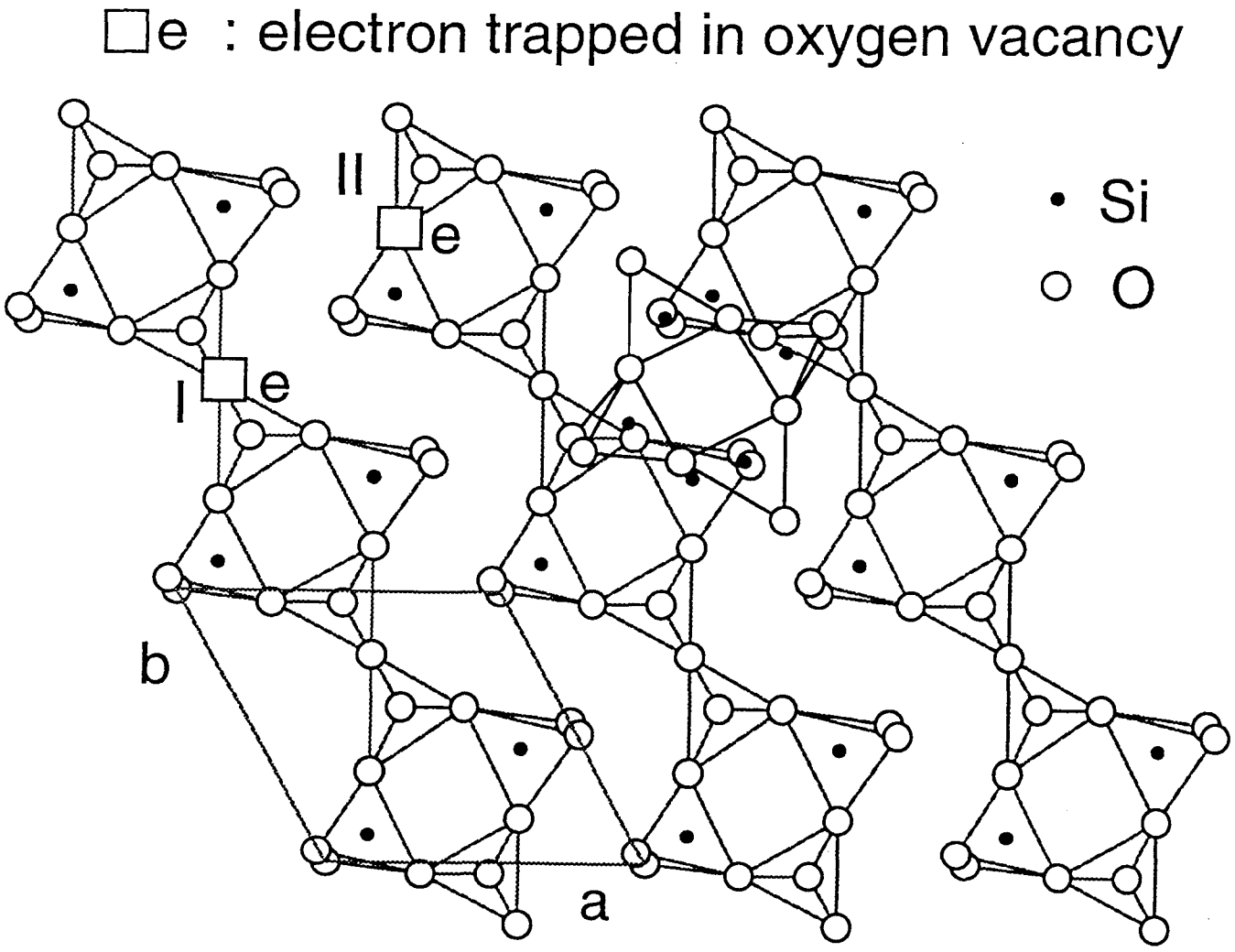

Fig. 2-11 Two oxygen vacancy sites are indicated as I and II in coesite. Axial and orthorhombic signals are ascribed to electron trapped oxygen vacancies at site I and site II, respectively.

2-4.Summary of E' centers in Quartz, Stishovite and Coesite

E' center (unpaired electron trapped at oxygen vacancy), the most intrinsic defect of Silica (SiO_2) is dealt in this chapter. Crystalline phase transition causes different lattice fields on the E' centers in the three polymorphs, quartz, stishovite and coesite, therefore the g-factors of the E' centers differ from each other. An almost axial type E' center was induced in stishovite, and two types (axial and orthorhombic) of SiO_3^{3-} radical were found in coesite.

Silicons surrounding the E'_1 center move considerably in quartz, because of noticeable flexibility of the crystal structure. This large lattice relaxation produces different lattice field on the electron from an SiO_3^{3-} radical, and large hyperfine constant of $A \approx 40$ mT.

X- and Q-band ESR observations indicate that the E' center in stishovite has an anisotropic g-factor of orthorhombic symmetry, $g_x = 2.0055$, $g_y = 2.0044$ and $g_z = 2.0023$. Hyperfine structures due to ^{29}Si ($I = 1/2$), $A_x = A_y = 1.2$ mT and $A_z = 8.5$ mT, for the E' center indicate that silicons in the neighborhood of the defect do not relax as much as in quartz. The g_z direction will be parallel to <110> in stishovite.

Doublets with apparent hf splitting parameters of $A_{\parallel} = 8.1$ mT and $A_{\perp} = 2.1$ mT associated with the axial E' center in coesite is very similar to the hf lines of E' center due to ^{29}Si in stishovite. It is possible that silicons surrounding E' center also do not move so much in coesite, as like as in stishovite.

Table 2-3. ESR parameters of E' centers in stishovite, coesite and quartz.

Mineral	Defect	g_x (A_x mT)	g_y (A_y mT)	g_z (A_z mT)	Comment	Ref.
stishovite	E' center	2.0055 (1.2)	2.0044 (1.2)	2.0023 (8.5)	$^{29}Si A_{shf}$=1.2 mT	present
coesite	SiO_3^{3-}	$g_{\perp} = 2.0027$	$g_{\parallel} = 1.9993$	($A_{\perp}$=1.2mT, $A_{\parallel}$ = 8.1 mT?)	axial	present
		$g_1 = 2.0004$	$g_2 = 1.9993$	$g_3 = 2.0047$	orthorhombic	
quartz	E'_1 center	2.00179 (45.3)	2.00053 (39.1)	2.00030 (39.1)	^{29}Si	2-4
	E'_2 center	$g_{\parallel}$ =2.0022	$g_{\perp} = 2.0006$	(41.2)	^{29}Si	2-14

References

2-1 R. A. Weeks: J. Appl. Phys. **27** (1956) 1376.

2-2 J. A. Weil: Phys. Chem. Minerals. **10** (1984) 149.

2-3 R. H. Shilsbee: J. Appl. Phys. **32** (1961) 1459.

2-4 M. G. Jani, R. B. Bossoli and L. E. Halliburton: Phys. Rev. **B 27** (1983) 2285.

2-5 D. L. Griscom: Phys. Rev. **B 20** (1979) 1823.

2-6 F. J. Feigel, W. B. Fowler and K. L. Yip: Solid State Comunn. **14** (1974) 225.

2-7 D. L. Griscom: Phys. Rev. **B 22** (1980) 4192.

2-8 J. K. Rudra and W. B. Fowler: Phys. Rev. **B 35** (1987) 8223.

2-9 E. G. Garrison, R. M. Rowlett, D. L. Cowan and L. V. Holroyd: Nature **290** (1981) 44.

2-10 A. Wieser and D. F. Regulla: Appl. Radiat. Isot. **40** (1989) 911.

2-11 J. K. Rudra, W. B. Fowler and F. J. Feigl: Phys. Rev. Lett. **55** (1985) 2614.

2-12 L. E. Halliburton, B. D. Perlson, R. A. Weeks, J. A. Weil and M. C. Wintersgill: Solid State Comunn. **30** (1979) 575.

2-13 R. B. Bossoli, M. G. Jani and L. E. Halliburton: Solid State Comunn. **44** (1982) 213.

2-14 R. A. Weeks: Phys. Rev. **130** (1963) 570.

2-15 D. L. Griscom: Rev. Solid State Sci. **4** (1990) 565.

2-16 R. J. Hill, M. D. Newton and G. V. Gibbs: J. Solid State Chem. **47** (1983) 185.

2-17 M. Ikeya: New Applications of Electron Spin Resonance (World Scientific, Singapore, 1993) Chapt. 2, p. 41.

2-18 V. P. Solntsev, M. Ya. Shcherbakova and E. V. Dvornikov: Zh. Strukt. Chim. **15** (1974) 217.

2-19 T. Zoltai and M. J. Buerger: Zeits. Krist. **111** (1959) 129.

3. Oxygen Hole Centers and Aluminum Hole Centers

3-1. Introduction of Oxygen Hole Centers and Aluminum Hole Center in Quartz and Fused Silica

(1) Oxygen Hole Centers (OHC)

Two types of distinct oxygen-associated trapped hole centers were found in high purity fused silica γ-rayed at room temperature [3-1]. One is a hole trapped in a single non-bonding $2p$ orbital of oxygen and called Non Bonding Oxygen Hole Center (NBOHC). It has an anisotropic g-factor of orthorhombic symmetry, $g_1 = 2.0010$, $g_2 = 2.0095$ and $g_3 = 2.078$ (weight average). A model for NBOHC in am-SiO_2 is ≡Si-O•. A proton is released from Si-OH by radiation and a hole trapped at the remaining oxygen, as shown in Fig. 3-1 (a).

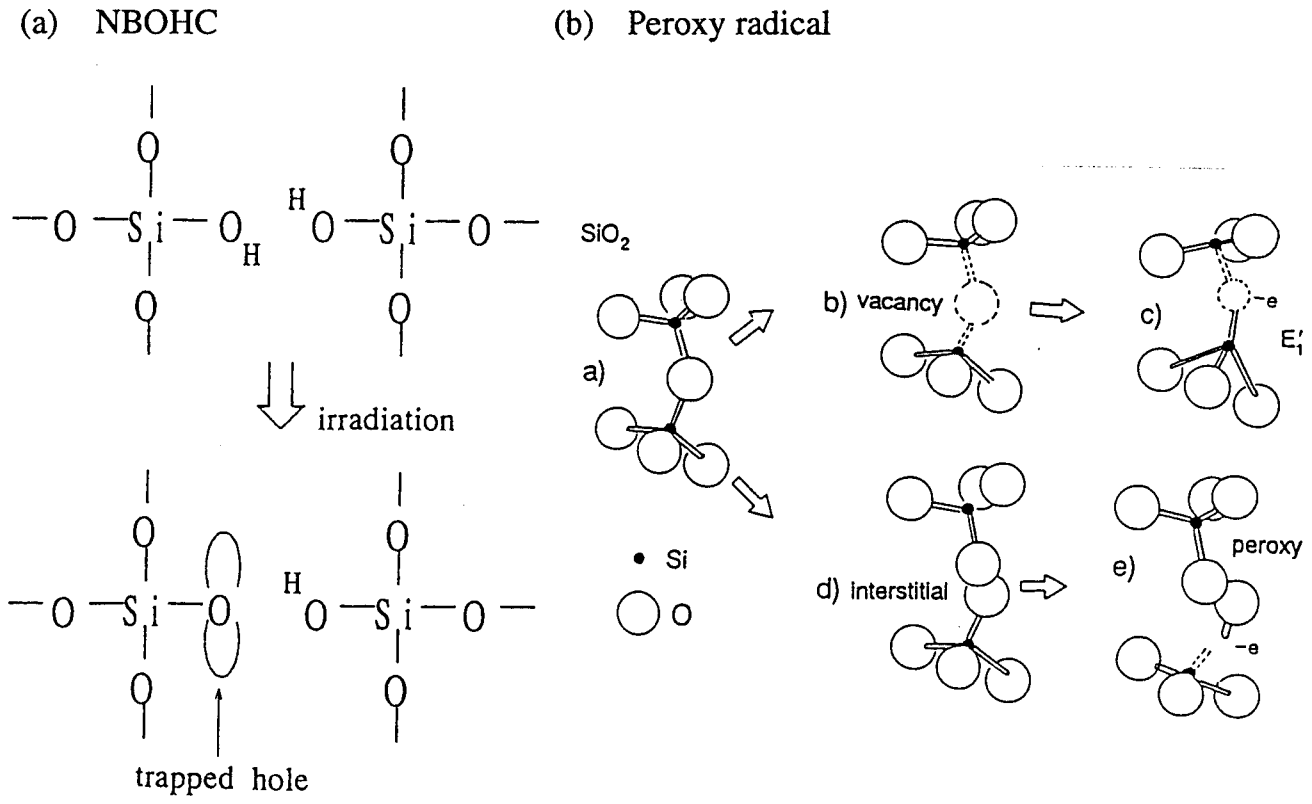

Fig. 3-1 (a) Suggested model for the formation of the NBOHC after [3-1]. (b) A formation scheme of the E'_1 center and peroxy radical: a) a normal SiO_2 sublattice, b) oxygen vacancy [V_-], c) E'_1 center, d) interstitial O^{2-} and e) peroxy radical after [1-1]

The other is a peroxy radical center. The intensity of this center is much larger than that of NBOHC in silica with low OH content. It also has an anisotropic g-factor of orthorhombic symmetry, $g_1 = 2.0014$, $g_2 = 2.0074$ and $g_3 = 2.067$ (weight average). In am-SiO_2, a model for the peroxy center is an antimorph (a complimentary center) of the E'_1 center in a Frenkel pair and is actually an intersticial oxygen ion O^- which bonds with O^{2-}, as shown in Fig 3-1 (b). It may be considered a hole trapped by two O^{2-} at an O^{2-} site, i.e., O_2^{3-} in the form of ≡Si-O-O• [3-2].

(2) Aluminum Hole Center

An ESR signal of a hole center associated with aluminum impurity in quartz has sextet hyperfine structure oriented from a nuclear spin $I = 5/2$ of the aluminum nuclei (100 % abundance) [3-3]. The electric structure was attributed to $[AlO_4]^0$ where a hole is trapped in a nonbonding p-orbital of an oxygen anion linking a substitutional aluminum impurity, as shown in Fig. 3-2 [3-4]. Therefore the aluminum hole center is one type of the oxygen hole centers in quartz. ESR parameters of the aluminum hole center is very similar to those of the OHCs, as shown in Table 3-1.

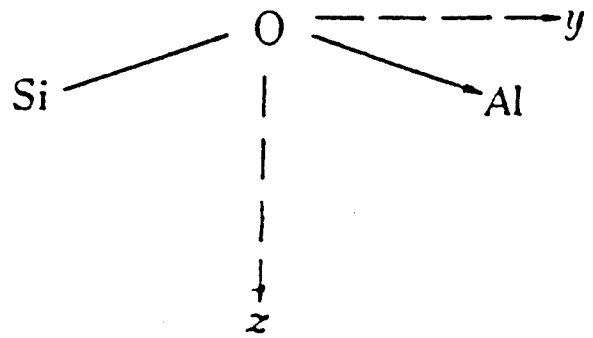

Fig. 3-2 A model of aluminum hole center in quartz after [3-4].

Table 3-1 ESR parameters of oxygen hole center and aluminum hole center in quartz.

Mineral	Signal	g_x (A_x mT)	g_y (A_y mT)	g_z (A_z mT)	Comment	Ref.
quartz	NBOHC	2.0010	2.0095	2.078 (av.)	≡Si-O•	3-1
and silica	peroxy	2.0014	2.0074	2.067 (av.)	≡Si-O-O•	3-2
quartz	Al center	2.0020(0.5)	2.0085(0.6)	2.0602(0.6)	$I = 5/2$	3-5

The hole moves back and forth between the two oxygens linking the aluminum impurity with long bonds [3-6]. Line width was observed to be broadened with increasing temperature [3-7]. The hole hopping process on four oxygens surrounding the aluminum impurity at room temperature is responsible for dielectric loss, therefore the signal can only be detected at low temperature due to the localization of the hole on one of the oxygen atoms [3-8].

The normal static state with Al substituted for Si is $[AlO_4/M^+]^0$, where M^+ is an ion for a charge compensator. A hole is created by irradiation on an oxygen ion nearest neighboring with the Al. The cation M^+ defuses away at the time of irradiation at room temperature and when the sample is warmed up after irradiation at liquid nitrogen temperature [3-9]. Consequently, the aluminum hole center, $[AlO_4]^0$, is formed by ionizing irradiation [3-10]. Other unstable aluminum hole centers, precursors of the $[AlO_4]^0$, have been reported, such as $[AlO_4/M^+]^+$ and $[AlO_4]^+$ [3-11, 12].

Newly found OHCs associated with aluminum impurities in stishovite and coesite are described in this chapter.

3-2.Aluminum Hole Center in Stishovite

(1) Abstract

ESR has been measured at X-band for stishovite synthesized from natural quartz and irradiated by γ-ray at 77 K. The prominent signal detected at 77 K has an anisotropic g-factor of orthorhombic symmetry, $g_x = 2.0155$, $g_y = 2.0094$ and $g_z = 2.0033$, and hyperfine sextets ($I = 5/2$) with $A_x = 0.394$ mT, $A_y = 0.372$ mT and $A_z = 0.436$ mT. The ESR parameters indicate that this signal is due to a two-center type hole center, O_2^{3-}, associated with an aluminum atom substituted at the silicon site in stishovite.

(2) Experimental and Results

Stishovite samples were synthesized from natural quartz including aluminum and titanium impurities. A ^{60}Co-γ-ray source was used to irradiate the samples, that were sealed in an evacuated sample holder and dipped in liquid nitrogen in a metal dewar, to the dose of 18 kGy at a dose rate of 3 kGy/h.

An ESR powder spectrum at 77 K of the stishovite is shown in Fig. 3-3 (a). This spectrum can be ascribed to a defect with an anisotropic g-factor of orthorhombic symmetry, $g_x = 2.0155$, $g_y = 2.0094$ and $g_z = 2.0033$ having sextets due to anisotropic hyperfine splittings by a nuclear spin of $I = 5/2$ with $A_x = 0.394$ mT, $A_y = 0.372$ mT and $A_z = 0.436$ mT. The ESR spectrum is simulated using the above parameters of the anisotropic g-factor and hyperfine A-values, as shown in Fig. 3-3 (b). Overall agreement of the hyperfine lines has been obtained at the central part. The disagreement might arise from the presence of overlapping signal due to an electron trapped in oxygen vacancy, E' center in stishovite (cf. Chapt. 2).

The signal at $g_x = 2.0155$ was observed clearly in a sample irradiated at room temperature, but that due to the E' center overlaps the line with $g_z = 2.0033$. The defect like E' center can not be observed clearly in the sample irradiated at 77 K in stishovite.

The signal is broadened up above -80 °C (193 K). The g-factor and hyperfine constants do not change appreciably from 77 K to 193 K. The signal becomes sextets, when the sample is cooled below 193 K again, and the signal intensity does not change at the same temperature from 77 K to 193 K. The defect is annealed at room temperature, then the E' center is produced. The ESR parameters of observed defect are tabulated in

Table 3-2 together with those of O_2^{3-} in anhydrite [3-13] and of aluminum hole center in quartz [3-5,14,15], for later comparison.

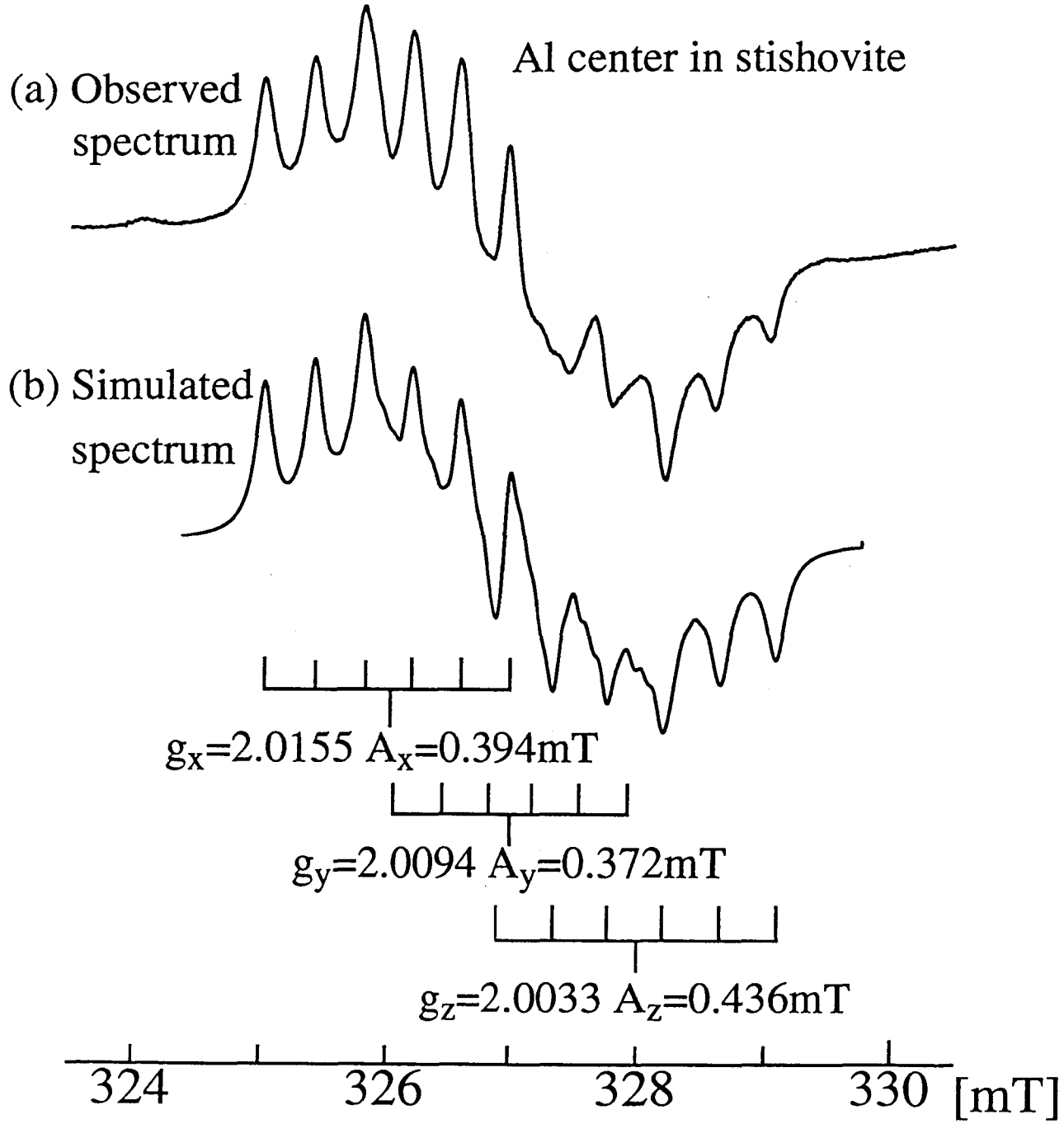

Fig. 3-3 (a) ESR spectrum of stishovite irradiated at 77 K. The ^{27}Al nucleus produces the hyperfine structure. (b) Simulation for the observed spectrum.

Table 3-2. Parameters for observed signals in stishovite together with those of related defects

mineral	signal	g_x (A_x mT)	g_y (A_y mT)	g_z (A_z mT)	comment	ref.
stishovite (SiO_2)	O_2^{3-}-Al^{3+}	2.0155 (0.394)	2.0094 (0.372)	2.0033 (0.436)	77K ^{27}Al I=5/2	present work
anhydrite ($CaSO_4$)	O_2^{3-}-Y^{3+}	2.0262 (0.49)	2.0122 (0.49)	2.0029 (0.63)	290K ^{89}Y I=1/2	3-13
	I*	2.0312 (0.45)	2.0078 (0.54)	2.0026 (0.52)	77K ^{89}Y I=1/2	3-13
	O_2^{3-}-Y^{3+}	2.0168 (0.47)	2.0078 (0.42)	2.0030 (0.42)	290K ^{89}Y I=1/2	3-13
	II*	2.0190 (0.40)	2.0062 (0.33)	2.0031 (0.38)	77K ^{89}Y I=1/2	3-13
quartz (SiO_2)	$[AlO_4]^0$	2.00 (0.51)	2.00 (0.60)	2.06 (0.60)	^{27}Al I=5/2	3-14
		2.0024 (0.50)	2.0091 (0.62)	2.0614 (0.62)	4.2K ^{27}Al I=5/2	3-15
		2.00195(0.50)	2.00854(0.62)	2.06021(0.61)	35K ^{27}Al I=5/2	3-5
		2.0045 (0.50)	2.0045 (0.63)	2.0590 (0.63)	77K ^{27}Al I=5/2	3-16

* Two different sites for O_2^{3-}-Y^{3+} exist in anhydrite ($CaSO_4$).

(3) Discussion

The g-factor larger than g_e = 2.0023, the nuclear spin I = 5/2 and the anisotropic hyperfine constants suggest that this signal is due to a hole center related to an aluminum atom located at the silicon site in the stishovite lattice as shown in Fig. 3-4. Each silicon is surrounded by an octahedron of oxygens in stishovite as shown in Fig. 3-4. A silicon atom forms tetrahedral bonds in SiO_2 polymorphs under about 8 GPa. The all six silicon-oxygen bonds are both covalent and ionic in stishovite. However simply, the structure may be considered as a combination of two sets of SiO_4 rectangular planes, one of which is perpendicular to the other. The bond between the silicon and oxygen at the pyramid top has the length of 1.809 Å, and the other ones forming the rectangular bottom of the pyramid have the length of 1.758 Å. The four nearest neighbor oxygen atoms form a SiO_4 rectangle having only four shortest bonds.

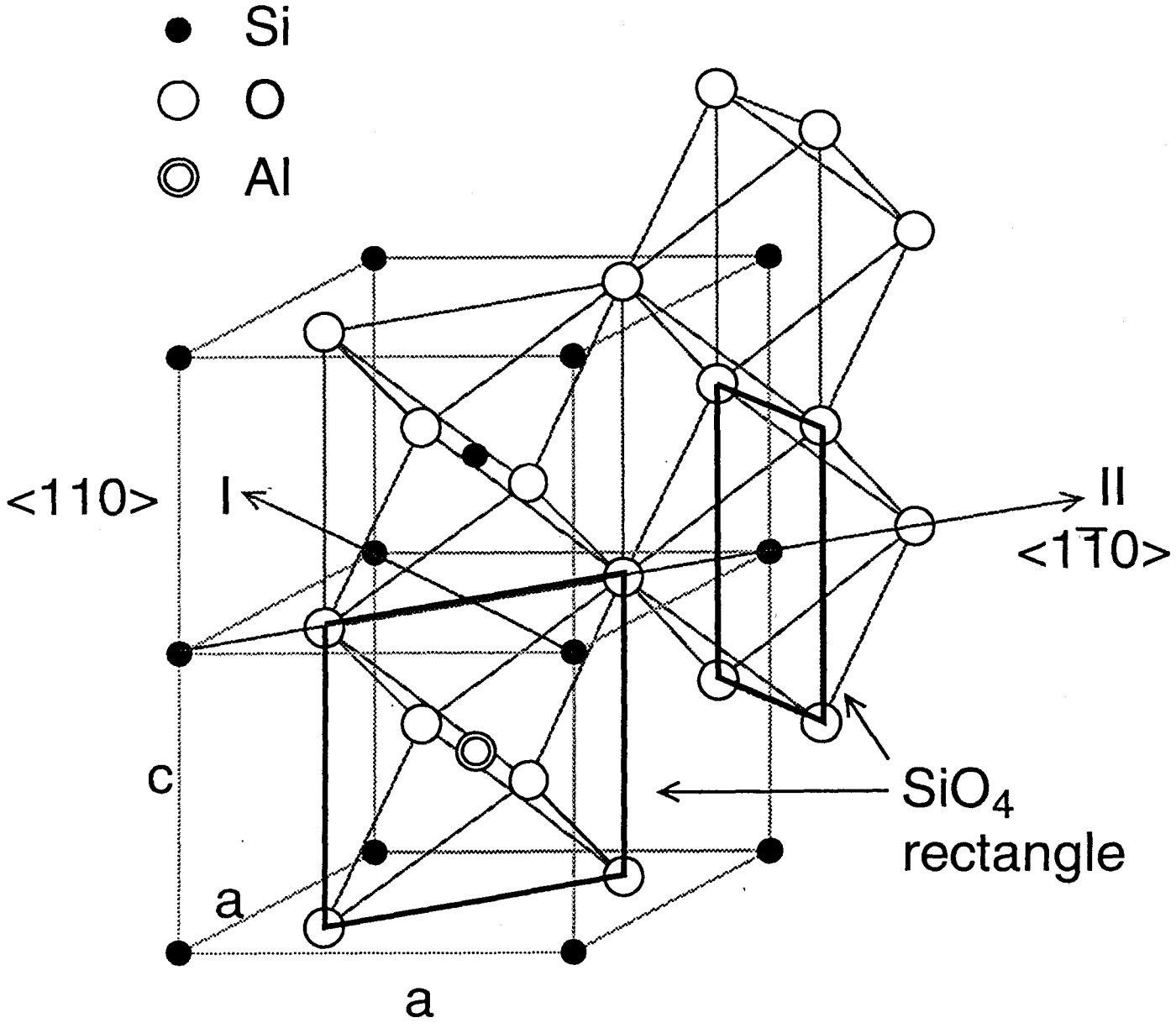

Fig. 3-4 A silicon atom is surrounded by six oxygen atoms octahedrally. Two SiO_4 rectangular planes form the structure for simplicity. a = 4.179 Å, c = 2.665 Å.

An aluminum atom can be an Al- ion by accepting an extra electron, and form an AlO_4 rectangle in stishovite. Each Al- ion should be accompanied by a positive ion as a charge compensator in SiO_2, to maintain the principle of charge neutrality as shown in Fig. 3-5 (a) and (b). Although only one oxygen atom provides the extra electron to the aluminum atom in Fig. 3-5, the dative bond may resonates with a bond from an equivalent oxygen atom existing on the right side, and may be shared by the two equivalent oxygen atoms.

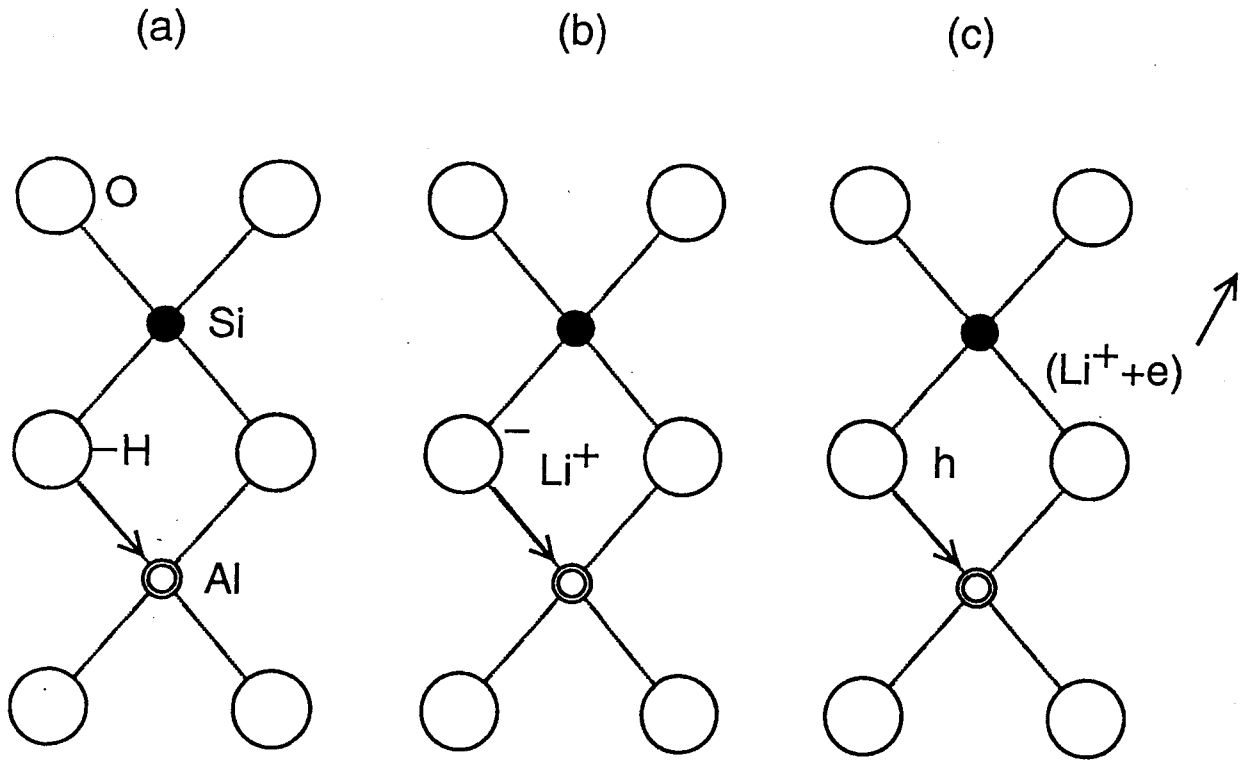

Fig. 3-5 Chemical bonding structure of SiO_4 rectangular planes. (a) and (b) before irradiation, and (c) after irradiation. The lines represent covalent bonds containing one electron from each atom, and the arrows represent dative bonds in which both electrons are provided by the atom at the tail of the arrow.

Irradiation produces a hole temporarily at a simple O^{2-} site but would move from the one site presumably due to Jahn-Teller distortion. Then the hole may be shared by the two oxygens forming an O_2^{3-} molecule-ion like a V_k center in alkali halides, as shown in Fig. 3-6.

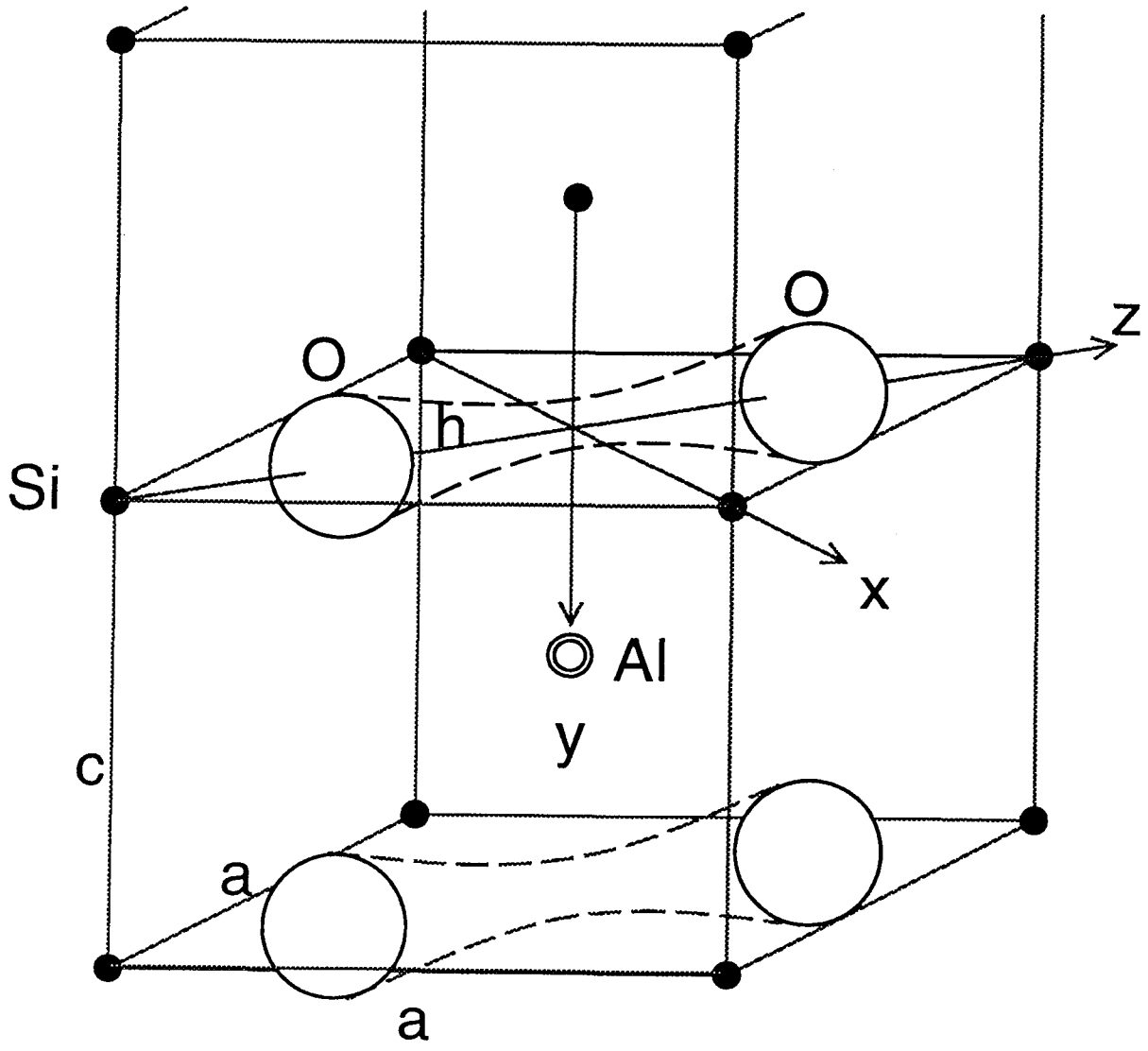

Fig. 3-6 A model of O_2^{3-} molecule-ion. Four oxygens that form the rectangle are written. The hole may be shared by the two equivalent oxygen atoms in middle of the scheme.

The O_2^{3-} molecule-ion is axially symmetric in free space. In stishovite the nearest neighbor aluminum and silicon atoms on the y-direction produce an orthorhombic field on the O_2^{3-} molecule-ion, as shown in Fig. 3-6. Therefore the g_x is not equal to the g_y, like as O_2^{3-}-Y^{3+} in anhydrite. In the Table 3-2 the directional notations of g-factors of O_2^{3-}-Y^{3+} are changed in concordance with those of O_2^{3-}-Al^{3+} model in stishovite.

In the O_2^{3-} molecule-ion model, the principal directions of the hyperfine interaction may be perpendicular to the oxygen-oxygen bond direction. Therefore the direction z' of the hyperfine structure may be the direction - y of the g-factor, and direct to the aluminum atom. However the directional notations of the hyperfine constants are not changed in this thesis for simplicity.

The ground-state wave function must contain some admixture of a wave function overlapping the aluminum nucleus because the hyperfine structure due to the aluminum appears. The hyperfine structure is almost isotropic. An s orbital on the aluminum atom should be mainly responsible, and may be the $3s$ orbital used in bonding.

The hyperfine interaction energy of an s electron is

$$A_s = (8\pi/3)g_e\beta_e g_n\beta_n|\Psi_0|^2 S\cdot I \qquad (3 - 1),$$

where $|\Psi_0|^2$ is the density of the wave function at the nucleus and $g_n\beta_n I$ is the nuclear moment. The $A_s/g_e\beta_e$ is 98.3 mT and $|\Psi_{3s}|^2$ is 2.355 a.u. = 15.82 Å^{-3} for aluminum atom [3-17]. The isotropic part of the hyperfine structure is taken to be the average value : $A = (A_x+A_y+A_z)/3$, calculated as 0.401 mT. If a term of $\delta|3s\rangle$ is added to the ground-state wave function, δ^2 must be 0.0041, which is a little smaller than the value of 0.0060 in quartz. This is so small that we can assume that the main part of the ground-state wave function is unaltered by this admixture.

The most available orbitals with an anisotropic hyperfine structure are the $3p$ orbitals that may be used in bonding. The interaction between the nucleus and an unpaired electron in a single p orbital is

$$A_p = (-5/2)g_e\beta_e g_n\beta_n\langle r^{-3}\rangle l_i S_i I_i \quad (3 -2),$$

where $l_y = -2/3$, $l_z = -1/3$, $l_x = -1/3$ for the orbital p_y. The $A_{3p}/g_e\beta_e$ is 2.16 mT and the value of $\langle r^{-3}\rangle$ substituted in this formula will be that on a neutral aluminum atom, $\langle r^{-3}\rangle$ = 1.088 a.u. = 7.31 Å^{-3} [3-17]. The maximum anisotropic part of the hyperfine structure is taken to be $|A_{3pmax.}| = (A_z-A_y)/3$, calculated as 0.021 mT. If a term of $\varepsilon|3p\rangle$ is added to the ground-

state wave function, ε^2 must be 0.0029. The maximum anisotropy in the hyperfine structure, $(A_z\text{-}A_y)/A$ of 16% is almost equal to that in quartz of 15% which is expected to be 16% from a simple tetrahedral bonding orbitals of the form ($|3s\rangle+|3p\rangle$) [3-4]. The broadening of the signal over 193 K is probably due to the hole hopping among the equivalent four oxygen atoms, as like in quartz. With heating the hole may move and be shared by another oxygen pair, which is perpendicular to the original O_2 molecule. Then another type O_2^{3-} molecule may be formed temporarily.

The E' center in stishovite is not produced obviously by irradiation at 77 K, presumably because an oxygen atom leaves two electrons in its vacancy and becomes an interstitial atom in stishovite lattice. The hole at O_2^{3-}--Al^{3+} radical may be released on heating to be trapped at the neutral oxygen vacancy with two electrons to form the E' center at room temperature.

3-3.Oxygen Hole Centers in Coesite

(1) Abstract

ESR has been measured for coesite synthesized from natural quartz and irradiated by γ-ray at 77 K. The prominent signal detected at 77 K have an anisotropic g-factor of orthorhombic symmetry, $g_1 = 2.0015$, $g_2 = 2.0055$ and $g_3 = 2.065$, and ascribed to an oxygen related hole center in coesite. No hyperfine structure due to aluminum nuclei is found.

(2) Experimental and Results

Coesite samples were synthesized from natural quartz including aluminum and titanium impurities, which was used for synthesis of the stishovite written above in this chapter. They were irradiated by γ-ray at liquid nitrogen temperature to the dose at 18 kGy. Observed and simulated ESR powder spectra at 77 K of coesite are shown in Fig. 3-7 (a) and (b), respectively.

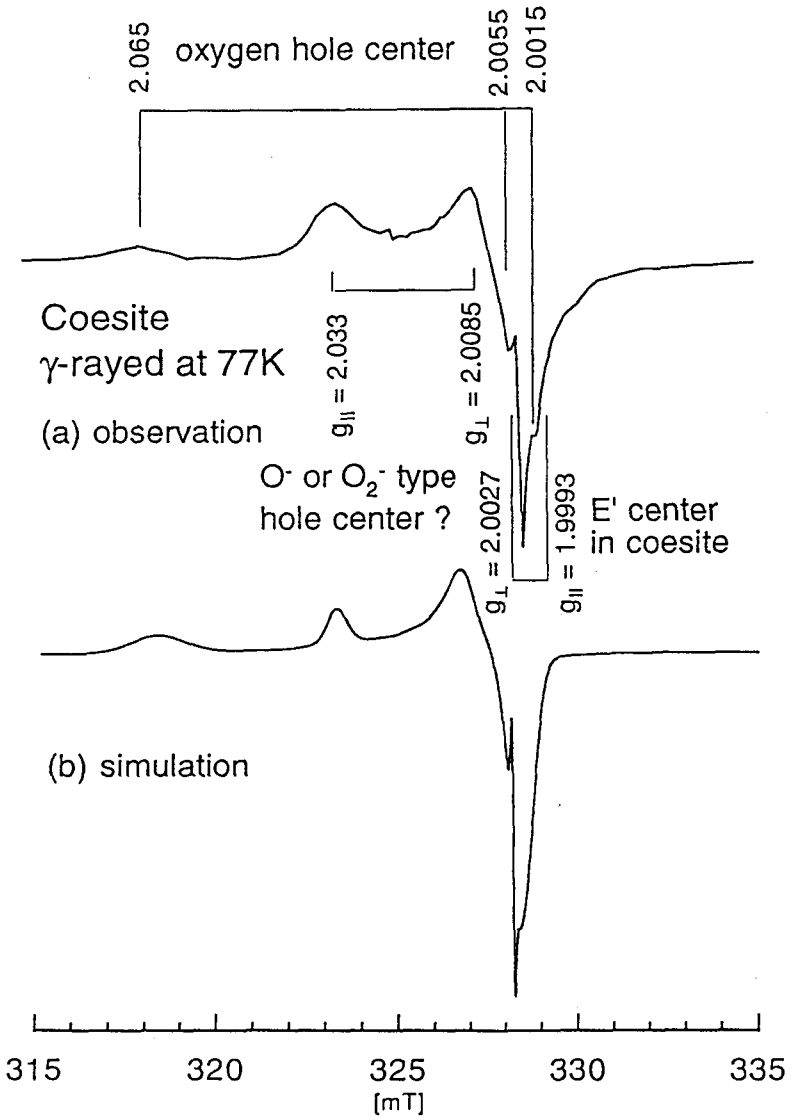

Fig. 3-7 ESR spectrum of coesite irradiated at 77 K. (a) observation and (b) simulation. Nuclei of ^{27}Al do not produce the hyperfine interaction on oxygen hole centers.

The observed signals can be ascribed to two newly found defects with anisotropic g-factors of orthorhombic symmetry, $g_1 = 2.0015$, $g_2 = 2.0055$ and $g_3 = 2.065$ and of axial symmetry, $g_{\parallel} = 2.0033$ and $g_{\perp} = 2.0085$, and an axial E' center in coesite ($g_{\perp} = 2.0027$ and $g_{\parallel} = 1.9993$) (cf. Chapt. 2). The former ones were annealed easily at room temperature, and then the ESR intensity of the E' center in coesite became larger. The ESR parameters of observed defects are tabulated in Table 3-3 together with those of oxygen related hole centers in quartz, amorphous silica and other minerals, for later comparison.

Table 3-3 Parameters for observed signals in coesite together with those of related defects

Defect	Mineral	g_1 (A_1 : mT)	g_2 (A_2: mT)	g_3 (A_3: mT)	Comment	Ref.
OHC	coesite	2.0015	2.0055	2.065		present
	stishovite		2.0095		NBOHC ?	Chapt. 2
	quartz and	2.0014	2.0074	2.067 (av.)	peroxy	3-1
	silica	2.0010	2.0095	2.078 (av.)	NBOHC	3-1
Al hole	quartz	2.0020(0.5)	2.0085(0.6)	2.0602(0.6)	35K $[AlO_4]^0$	3-5
center	stishovite	2.0155(0.4)	2.0094(0.4)	2.0033(0.4)	77K O_2^{3-}-Al^{3+}	present
O- or O^{2-}	coesite	2.033 ($g_{\parallel}$)	2.0085 ($g_{\perp}$)			present
O- type	alkali-	2.0301(0.9)	2.0034(0.9)	2.0094(0.9)	Al-O-Al	3-18
hole center	-feldspar	2.0342(0.9)	2.0043(0.9)	2.0099(0.9)	Al-O-Al	3-18
	kaolinite	2.039 ($g_{\parallel}$)	2.009 ($g_{\perp}$)		A' center	3-19
	gypsum	2.037	2.000	2.002	OH	3-20
O_2- type	dry ice	2.0360(1.8)	2.0055(1.9)	2.0040(1.3)	HO_2	3-21
hole center	ice	2.0353(1.4)	2.0086(0.4)	2.0042(1.6)	HO_2	3-22

(3) Discussion

The anisotropic g-factor of $g_1 = 2.0015$, $g_2 = 2.0055$ and $g_3 = 2.065$ is similar to those of oxygen hole centers in fused silica or natural quartz, as shown in Table 3-3. An expected oxygen hole center with hyperfine structure due to a nuclear spin $I = 5/2$ of an aluminum nucleus was not observed in coesite irradiated at 77 K, though the starting material has aluminum impurities. We consider the orthorhombic signal is due to a hole trapped at an oxygen atom nearby an aluminum atom substituted at silicon site in coesite: the hole will not interact with the nuclear spin $I = 5/2$ of the aluminum atom in this case on the contrary to quartz and stishovite.

Four silicon-oxygen tetrahedra make one unit, and the units make the framework in coesite, as shown in Fig. 3-8. An aluminum atom can be an Al- ion by accepting an extra electron, and form an AlO_4 tetrahedron in coesite.

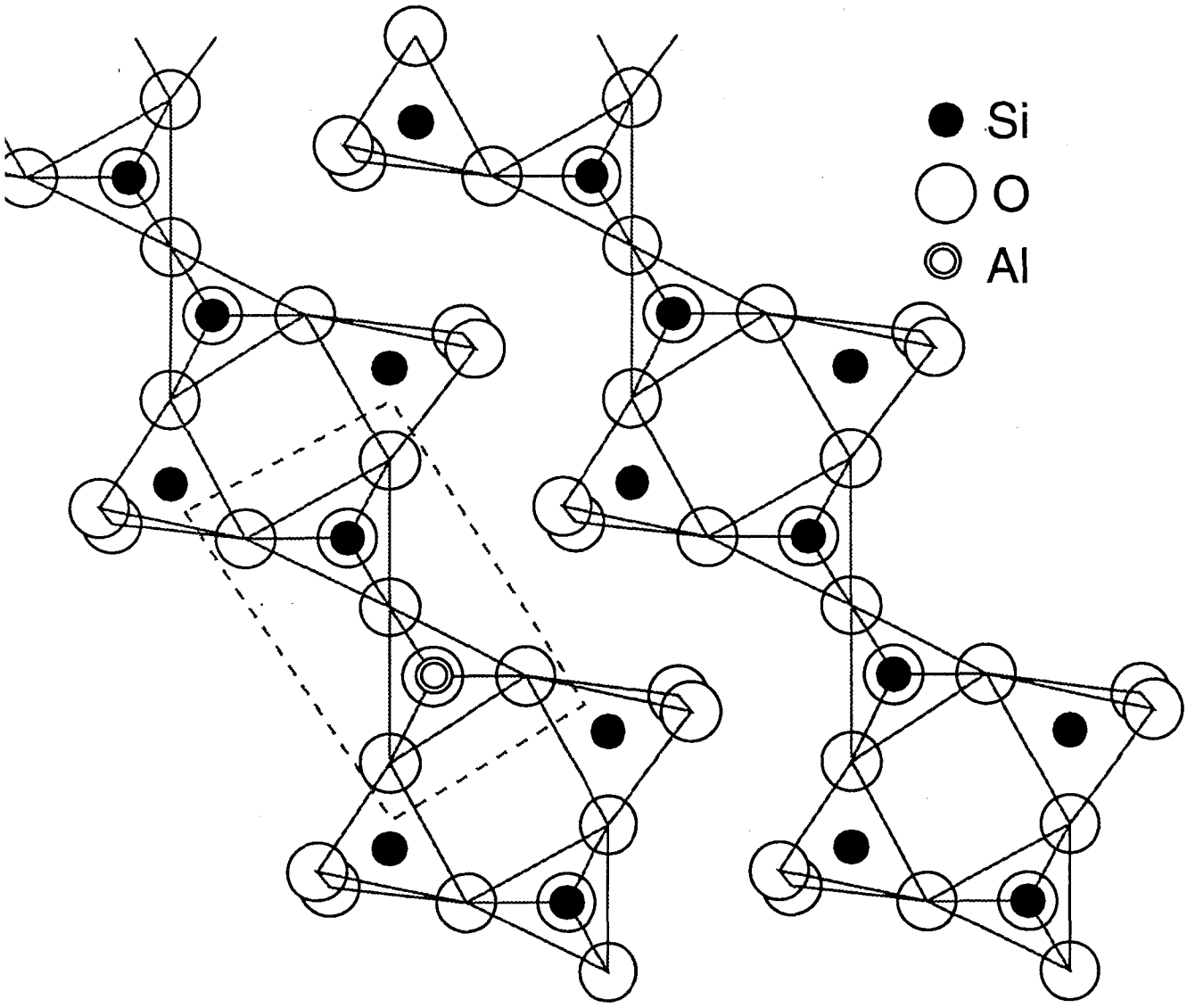

Fig. 3-8 An aluminum atom can be an Al- ion by accepting an extra electron from a charge compensator, and form an AlO_4 tetrahedron in coesite.

Each Al- ion should be accompanied by a positive ion as a charge compensator in coesite, to maintain the principle of charge neutrality as shown in Fig. 3-9 (a): this is similar to the Al- ion in quartz. The charge compensator atom leaves a hole at the oxygen atom between the silicon atom and the aluminum atom, as shown in Fig. 3-9 (b) on γ-ray irradiation.

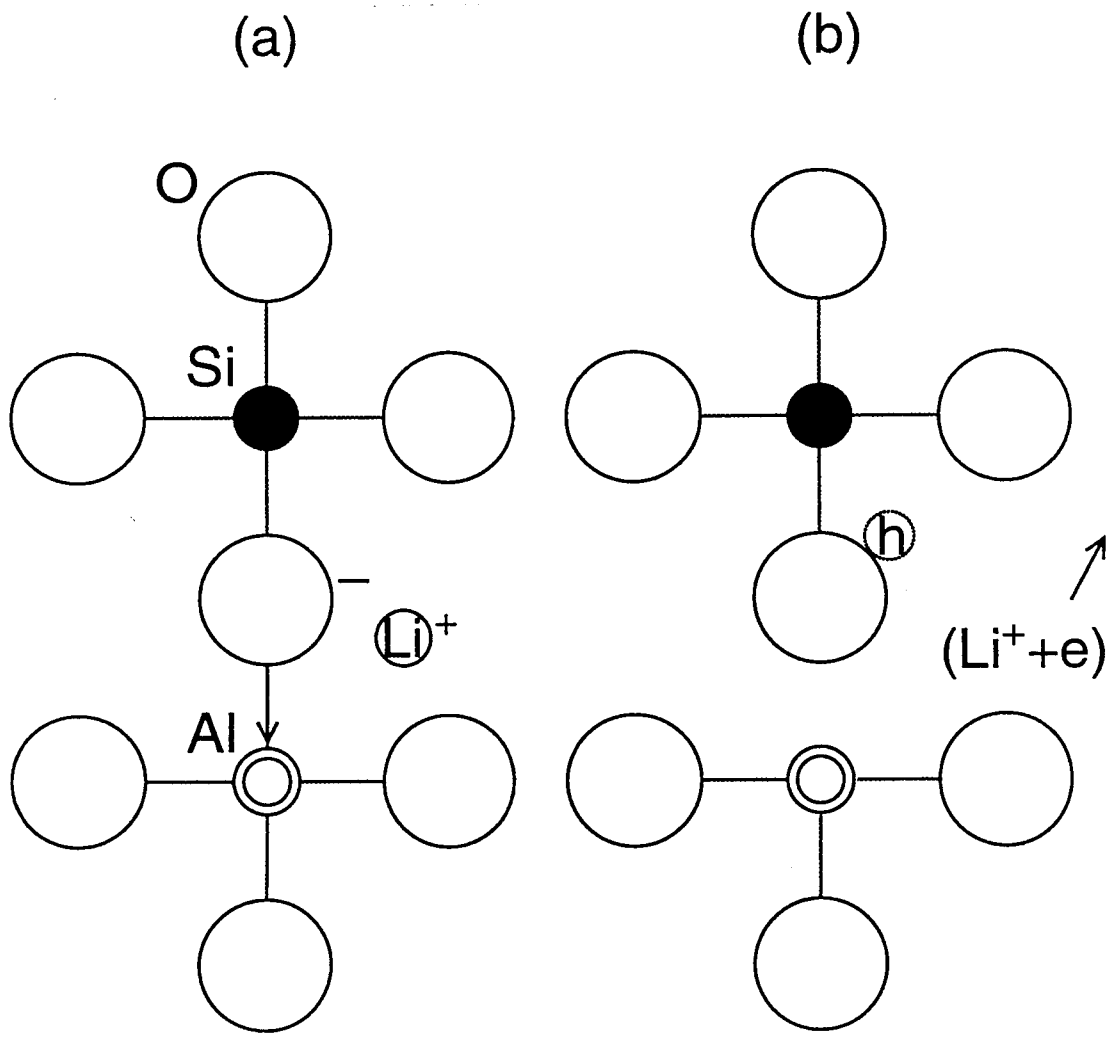

Fig. 3-9 Chemical bonding structure of coesite including an aluminum impurity center. (a) before irradiation and (b) after irradiation. The lines represent covalent bonds containing one electron from each atom, and the arrow represents a dative bond in which both electrons are provided by the atom at the tail of the arrow.

The aluminum atom will relax in the opposite direction to the hole and make an AlO_3 pyramid or triangle in coesite. Then the dative electron from the oxygen atom will not be necessary to make the AlO_4 tetrahedron as shown in Fig. 3-10 (a). This is contrary to the case of $[AlO_4]^0$ in quartz shown in Fig. 3-10 (b) where the dative bond exists to maintain the crystal structure of quartz which has no unit made of SiO_4 tetrahedra as like in coesite.

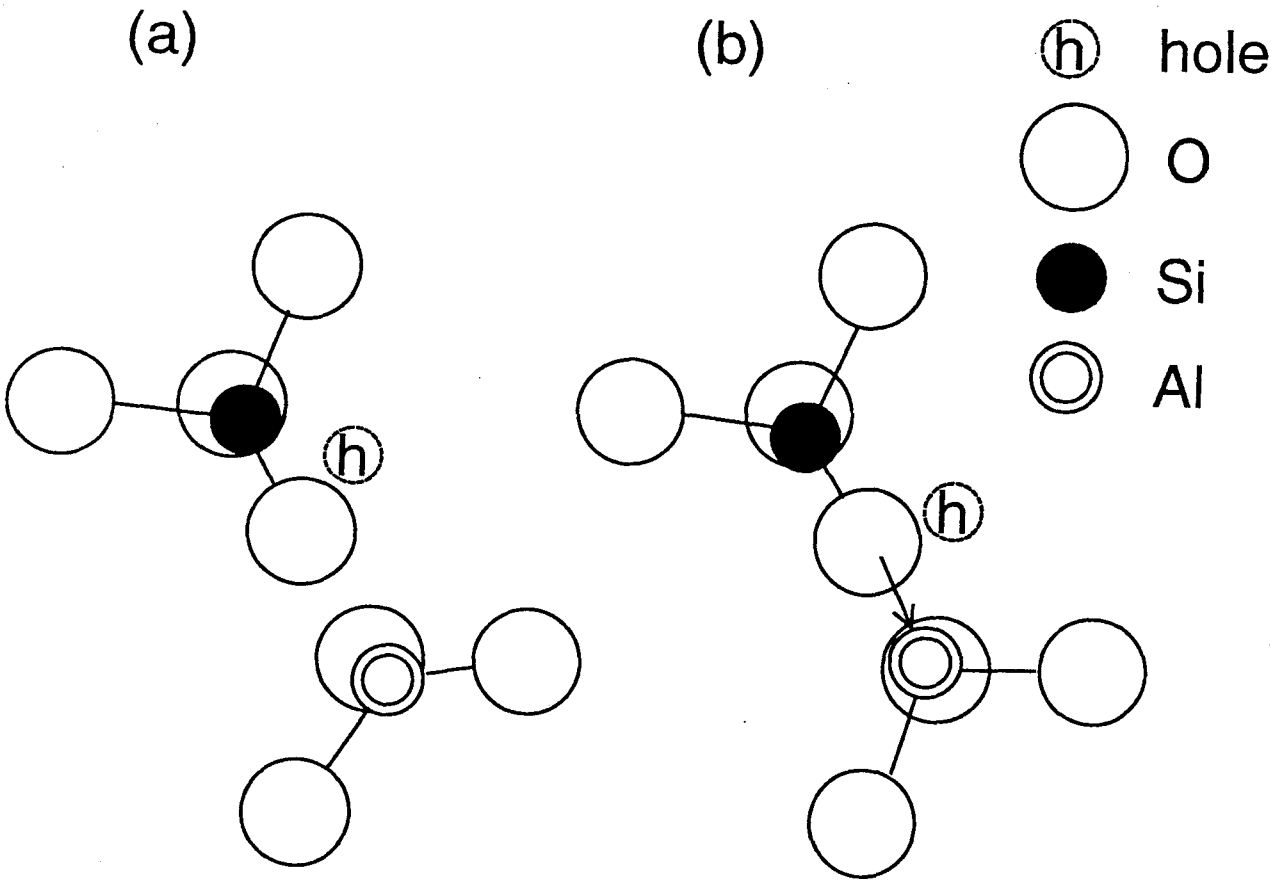

Fig. 3-10 (a) A model of oxygen hole center in coesite. The hole may be shared by an oxygen atom neighboring the aluminum impurity center, then the aluminum atom has only three bonds. The aluminum atom might move from the original point by crystal relaxation. The hole may not interact with the aluminum nucleus. (b) An aluminum associated oxygen hole center $[AlO_4]^0$ in quartz. The hole is trapped at one of oxygens nearby an aluminum atom substituted at silicon site under 77 K. The dative bond is necessary to maintain the crystal structure of quartz.

If the lattice relaxation of the aluminum atom occurs in coesite, the grand-state wave function of the hole may contain no admixture of a wave function overlapping the aluminum nucleus. There might also be an oxygen hole center with the same *g*-factor having no relation to the aluminum impurity center. Oxygen hole centers including $[AlO_4]^0$ in quartz have similar *g*-factors arisen from similar defect structures as shown in Table 3-3.

It is possible that the defect is the OHC in amorphous SiO_2 included in the crystals of coesite or covering coesite. However the defect in coesite has not been produced by irradiation at room temperature, and disappears at room temperature, though oxygen hole centers in amorphous SiO_2 are stable up to about 300 °C.

The E' centers have been easily produced with annealing of the oxygen hole centers in coesite at room temperature. This is similar to the case in quartz and may also be presumably because some oxygen atoms leave two electrons in their own vacancies and become interstitial atoms in coesite lattice on irradiation at 77 K. The holes at oxygen atoms nearby aluminum atoms may be released on heating to be trapped at the neutral oxygen vacancies with two electrons to form the E' centers at room temperature.

The signal of $g_{\parallel} = 2.0033$ and $g_{\perp} = 2.0085$ may be a hole type one, considering the *g*-factor larger than the free electron value $g_e = 2.0023$. Similar signals of O^- and O^{2-} radicals at $g_{\parallel} = 2.003$ and $g_{\perp} = 2.009$ are observed in some minerals and in solid CO_2 and H_2O irradiated at 77 K, as shown in Table 3-3, indicating the possibility of a different type oxygen hole center, O^- or O_2^- in coesite.

3-4.Summary of Oxygen Hole Centers Associated with Aluminum Impurities in Quartz, Stishovite and Coesite

Oxygen hole centers associated with aluminum impurities substituted for silicons are dealt in this chapter. A hole at an oxygen atom bonding an aluminum impurity atom interacts with nuclear spin, I = 5/2, of the aluminum and shows sextet ESR lines of an anisotropic g-factor of orthorhombic symmetry, g_x = 2.0020, g_y = 2.0085 and g_z = 2.0602, and hyperfine sextets (I = 5/2) with A_x = 0.5 mT, A_y = 0.6 mT and A_z = 0.6 mT at low temperature in quartz.

The prominent signal detected at 77 K in stishovite γ-rayed at 77 K has an anisotropic g-factor of orthorhombic symmetry, g_x = 2.0155, g_y = 2.0094 and g_z = 2.0033, and hyperfine sextets (I = 5/2) with A_x = 0.394 mT, A_y = 0.372 mT and A_z = 0.436 mT. The g-factor and the hyperfine structure indicate that this signal is due to a two-center type hole center, O_2^{3-}, associated with an aluminum atom substituted at the silicon site in stishovite.

Two types of oxygen hole centers were observed in coesite synthesized from natural quartz including aluminum impurities after γ-ray irradiation at 77 K. The prominent signal detected at 77 K has anisotropic g-factor of orthorhombic symmetry, g_1 = 2.0015, g_2 = 2.0055 and g_3 = 2.065 and ascribed to an oxygen hole center like NBOHC in quartz. The observed signal at $g_{\parallel}$ = 2.0033 and $g_{\perp}$ = 2.0085 might be related with an O^- or O_2^- type hole center. These centers have no hyperfine structures due to aluminum nuclei (I = 5/2). Gamma-ray irradiation will not only produce a hole at an oxygen atom of an [AlO_4] tetrahedron but also let the aluminum impurity atom relax to the center of the other three oxygens of the tetrahedron in coesite.

The oxygen hole centers associated with aluminum impurities in stishovite and coesite are produced by γ-ray irradiation at 77 K, and annealed easily at room temperature. Detrapped holes will go to oxygen vacancies with two electrons and form E' centers in both minerals. Similar process occurs in heating experiment at 200 to 300 °C on $[AlO_4]^0$ and E'_1 centers in quartz.

References

3-1 M. Stapelbroek, D. L. Griscom, E. J. Friebele and G. H. Jr. Sigel: J. Non-crystal. Solids **32** (1979) 313.

3-2 E. J. Friebele, D. L. Griscom and M. Stapelbroek: Phys. Rev. Lett. **42** (1981) 1346.

3-3 J. H. E. Griffith, J. Owen and I. M. Ward: Nature **173** (1954) 439.

3-4 M. C. M. O'Brien: Proc. Roy. Soc. (London) **A 231** (1955) 404.

3-5 R. H. D. Nuttal and J. A. Weil: Can. J. Phys. **59** (1981) 1696.

3-6 A. L. Taylar and G. W. Farnell: Can. J. Phys. **42** (1964) 595.

3-7 R. Schnadt and A. Räuber: Solid State Commun. **9** (1971) 159.

3-8 R. Schnad and J. Schneider: Phys. Condens. Mater. **11** (1970) 19.

3-9 K. B. Hitt and J. J. Martin: J. Appl. Phys. **54** (1983) 5030.

3-10 J. A. Weil: Phys. Chem. Mineral. **10** (1984) 149.

3-11 R. H. D. Nuttal and J. A. Weil: Can. J. Phys. **59** (1981) 1709.

3-12 R. H. D. Nuttal and J. A. Weil: Can. J. Phys. **59** (1981) 1886.

3-13 L. V. Bershov, V. O. Martirosyan, A. S. Marfunin and A. V. Speranskii: Phys. Status. Solid **(b) 44** (1971) 505.

3-14 J. H. Griffith, J. Owen and I. M. Ward: Bristol Conference, London, 1955. Phys. Soc. London, Engl. (1955) 88.

3-15 P. R. Barker: J. Phys. **C 8** (1975) 142.

3-16 J. H. Jr. Mackey, J. W. Boss and D. E. Wood: J. Mag. Res. **3** (1970) 44.

3-17 R. E. Watson and A. J. Freeman: Phys. Rev. **123** (1961) 521.

3-18 B. Speit and G. Lehmann: Phys. Chem. Minerals. **8** (1982) 77.

3-19 J. P. E. Johnes, B. R. Angel and P. L. Hall: Cray Miner. **10** (1974) 257.

3-20 M. Hirai, M. Ikeya, Y. Tsukamoto and C. Yamanaka: J. Appl. Phys. Lett. **33** (1994) 1453.

3-21 A. R. P. L. Albuquerque and S. Isotani: Phys. Soc. Jpn. **51** (1982) 1111.

3-22 S. J. Wyard, R. C. Smith and F. J. Adrian: J. Chem. Phys. **49** (1968) 2780.

4. Atomic Hydrogen Centers

4-1.Introduction of Atomic Hydrogen in Quartz

Irradiation at low temperature produces atomic hydrogens, H^0, in quartz exhibiting sharp doublet hyperfine (hf) lines due to $I = 1/2$ of proton with hf constant $A \approx 50$ mT [4-1-3]. The exact sources of the H^0 are still not clear, but one possible candidate may be the $[AlO_4/H^+]^0$ centers [4-4-6]. The trapped H^0 atoms are trapped in the SiO_4 framework of quartz, as shown in Fig. 4-1. They are detrapped and disappear if the quartz is allowed to warm much above 100 K [4-3]. Recombination of an H^0 with a hole center might follow the reaction, which will give luminescence. The recombination luminescence due to hydrogen migration and reaction with a hole center of O^- were studied in OH^- doped KCl [4-7]. Atomic hydrogen centers induced by γ-ray irradiation at room temperature in coesite and stishovite are described in this chapter.

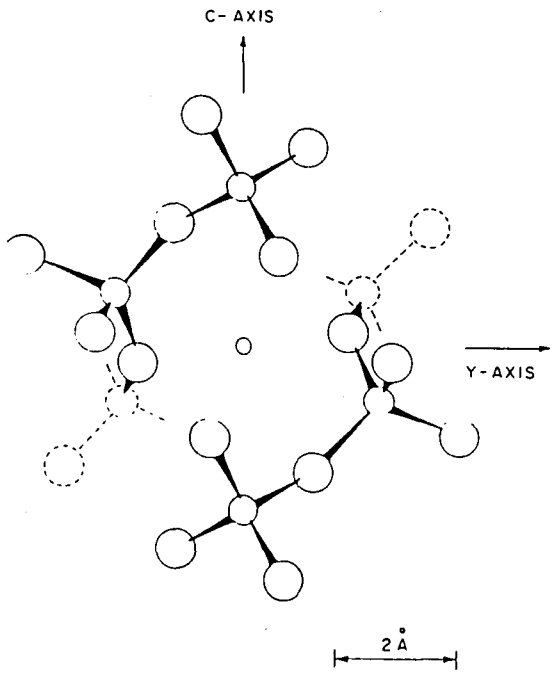

Fig. 4-1 A model view of an atomic hydrogen center in α-quartz, after [4-3]. It is seen with two-fold axis $\boldsymbol{b}_1$ at the center and normal to the plane of the figure, pointing upward. The circles in decreasing size represent oxygen, silicon and hydrogen, respectively. The center of the nearest large *c*-axis channel occurs 1.30 Å below the intersection of capping Si-Si direction with $\boldsymbol{b}_1$. The hydrogen atom is shown located at this interaction.

4-2.Atomic Hydrogen Centers in High Pressure Synthesized SiO_2 Samples

(1) Abstract

Similar TL glow curves and ESR hyperfine lines are observed in coesite and stishovite after γ-ray irradiation at room temperature. Isochronal annealing data for the sharp ESR hyperfine lines are consistent with the thermal stability parameters obtained from the large TL peak. The TL peak at about 200 °C and the sharp ESR hyperfine lines are due to the same defects; atomic hydrogen centers in high density amorphous SiO_2. The broad ESR hyperfine lines are due to atomic hydrogen centers in crystalline coesite and stishovite.

(2) Experimental and Results

(a) Thermoluminescence (TL)

Coesite and stishovite samples synthesized from high purity SiO_2 glass used for ESR sample tube were irradiated by γ-ray from a ^{60}Co-source at 3 kGy at a dose rate of 100 Gy/hour at room temperature.

TL curves were observed with a home-made TL apparatus from room temperature to 400 °C at the heating rate of 5 °C/s with no optical filter. Observed TL glow curves of the γ-rayed coesite and stishovite are shown in Fig. 4-2 (a) and (b), respectively. A large peak at 205 °C is observed in both minerals. Activation energies and pre-exponential frequency factors of the defects were obtained using an equation for first order (monomolecular) kinetics as follows,

$$I(T) = n_0 s \exp(-E/kT) \exp\left[-(s/\beta)\int_{T_0}^{T} \exp(-E/kT)dT\right] \quad (4\text{-}1),$$

where I is integration of TL peak, T, absolute temperature, n_0 is number of the radicals at $t = t_0$, starting time, s, pre-exponential frequency factor, E, activation energy, k, Boltzman factor and β, heating rate [4-9]. The calculated curves obtained by the least square best fitting to equation (3-1) are given by curves in broken lines.

Pre-exponential frequency factors, s, were calculated to be 1.3±0.1 x 10^{12} Hz for all TL peaks. The first peak temperature is 205 °C with an activation energy, E_I = 1.20±0.01 eV. Small second peaks at 240 °C and at 255 °C are obtained by subtraction of the large peaks simulated using theoretical TL curves. Activation energies, E_{II} = 1.27±0.01 eV and

1.32±0.01 eV were obtained for the small peaks of coesite and stishovite, respectively.

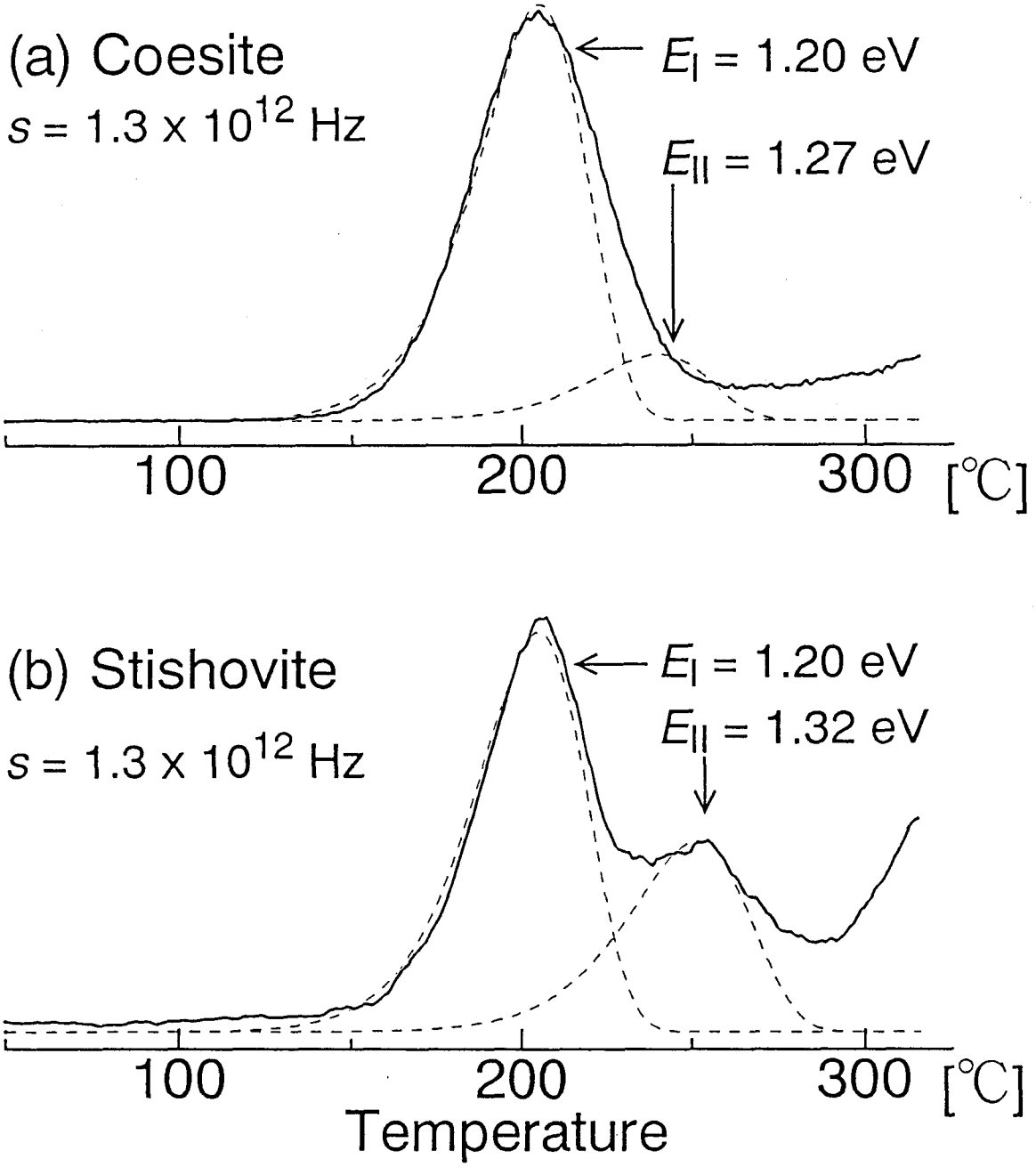

Fig. 4-2 TL curves for (a) coesite and (b) stishovite after 3 kGy γ-ray irradiation. The same pre-exponential factor of 1.3±0.1 x 10^{12} Hz and activation energy of 1.20±0.01 eV were obtained by simulation for the first TL peak at 205 °C in the both minerals using first order kinetic equation. Small TL peaks were obtained by subtraction of simulated the first peak from the observed TL curves.

Table 4-1. TL parameters in coesite and stishovite

Mineral	ν_0 [Hz]	E_I [eV]	E_{II} [eV]	Remarks
coesite	1.3±0.1 x 10^{12}	1.20±0.01	1.27±0.01	I and II are due to H^0 in densified amorphous
stishovite	1.3±0.1 x 10^{12}	1.20±0.01	1.32±0.01	and in crystalline phases, respectively.

(b) ESR and Thermal Stability of the Signals

ESR spectra for γ-rayed synthetic coesite and stishovite are shown in Fig. 2 (a) and (b), respectively. The similar ESR spectrum observed for γ-rayed natural stishovite from Arizona meteor impact crater by Devine and Hübner [4-8], as shown in (c). ESR parameters of g = 2.002, and $A \approx 50$ mT are confirmed by calculation of resonance magnetic field using the following equation including second order perturbation;

$$H(m_I,\theta) = \frac{h\nu_0}{g\beta} + \left(\frac{K}{g\beta}\right)m_I - \frac{A_\perp^2}{4g\beta h\nu_0}\left(\frac{A_{//}^2+K^2}{K^2}\right)\left[I(I+1)-m_I^2\right]$$
$$-\frac{1}{2g\beta h\nu_0}\left(\frac{A_{//}^2-A_\perp^2}{K}\right)\left(\frac{g_{//}g_\perp}{g^2}\right)^2 \sin^2\theta\cos^2\theta m_I^2 \qquad (4\text{-}2),$$

with $g^2 = g_{//}^2\cos^2\theta + g_\perp^2\sin^2\theta$ and $K^2 = (A_{//}^2 g_{//}^2\cos^2\theta + A_\perp^2 g_\perp^2\sin^2\theta)/g^2$,

where θ is the angle between the applied magnetic field and the principal axis of the defect or impurity and ν_0 is the applied microwave frequency, on an axial symmetric assumption, $g_\perp = \sqrt{(g_1^2\sin^2\phi + g_2^2\cos^2\phi)}$ and $A_\perp^2 g_\perp^2 = (A_1^2 g_1^2\sin^2\phi + A_2^2 g_2^2\cos^2\phi)$. All of g-factors are 2.002±0.0005 and hyperfine constants are calculated as $A_\perp$ = 46±0.2 mT and $A_{||}$ = 59±0.2 mT for sharp lines, and $A_\perp$ = 50±0.2 mT and $A_{||}$ = 53±0.2 mT for broad lines. Obtained parameters for synthetic coesite and stishovite are very similar to those for natural stishovite, g = 2.002 $A_\perp$ = 45.7 mT and $A_{||}$ = 59.0 mT for sharp lines, and $A_\perp$ = 50.3 mT and $A_{||}$ = 52.5 mT, except for the line width [4-8]. These spectra with sharp and broad lines are designated as H_I and H_{II}, respectively.

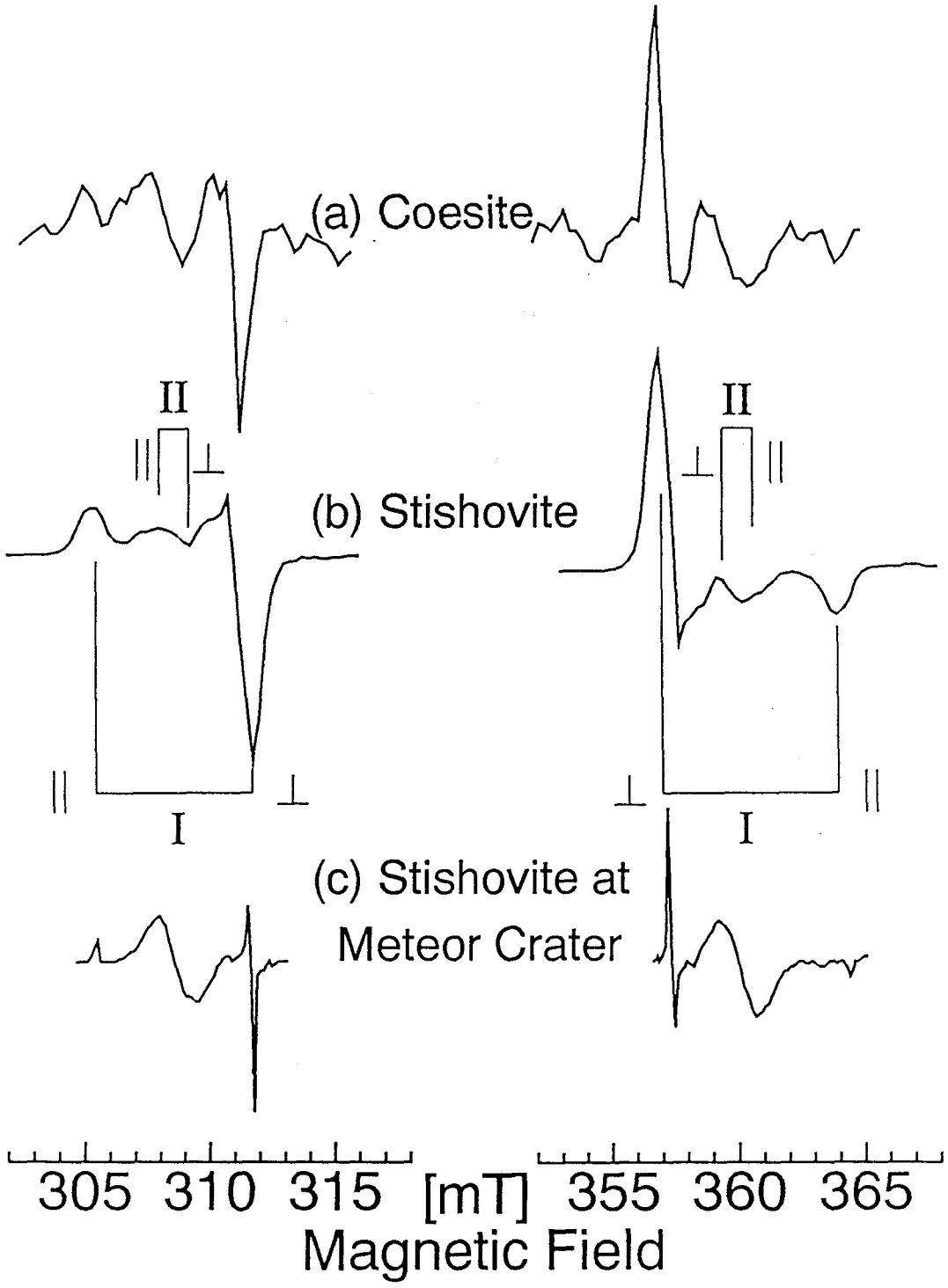

Fig. 4-3 ESR spectra of (a) Coesite, (b) Stishovite and (c) Stishovite at the Arizona meteor crater. The spectrum in (c) is modified the range of the magnetic field from that by Devine and Hübner [4-8].

Microwave power dependence of the H_I intensities in coesite and in stishovite are shown in Fig. 4-4. The H_I intensities reach maximum at nearly same power of 5 mW and 3 mW for coesite and stishovite, respectively. The dependence for the H_{II} is difficult to plot.

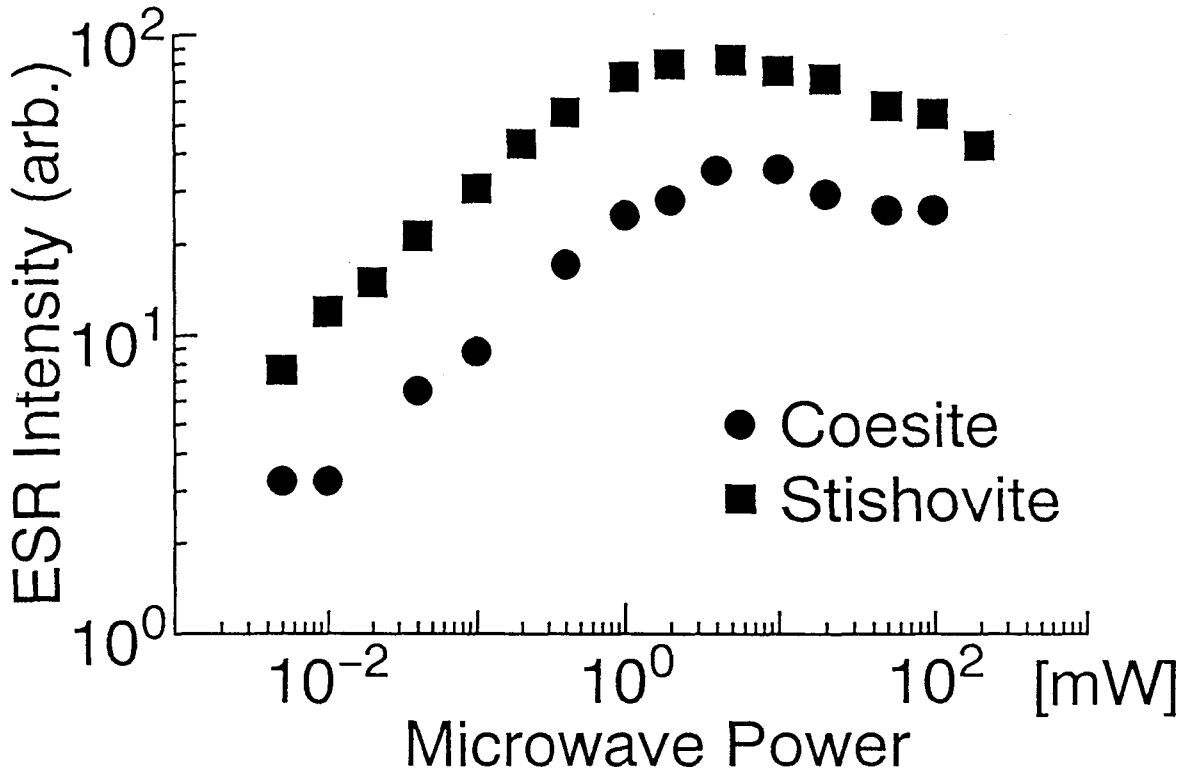

Fig. 4-4 Microwave power dependence of the hyperfine doublet lines, H_I, observed in γ-rayed coesite and stishovite and ascribed to H^0 in high density amorphous SiO_2.

Isochronal annealing data for the H_I for both minerals and the H_{II} in stishovite are plotted in Fig. 4-5. The curves were simulated using a function of $I_i = I_{i-1}\exp(-t_a/\tau)$, where $t_a = 900$ s with the life time $\tau = (1/s)\exp(E/kT)$, giving the s = 1.3 x 10^{12} Hz, the E_I = 1.20 eV for the H_I and E_{II} = 1.32 eV for the H_{II} for the TL of stishovite [4-10].

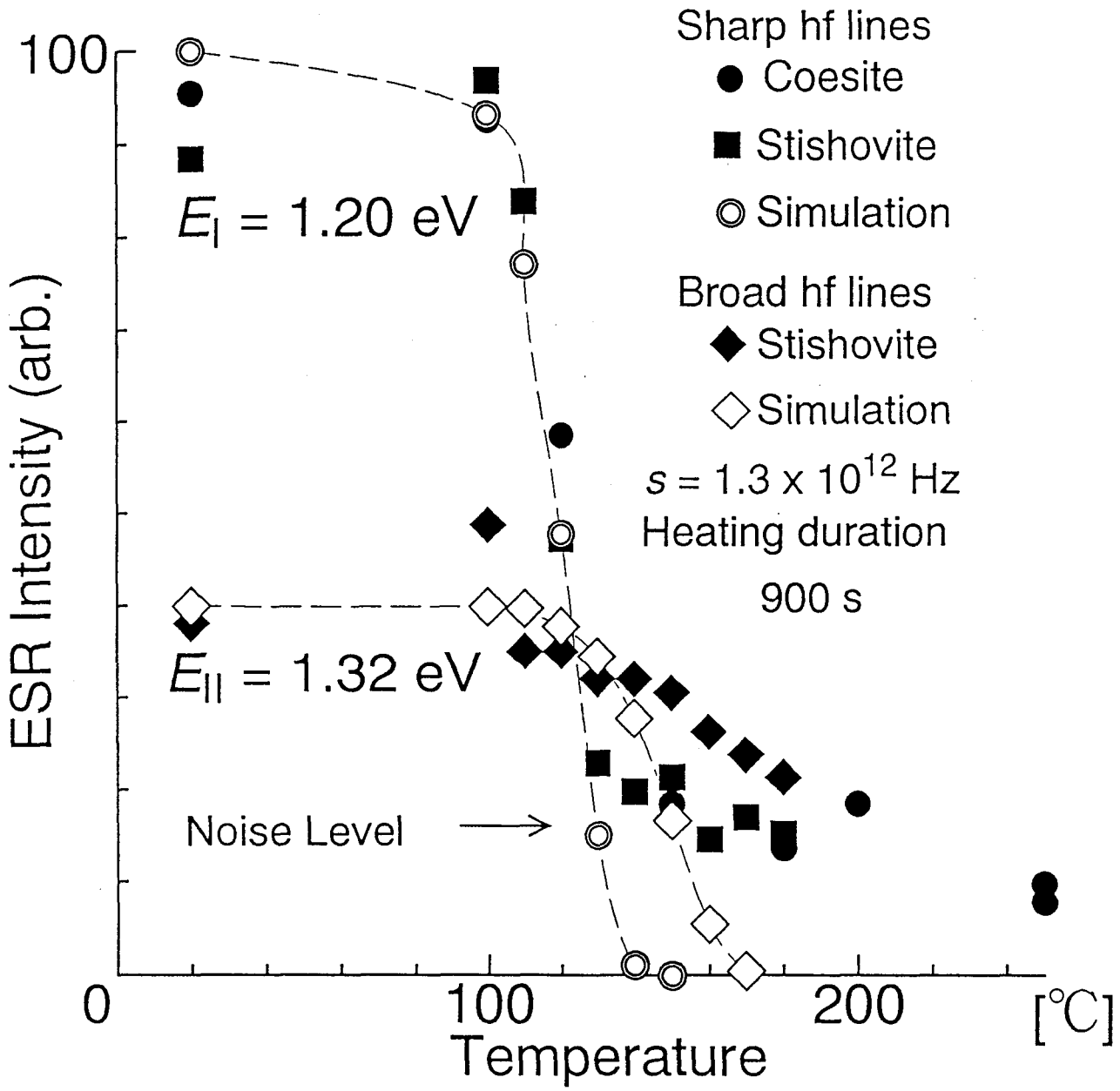

Fig. 4-5 Isochronal annealing curves for the hyperfine lines observed in γ-rayed coesite and stishovite. Simulation using $I_i = I_{i-1}\exp(-t_a/\tau)$, where t_a = 900 s with the life time $\tau = (1/s)\exp(E/kT)$ [4-10], s = 1.3 x 10^{12} Hz and E_I = 1.20 eV resulted in good agreement for the data of lines sharp lines. Similar simulation with E_{II} = 1.32 eV for the broad lines did not agree observed data due to poor S/N ratio.

The microwave power dependence and the isochronal annealing for the sharp hf lines in coesite and in stishovite are very similar. Simulation for the annealing data resulted in good agreement for the intensities of the H_I but in disagreement for the H_{II}. Obtained parameters for the centers are tabulated in Table 4-2 with those of atomic hydrogen and E' centers in quartz and in stishovite.

Table 4-2. ESR Parameters for atomic hydrogens, H^0, in coesite, stishovite and quartz together with E' centers in quartz and stishovite.

Signal		Site	g-factor	$A_\perp$/mT	$A_\parallel$/mT	Comment	Ref.
H^0 coesite	H_I	am	2.0020(5)	46.0(2)	59.0(2)	E_I = 1.20(1) eV	present
	H_{II}	cr	2.0020(5)	50.0(2)	53.0(2)	E_{II} = 1.27(1) eV	work
stishovite	H_I	am	2.0020(5)	46.0(2)	59.0(2)	E_I = 1.20(1) eV	
	H_{II}	cr	2.0020(5)	50.0(2)	53.0(2)	E_{II} = 1.32(1) eV	
stishovite	H_I	am	2.002	45.7	59.0	Previously identified as E'	4-8
at crater	H_{II}	cr	2.002	50.3	52.5	centers in cr (H_I) and am (H_{II}).	
			g_1 (A_1/mT)	g_2 (A_2/mT)	g_3 (A_3/mT)		
quartz		cr	2.002179 (51.6981)	2.002143 (51.9235)	2.002094 (51.7832)	Data at 40 K. H^0 disappears above 100 K.	4-3
E'_1 center in quartz		cr	2.00179 (45.3)	2.00053 (39.1)	2.00030 (39.1)	split by I = 1/2 of ^{29}Si	4-11
E' center in stishovite		cr	2.0055 (1.2)	2.0044 (1.2)	2.0023 (8.5)	split by I = 1/2 of ^{29}Si	Chapt. 2

cr: in crystalline part, am: in amorphous part

(3) Discussion

The TL spectra are very similar in coesite and stishovite, as shown in Fig. 1 (a) and (b). The H_I has the same thermal stability given by s and E_I of the large TL signals for both minerals, as shown in Fig. 4. The origin of the TL peaks will be related with the same defect.

Devine and Hübner ascribed the ESR doublets, H_I and H_{II}, shown in Fig. 2 to hyperfine structures of E' centers due to a nuclear spin I = 1/2 of ^{29}Si (natural abundance of 4.7 %) in stishovite and to densified amorphous SiO_2, respectively [4-8]. However, the same doublets are detected also in coesite, as shown in Fig. 2. Furthermore, we found other hyperfine lines of E' center due to the nuclear spin I = 1/2 of ^{29}Si with much smaller splitting constants of $A_\parallel$ = 8.5 mT and $A_\perp$ = 1.2 mT in stishovite separately, as shown in Chapt. 2.

Atomic hydrogen centers, H^0, are produced in quartz by irradiation at low temperature and annealed above 100 K. (Total hydrogen content in quartz crystals seems to be in the range $\leq 10^4$ ppm H/Si [4-12].) Gamma-ray irradiation at room temperature gives H^0 in some minerals like hydroxyapatite soon after irradiation [4-10]. The hyperfine constants of H^0 is generally about 50 mT. The ESR lines are almost isotropic because the unpaired electrons exist in 1s orbital of hydrogens. Small anisotropic perturbation of 0.1 mT is produced by surrounding atoms in quartz [4-1-3].

We concluded that the sharp signals with the same large A values (H_I) in both coesite and stishovite are due to H^0 in a densified amorphous state of SiO_2 and that the broad signals with different A values (H_{II}) in crystalline coesite and stishovite are due to H^0 in the crystalline phases. Isotropic hyperfine constants observed in coesite and stishovite are calculated as $A_{iso} = (A_{||}+2A_{\perp})/3$ to be 50.1 mT for the H_I and 51.0 mT for the H_{II}, respectively. These are very similar to the A-value of 50.8 mT for H^0.

Anisotropic hyperfine constants observed in coesite and stishovite are calculated as $A_{ani} = (A_{||}-A_{\perp})/3$ to be 4.4 mT for the H_I and 0.7 mT for the H_{II}, respectively. The anisotropic part for the H_I is very larger than that of 0.1 mT in quartz, presumably because local structure bonding characteristic for high density amorphous SiO_2 produces larger influence on a wave function of the unpaired electron of H^0 than that in quartz.

I suggest a model for the local structure of the H^0 trapping site in deisified amorphous SiO_2, as shown in Fig. 4- 6. A hydrogen atom trapped at the center of the structure will feel strong axial crystal field along the z axis. It is necessary to establish detailed models on the hydrogen sites and the hydrogen wave function in coesite and stishovite lattice.

The high density packing of atoms may cause the higher stability of the atomic hydrogens in crystalline high pressure phases. Activation energies over 1.20 eV for hydrogen dissociation and diffusion are very large: the activation energy for hydrogen diffusion was calculated to be about 1 eV in other silicates and in polysilicon CVD film [4-13-15]. Hydrogens trapped in crystalline phases will be more stable than those in densified amorphous SiO_2, as shown in Fig. 4-5.

The first TL peak may be due to recombination of the H^0 centers with undefined hole centers. Almost all of the hole centers may associate with H^0 for coesite, while some of them still remain in stishovite. The second TL peak, very weak for coesite and relatively

comparable as the first peak in stishovite may be due to recombination of the holes with other electron centers.

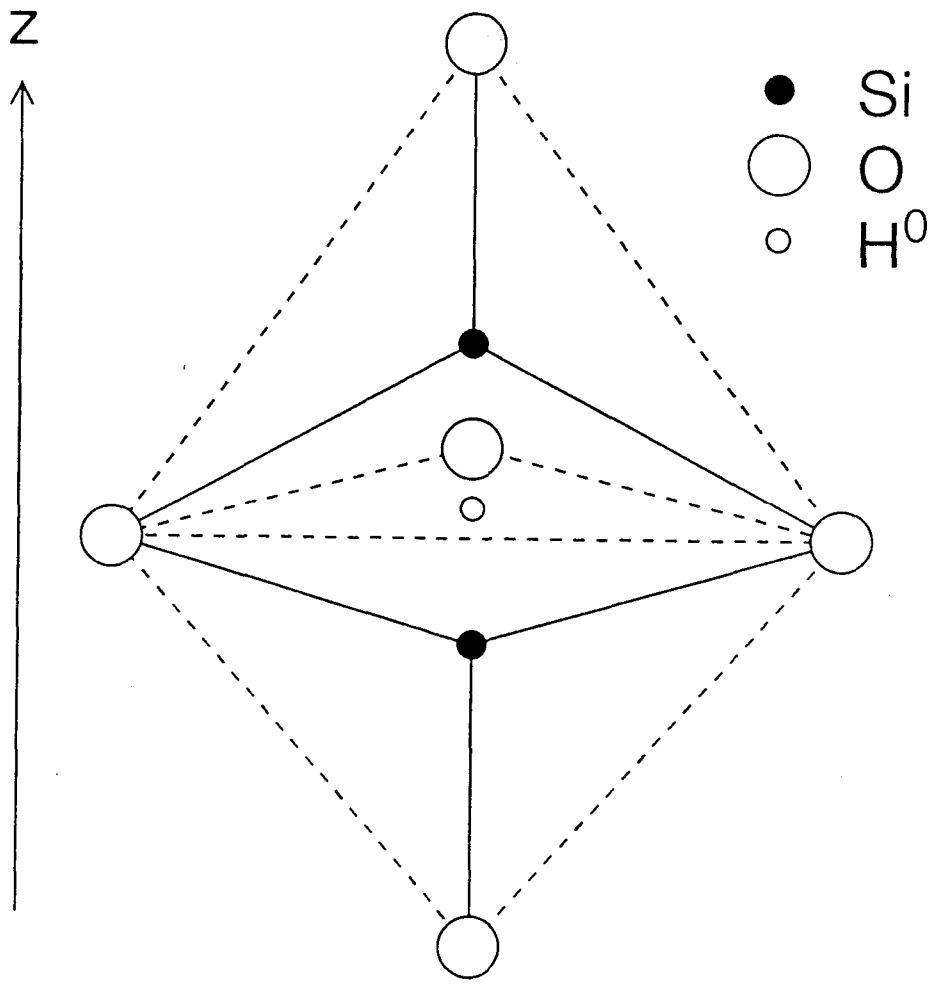

Fig. 4-6 A model for the local structure of the H^0 trapping site in deisified amorphous SiO_2. Two SiO_4 tetrahedra share an O_3 triangle. A radiation-induced hydrogen atom is trapped at the center of the O_3 triangle, and feel strong axial crystal field along the z axis.

4-3.Summary of Atomic Hydrogens in Densified Amorphous SiO_2, Coesite, Stishovite and Quartz

Thermoluminescence (TL) of coesite and stishovite samples has been measured after γ-ray irradiation at room temperature from ^{60}Co. Analysis of the first TL peaks at 205 °C indicates an activation energy, E_I = 1.20 eV and a pre-exponential frequency factor, s = 1.3 x 10^{12} Hz; the second peaks are at 240 °C and at 255 °C giving E_{II} = 1.27 eV and 1.32 eV for coesite and stishovite, respectively.

ESR lines at g = 2.002 with $A_\perp$ = 46 mT and $A_\parallel$ = 59 mT show the same isochronal annealing behavior with the same parameters of thermal stability as those of the first TL peaks. Other ESR lines at g = 2.002 with $A_\perp$ = 50 mT and $A_\parallel$ = 53 mT are stable to high temperature.

Atomic hydrogens, H^0, in densified amorphous and in crystalline parts are responsible for the ESR signals and the release of trapped H^0 leads to recombination with a hole center emitting the TL light. The atomic hydrogen centers are stable thermally even at 100 °C in the high pressure synthesized SiO_2 samples because of high density packing, though the atomic hydrogens are induced by irradiation only at low temperature and disappear above 100 K in quartz.

References

4-1 J. C. Brice: J. Mater. Sci. **15** (1980) 161.

4-2 R. A. Weeks and M. Abraham: J. Chem. Phys. **42** (1965) 68.

4-3 J. Isoya and J. A. Weil: J. Phys. Chem. Solids **44** (1983) 335.

4-4 R. H. D. Nuttal and J. A. Weil: Can. J. Phys. **59** (1981) 1709.

4-5 R. H. D. Nuttal and J. A. Weil: Can. J. Phys. **59** (1981) 1696.

4-6 L. E. Halliburton, N. Koumvakalis, M. E. Marks and J. J. Martin: J. Appl. Phys. **52** (1981) 3565.

4-7 M. Ikeya, L. O. Schwan and T. Miki: Solid State Commun. **27** (1978) 891.

4-8 R. A. B. Devine and K. Hübner: Phys. Rev. **B 40** (1989) 7281 .

4-9 S. W. S. Mckeever: Thermoluminescence of Solids, ed. R. W. Cahn, E. A. Davis and I. M. Ward (Cambridge University Press, Cambridge, 1985).

4-10 M. Ikeya: New Applications of Electron Spin Resonance (World Scientific, Singapore, 1993).

4-11 M. G. Jani, R. B. Bossoli and L. E. Halliburton: Phys. Rev. **B 27** (1983) 2285.

4-12 B. D. Perlson and J. A. Weil: J. Magn. Res. **15** (1974) 594 .

4-13 C. M.Graham: Contib. Mineral. Petrol. **76** (1981) 216.

4-14 R. Freer: Contib. Mineral. Petrol. **76** (1981) 440.

4-15 M. Ikeya and M. Yamamoto: Jpn. J. Appl. Phys. Lett. **33** (1994) 1087.

5. Summary

Irradiation induces defects in stishovite and coesite, high pressure phases of SiO_2. E' centers, oxygen hole centers associated with aluminum impurities, and atomic hydrogen centers are studied, and some models are suggested for them except for atomic hydrogens in this thesis.

All of the E' centers are produced easily by γ-ray irradiation at room temperature. Though the E' center is not produced at 77 K as like as E'_1 center in quartz, the axial type E' center in coesite is a little produced by irradiation at 77 K. Silicons surrounding the unpaired electrons in stishovite and coesite do not move so much as those in quartz, according to hyperfine structures due to nuclear spin $I = 1/2$ of ^{29}Si.

Oxygen hole centers associated with aluminum impurities are produced by γ-ray irradiation at 77 K, but little produced at room temperature. ESR lines become sextet in stishovite due to nuclear spin, $I = 5/2$, of the aluminum nucleus. However no hyperfine split occurs in ESR lines in coesite, though the starting materials for synthesis of both minerals are same natural quartz including aluminum impurities.

The models of the defects are suggested on crystal structures of the both minerals. The hole is trapped by two oxygen atoms forming O_2^{3-}-Al^{3+} molecule ion in stishovite. The aluminum impurity atom will move to the opposite of the hole trapping oxygen atom, therefore hyperfine interaction with the aluminum nucleus will disappear in coesite.

Both of the oxygen hole centers related to aluminum impurities are annealed at room temperature, at the same time the E' centers are formed largely. The hole will be released by heating and move to oxygen vacancies trapping two electrons forming the E' centers. This process is very similar to $[AlO_4]^0$ decrease and E'_1 increase combination process in quartz at 200 to 300 °C.

Atomic hydrogen centers are produced by irradiation at room temperature in samples of the both minerals, though the atomic hydrogen disappears above 100 K in quartz. Sharp and broad ESR lines are ascribed to the atomic hydrogens in amorphous and crystalline phase, respectively. An isochronal annealing experiment on the ESR signals indicates same thermal stabilities of obtained by an analysis of thermoluminescence curves.

Sharp hyperfine lines have much axial symmetry, though the wave function of a hydrogen atom is 1*s* orbital. The large anisotropy will be due to a characteristic structure

of the hydrogen trapping local site of densified amorphous silica made under high pressure condition. Some anisotropic symmetry are found in atomic hydrogen centers in hydroxyapatite produced by irradiation at room temperature. The atomic hydrogens in high pressure synthesized samples are detrapped by heating and will combine some hole centers emitting light.

A little study has been performed on the radiation induced defects in high pressure phases of SiO_2 in this thesis, as summarized below in Table. 5. I hope this work make some contribution in physics of radiation induced defects and in dating study on meteor impact craters of terrestrial planets someday.

Table 5. ESR parameters of radiation induced defects in stishovite and coesite with those of related defects in quartz.

Defect	Mineral	g_x (A_x mT)	g_y (A_y mT)	g_z (A_z mT)	Comment	Ref.
E' center	stishovite	2.0055 (1.2)	2.0044 (1.2)	2.0023 (8.5)	^{29}Si A_{shf} = 1.2 mT	Chapt. 2
	coesite	$g_\perp$ = 2.0027	$g_\parallel$ = 1.9993	($A_\perp$=1.2mT, $A_\parallel$ = 8.1 mT?)	axial	Chapt. 2
		g_1 = 2.0004	g_2 = 1.9993	g_3 = 2.0047	orthorhombic	Chapt. 2
	quartz E'_1	2.00179 (45.3)	2.00053 (39.1)	2.00030 (39.1)	^{29}Si	2-4
	E'_2	$g_\parallel$ =2.0022	$g_\perp$ = 2.0006	(41.2)	^{29}Si	2-14
OHC	stishovite		2.0095		NBOHC ?	Chapt. 2
	coesite	2.0015	2.0055	2.065	Al related ?	Chapt. 3
		$g_\parallel$ = 2.033	$g_\perp$= 2.0085		O^- or O^{2-}	Chapt. 3
	quartz and	2.0014	2.0074	2.067 (av.)	peroxy	3-1
	silica	2.0010	2.0095	2.078 (av.)	NBOHC	3-1
Al hole	stishovite	2.0155(0.4)	2.0094(0.4)	2.0033(0.4)	77K O_2^{3-}-Al^{3+}	Chapt. 3
center	quartz	2.0020(0.5)	2.0085(0.6)	2.0602(0.6)	35K $[AlO_4]^0$	3-5
H^0 center	Stishovite	g = 2.0020	$A_\perp$ = 46.0	$A_\parallel$ = 59.0	am sharp	Chapt. 4
	and coesite	g = 2.0020	$A_\perp$ = 50.0	$A_\parallel$ = 53.0	cr broad	Chapt. 4
	quartz	2.002179 (51.6981)	2.002143 (51.9235)	2.002094 (51.7832)	cr disappears above 100 K.	4-3

cr: in crystalline part, am: in amorphous part.

Followings are my works done in graduate school but not much related with the present theses work on physics of lattice defects. Reprints are duplicated as Appendix.

Appendix A Calculation of Dose-rate Data for ESR and TL Dating

Confirmation and Re-calculation of Dose-rate Data for TL and ESR Dating

[1]K. Ogoh, [2]S. Ikeda, [1]M. Ikeya
[1]Department of Earth and Space Science, Faculty of Science,
Osaka University
Toyonaka, Osaka 560, Japan

[2]Department of Physics, Faculty of Science,
Kwansei Gakuin University
Nishinomiya, Hyogo 662, Japan

Abstract

The annual dose data for TL and ESR dating have been given by Bell (1977, 1979), Carriveau and Troka (1978), Aitken (1983), and Nambi Aitken (1986). Recently, Liritzis and Kokkoris (1992) provided useful lists of radiation energies and revised dose-rate data somewhat larger than the previous work. Confirmation and re-calculation were performed on their data and supplemented data of ^{208}Tl missing in their table. The result of the present work almost agrees with that of Nambi and Aitken (1986).

The TL and ESR dating methods require not only in situ radiation energy measurements, but also estimation of annual dose from radioactive isotope concentration. Liritzis and Kokkoris (1992) provided convenient lists of radiation energies of α, β and γ particles released from ^{238}U, ^{235}U, ^{232}Th, ^{40}K, ^{87}Rb and their daughter nuclides. We have followed their calculation and arrived at different results. In the present work, the annual dose data are modified by re-calculation on radiation energies listed in their table.

Used data of half-life, energy and fraction are those written in their table1 (Liritzis and Kokkoris 1992). Used parameters are written below.

$$1[\text{eV}] = 1.6021 \times 10^{-19}[\text{J}] \qquad [1]$$

$$1[\text{mol}] = 6.022045 \times 10^{23}[\text{piece}] \qquad [2]$$

The annual dose is calculated with the equation as,

$$D\,[\text{mGy/y}] = 1.6021 \times 10^{-10}\,[\text{mGy/MeV}] \times \lambda\,[1/\text{y}] \times N \times E[\text{MeV}]. \qquad [3]$$

$$\lambda\,[1/\text{yr}] = \log_e 2 \,/\, \tau = 0.693147/\,\tau, \quad [4]$$

where, λ : decay constant, τ : half life and N : number of atoms of the nuclei. The data of radiation energies of ^{238}U, ^{235}U, ^{232}Th, ^{40}K, ^{87}Rb and their daughter products are listed in Table 1, 2, 3 and 4. The energy of conversion

electron is included in β ray. The annual dose data are estimated for 1ppm ^{232}Th, ^{238}U, 7.11 x 10^{-3} ppm ^{235}U (considering its abundance ratio of 0.72%), 1% K_2O and Rb_2O in 1kg matrix. The annual dose for calculation of radioactive equilibrium and disequilibrium are listed in Table 5. The recent calculated annual dose data for the isotopes are compared with those of previous works in Table 6.

The differences between the present work and the calculation by Liritzis and Kokkoris (1992) may be resulted from points shown below.

1. They did not show Tl-81-208 in their table 1(c) for ^{232}Th series.
2. For ^{210}Tl, they may have not multiplied the branching ratio.
3. For ^{235}U, they might divide the mass of 1ppm U by 235, not by 238.0289 (: averaged atomic weight of U), to obtain the *N* of ^{235}U. (*N* : number of atoms of ^{235}U)
4. Other differences are found as indicated in each table.

Table. 1 Radiation energy of Th-90-232 series

			Energy[MeV] (Fraction [%])		
	decay	half life	α	β	γ
Th-90-232	α	14.05 x10^9[y]	4.010 (77)	0.01043	0.0013
			3.952 (23)		
Ra-88-228	β	5.75[y]		0.01437	
Ac-89-228	β	6.31[h]		0.4516	0.9287
Th-90-228	α	1.9131[y]	5.396	0.01837	0.00322
Ra-88-224	α	3.66[day]	5.674	0.002115	0.00989
Rn-86-220	α	55.6[s]	6.282		0.000385
Po-84-216	α	0.15[s]	6.779		1.61x10^{-5}
Pb-82-212	β	10.64[h]		0.1702	0.148
Bi-83-212	α,β	60.55[m]	2.172	0.4669	0.1846
Po-84-212	α	0.305[μs]	5.633		
		branching ratio 64.1%			
Tl-81-208	β	3.0533[m]		0.2147	1.211
		branching ratio 35.9%			
[MeV]	total (100% Rn loss)		**35.93 (15.07)**	**1.341 (0.4969)**	**2.488 (0.9445)**
[mGy/y]	total (100% Rn loss)		**0.737 (0.309)**	**0.0275 (0.0102)**	**0.0510 (0.0194)**
Liritzis and Kokkoris	total (100% Rn loss)		0.731 (0.307)	0.0231 (0.0101)	0.0260 (0.0192)

Liritzis and Kokkoris (1992) did not show the energy and fraction data of ^{208}Tl in their table 1(c). However when they estimated the total annual dose for ^{232}Th series (shown in their table 2-5), they might calculate with the data of ^{208}Tl. For our calculation, the missing data of ^{208}Tl is supplemented by the Table of Radioactive Isotopes (1986). For their calculation, the data of ^{208}Tl are neglected in this table.

Table. 2 Radiation energy of U-92-238 series.

			Energy[MeV] (Fraction [%])		
	decay	half life	α	β	γ
U-92-238	α	4.468×10^9 [y]	4.198 (77)	0.00815	0.00136
			4.149 (23)		
Th-90-234	β	24.1 [d]		0.051 (73)	0.00935
				0.025 (19)	
Pa-91-234	β	1.17 [m]		0.825 (98)	0.0188
U-92-234	α	244500 [y]	4.773 (72)	0.011	0.00172
			4.721 (28)		
Th-90-230	α	77000 [y]	4.688 (76)	0.0127	0.00154
			4.621 (23)		
Ra-88-226	α	1600 [y]	4.785 (94.4)	0.0034	0.00674
			4.602 (5.6)		
Rn-86-222	α	3.8235 [d]	5.490 (99.9)	0.00000834	0.510 (0.00078)
Po-84-218	α,β	3.05 [m]	6.003 (100)	0.0705 (0.0002)	0.00000837
Pb-82-214	β	26.8 [m]		0.207 (48)	0.249
	branching ratio		99.9815%	0.227 (42)	
At-85-218	α	2 [s]	0.00124		
	branching ratio		0.0185%		
Bi-83-214	α,β	19.9 [m]		0.648	0.609 (46)
Tl-81-210	β	1.3 [m]		5.67E-08	0.000000114
	branching ratio		0.021%		
Po-84-214	α	0.1643 [s]	7.685		0.00008
	branching ratio		99.979%		
Pb-82-210	β	22.3 [y]		0.0321	0.00481
Bi-83-210	β	5.012 [d]		0.389	
Po-84-210	α	138.38 [d]	5.297		
[MeV]	total (100% Rn loss)		**42.81 (18.33)**	**2.270 (0.913)**	**1.752 (0.0395)**
[mGy/y]	total (100% Rn loss)		**2.691 (1.153)**	**0.143 (0.0574)**	**0.110 (0.00248)**
Liritzis and Kokkoris	total (100% Rn loss)		2.727 (1.188)	0.150 (0.0575)	0.110 (0.0019)

The data of Liritzis and Kokkoris (1992) are listed for comparison.

Dose	α		β		γ	
[mGy/y]	Present	Liritzis and Kokkoris	Present	Liritzis and Kokkoris	Present	Liritzis and Kokkoris
Pa-91-234					1.180×10^{-3}	5.869×10^{-4}
U-92-234	0.2990	0.33178	6.913×10^{-4}	7.671×10^{-4}	1.083×10^{-4}	1.201×10^{-4}
Th-90-230	0.2905	0.29303				
Rn-86-222			5.24×10^{-7}	4.40×10^{-7}		
At-85-218	7.8×10^{-5}	8.5×10^{-5}	: They might multiply the branching ratio as 0.02%.			
Bi-83-214			0.04076	0.04771		
Tl-81-210			3.57×10^{-9}	1.70×10^{-5}	7.18×10^{-9}	3.42×10^{-5}

: They did not multiply the branching ratio on β & γ rays.

Table. 3 Radiation energy of U-92-235 series.

			Energy[MeV] for abundance (0.720%)		
	decay	half life	α	β	γ
U-90-235	α	7.308 x10^8[y]	4.391	0.04025	0.1542
Th-90-231	β	25.52[h]		0.1454	0.02548
Ac-89-227	α,β	21.773[y]	0.06789	0.01398	0.0001793
Pa-91-231	α,β	32760[y]	4.954	0.0445	0.03914
Th-90-227	α	18.718[d]	5.838	0.03578	0.1057
Fr-87-223	β	21.8[m]		0.3837	0.05855
Ra-88-223	α	11.434[d]	5.650	0.06669	0.1328
Rn-86-219	α	3.96[s]	6.754	0.006019	0.05553
Po-84-215	α	1.78[ms]	7.379		0.0001755
Pb-82-211	β	36.1[m]		0.4541	0.05029
Bi-83-211	α,β	2.14[m]	6.555	0.009487	0.04651
Po-84-211	α	0.516[s]	0.02083	4.202E-07	0.00002181
		branching ratio	0.28%		
Tl-81-207	β	4.77[m]		0.4916	0.002205
		branching ratio	99.72%		
[MeV]	total (100% Rn loss)		**41.61 (20.90)**	**1.692 (0.7303)**	**0.6708 (0.516)**
[mGy/y]	total (100% Rn loss)		**0.1196 (0.0600)**	**0.00486 (0.00210)**	**0.00193 (0.00148)**
Liritzis and Kokkoris	total (100% Rn loss)		0.1218 (0.0611)	0.00496 (0.00214)	0.00198 (0.00153)

Liritzis and Kokkoris (1992) calculated annual dose of ^{235}U series for 7.25261 x 10^{-3}ppm ^{235}U in 1kg matrix. They may have considered the abundance ratio of 0.720% in natural U. However they may have used the abundance ratio as weight abundance. The meaning of abundance ratio is in the number of isotopes. The *N* should be obtained as below.

$$N = \{ M / A.W. \} \times A.R. \quad [5]$$

where *M*: mass of natural U, *N* : the number of ^{235}U atoms, *A.W.* : averaged atomic weight of natural U and *A.R.* : abundance ratio of ^{235}U. However they may have divided *M* by 235, not by 238.0289 : *A.W.*, to obtain the *N* of ^{235}U. As a result their annual dose of ^{235}U series is about 2% larger than that of the present work

Table. 4 Radiation energy of K_2O and Rb_2O

K_2O 1%	decay	half life		Energy [MeV]	
K-19-40	β	1.28 x10^9[y]	α	β	γ
[MeV]				0.5224	0.1563
[mGy/y]				0.6780	0.2029
Liritzis and Kokkoris				0.6824	0.2042

Rb_2O 1%	decay	half life		Energy [MeV]	
Rb-37-87	β	4.7 x 10^9[y]	α	β	γ
[MeV]				0.1115	
[mGy/y]				4.724	
Liritzis and Kokkoris				4.643	

K_2O1% & Rb_2O 50ppm	α	β	γ
[mGy/y]		0.7016	0.2029
Liritzis and Kokkoris		0.7057	0.2042

The used averaged atomic weight are shown below. K : 39.0983, Rb : 85.4678 and O : 15.9994. It is not clear why the results of their calculation on K_2O and Rb_2O differ from those of the present work.

Table. 5 The annual dose data for radioactive equilibrium and disequilibrium

[mGy/y]	α	β	γ
U (1ppm) (100% Rn loss)	2.792 (1.204)	0.1466 (0.05907)	0.1113 (0.003948)
^{238}U (1ppm) (100% Rn loss)	2.691 (1.153)	0.1427 (0.05738)	0.1102 (0.00248)
^{232}Th (1ppm) (100% Rn loss)	0.737 (0.309)	0.0275 (0.0102)	0.0510 (0.0194)
K_2O (1%)		0.6780	0.2029
Rb_2O (1%)		4.724	
K_2O (1%) & Rb_2O (50ppm)		0.7016	0.2029
^{238}U-^{234}Pa	0.2632	0.05568	0.001854
^{234}U	0.2990	0.00069	0.0001083
^{230}Th-^{206}Pb (100% Rn loss)	2.129 (0.5906)	0.0864 (0.00101)	0.1082 (0.000521)
^{226}Ra-^{206}Pb (100% Rn loss)	1.839 (0.300)	0.0856 (0.000214)	0.1081 (0.000424)
^{222}Rn-^{206}Pb	1.539	0.08533	0.1077
^{235}U-^{207}Pb	0.1196 (0.060)	0.00486 (0.00210)	0.00193 (0.00148)

Table. 6 The comparison of annual dose

[mGy/y]	[mGy/y] α	β	γ	total	ratio Previous / Present
ThO_2(1ppm) = Th(1ppm)x0.8788					
Bell 1977, 1979				0.7193	1.0036
Carriveau and Troka 1978				0.7139	0.9960
Nambi and Aitken 1986	0.6494	0.0251	0.0458	0.7204	1.0051
Liritzis and Kokkoris 1992	0.6423	0.0241	0.0444	0.7108	0.9917
Present work. 1993	**0.6477**	**0.0242**	**0.0449**	**0.7167**	
UO_3 (1ppm) = U (1ppm)x0.8322					
Bell 1977, 1979				2.5353	0.9989
Carriveau and Troka 1978				2.5464	1.0033
Nambi and Aitken 1986	2.3143	0.1223	0.0945	2.5312	0.9973
Liritzis and Kokkoris 1992	2.3564	0.1222	0.1109	2.5895	1.0203
Present work. 1993	**2.3235**	**0.1220**	**0.0926**	**2.5381**	
K_2O (1%)					
Bell 1977, 1979				0.8870	1.0069
Carriveau and Troka 1978				0.8720	0.9899
Nambi and Aitken 1986		0.6760	0.2020	0.8780	0.9967
Liritzis and Kokkoris 1992		0.6824	0.2042	0.8866	1.0065
Present work. 1993		**0.6780**	**0.2029**	**0.8809**	
Rb_2O (1%)					
Carriveau and Troka 1978				3.7800	0.8002
Nambi and Aitken 1986			4.2800	4.2800	0.9060
Liritzis and Kokkoris 1992			4.6432	4.6432	0.9829
Present work. 1993			**4.7240**	**4.7240**	
1% K_2O & 50ppm Rb_2O					
Nambi and Aitken 1986		0.6974	0.2020	0.8994	0.9944
Liritzis and Kokkoris 1992		0.7056	0.2042	0.9098	1.0059
Present work. 1993		**0.7016**	**0.2029**	**0.9045**	

The results of the present calculation almost agree with those of Nambi and Aitken (1986) except for Rb_2O. Liritzis and Kokkoris (1992) estimated too large dose for ^{238}U and ^{235}U series. The averaged atomic weight 238.0289 for U and 232.0381 for Th are used for the calculation.

Acknowledgements

The authors thank Mr. M. Okabe for checking data. This work is partially supported by the grant for Fellowships of the Japan Society for the Promotion of Science for Japanese Junior Scientists. (No. 1455 of 1993)

Reference

Aitken M. J. (1983)
Radioactivity data using SI units
PACT **9**, 70-71

Bell W. T. (1977)
Thermoluminescence dating : revised dose- rate data
Archaeaometry **19**, 99-100

Bell W. T. (1979)
Thermoluminescence dating : revised dose- rate data
Archaeometry **21**, 243-245

Carriveau G. T. and Troka W. (1978)
Annual dose- rate calculations for thermoluminescence dating
Archaeophysica **10**, 406-422

ICRP (1983)
Annals of the ICRP. Radionuclide Transformations : Energy and Intensity of Emissions,Vol. 11-13.

Liritzis Y. and Kokkoris M. (1992)
Revised Dose-rate Data for Thermoluminescence / ESR Dating
*Nucl. Geophys.*Vol. 6, **3**, 423-443

Nambi K. S. V. and Aitken M. J. (1986)
Annual dose conversion factors for TL and ESR dating
Archaeaometry **28**, 202-205

Shirley V. S. (1986)
Table of Radioactive Isotopes
John Wiley & Sons, Inc.

Ikeya M. (1987)
Electron spin resonance (ESR) Dating (in Japanese), 59-74
Ionics, Tokyo

Appendix B Dating of a Caldera Using Defects in Quartz

Cooling History of the Valles Caldera, New Mexico Using ESR Dating Method

[1]K. OGOH, [1]S. TOYODA, [1]S. IKEDA, [1]M. IKEYA, and [2]F. GOFF

[1]Department of Physics, Faculty of Science
Osaka University
Toyonaka, Osaka 560, Japan

[2]Earth and Space Sciences Division
Los Alamos National Laboratory
Los Alamos, New Mexico 87545

ESR dating was made at the Valles caldera by using the Al center and Ti center in quartz grains separated from the layers of the Valles Rhyolite. Obtained ESR ages were much younger than those by other methods (fission track and ^{39}Ar-^{40}Ar). A reported thermal event of about 10-40 ka ago might explain the difference between the above ages.

KEYWORDS: ESR dating; the Valles caldera; Al center; Ti center; quartz; geothermal.

INTRODUCTION

Quartz has been used for electron spin resonance (ESR) dating. Volcanic ashes (e.g., Imai *et al.*, 1985), volcanic rocks (Shimokawa and Imai, 1987), geothermal materials (Ikeya, 1983), and sediments heated by lava flows or intrusions (Yokoyama *et al.*, 1985; Ikeya and Toyoda, 1991) have been used for ESR dating. Quartz has been also used for the studies on ESR dating of fault movements (Ikeya, 1982; Fukuchi, 1989).

ESR ages have been reported using impurity (Ge, Al and Ti) centers and defect (E' and oxygen hole) centers in quartz. The ages obtained by using several defects, with different thermal stabilities, should be the same if the sample has cooled rapidly. On the other hand, different ages may be obtained when the sample has cooled slowly. Thermal histories of samples have been investigated by using some impurity centers, each of which has a different thermal stability (Shimokawa and Imai, 1987): the thermal stabilities of Ge, oxygen hole, and Al centers in quartz were reported (Shimokawa and Imai, 1987). Recently, thermal stabilities of E', Al, and Ti centers were studied systematically (Toyoda and Ikeya, submitted). ESR ages obtained from many different centers with different stabilities will give the history of cooling.

GEOLOGY OF VALLES CALDERA

The Jemez Mountains volcanic field, New Mexico (Fig. 1), has a record of continuous volcanism for more than 13 Ma (Gardner *et al.*, 1986). The most significant and famous activity in the field was the formation of the Toledo and Valles caldera associated with the Otowi and Tshirege Members of the Bandelier Tuff, which were erupted at 1.50 and 1.13 Ma, respectively (Spell *et al.*, 1990). The Valles Rhyolite (Bailey *et al.*, 1969), the product of the post-Valles caldera activity, erupted from the ring fracture zone in caldera.

The youngest post-caldera event consists of three members, the Battleship Rock Member, the El Cajete Member and the Banco Bonito Member. Figure 1 shows the distributions of the members. The Battleship Rock Member is composed of non-welded to densely-welded ash flow deposits. The El Cajete Member consists of well- bedded to crudely bedded pumice fall deposits. The Banco Bonito Member is a thick flow of porphyritic obsidian (Smith *et al.*, 1970). The previous two members were considered to be precursors to the formation of the Banco Bonito Member (Self *et al.*, 1988). The fission track and U-series ages obtained for the three members are: Battleship Rock 130-180 ka: El Cajete 150-170 ka: Banco Bonito 130-140 ka (Self *et al.*, 1988). More recently, Self *et al.* (1991) have obtained ^{39}Ar-^{40}Ar dates from these units and have suggested that the Banco Bonito Member is 170-240 ka. These members and the recently discovered VC-1 Rhyolite whose age is 365 ka and the VC-1 Tuffs (Goff *et al.*, 1986) have a distinct feature of relatively low-silica composition as compared to the older members of the Valles Rhyolite and the Bandelier Tuff.

EXPERIMENTAL

Sample Preparation.

Seven samples were collected from outcrops of the Valles Rhyolite (Fig. 1). Two are from the Battleship Rock (BSR) Member, three are from the El Cajete Member (EC), one is from the Banco Bonito Member (BBO) and the last is from the South Mountain Rhyolite (SMR) with K-Ar ages of 0.49 Ma, and 0.60 Ma (Self *et al.*, 1988). Three samples were obtained from the VC-1 core (Goff *et al.*, 1986). One sample corresponds to the BSR Member, whereas the other two samples come from the VC-1 Tuffs.

The original quartz phenocryst samples were soaked with 3% HCl for 20 minutes, placed into an ultrasonic bath for 8 to 9 minutes within 5% HF, and soaked with HNO_3 for 30 minutes. They were examined under a microscope to ensure the crystals were clean, if not, HF treatment was repeated for 3 minute periods. After the above treatments, samples were etched in 20% HF for an hour to remove defects caused by alpha emitters in the original matrix. The diameter of the quartz grains was about 1 mm. They were crushed with a mortar, and sieved to obtain 75-250 μm. Eight 150 mg aliquots for each sample were prepared.

ESR dating.

ESR signals of Al and Ti centers were observed with a commercial X-band ESR spectrometer (JEOL-RE-1X) at liquid nitrogen temperature with 100 kHz field modulation using an amplitude of 0.1 mT and with microwave power of 5 mW. A ^{60}Co γ-ray source was used to irradiate a sample at a dose rate of 35 Gy/h. Eight aliquots were irradiated for each sample. The signal growth was fitted to a straight line by using the least-square method. The parameters and standard deviations of the parameters were obtained. The production efficiency of centers was obtained from the slope. The equivalent dose (ED) was obtained by extrapolating the growth line to zero ordinate.

The annual dose rate (D) was calculated from K, U and Th contents that were obtained by neutron activation analysis in the rhyolite from which the quartz sample was separated. The effective β-ray dose was calculated to be 45% for ^{232}Th, 40% for ^{238}U, and 33% for K from Fig. A-2 of Grün (1989). Radioactive equilibrium was assumed. The ESR age was calculated by dividing the equivalent dose by the annual dose rate. The error of *ED* was calculated from the errors of parameters and from the correlation between them.

Thermal stabilities of Al and Ti centers.

Thermal stabilities of Al and Ti centers were investigated by an isothermal heating experiment of sample 90-11 at several temperatures from 170 to 290°C for 130 to 210 min. The signal intensities of Al and Ti centers decreased after heating. The inverse of signal intensities form a linear relation as a function of time. This process is caused by the second order kinetic reaction (Toyoda and Ikeya, in press). The activation energies of 1.75 and 2.10 eV for Al and Ti centers, respectively were obtained from an Arrhenius diagram plotting decay factors.

RESULTS

ESR ages.

Obtained ESR ages are listed in Table 1. They are much younger than those obtained by other methods, and range from 1.7 to 45 ka, except one, 90-6 of 120-200 ka. There is, however, a relative correlation with ages obtained by other methods in that the ages for BSR, EC and BBO are about the same, and that of SMR is much older. Ages in VC-1 core hole systematically decrease with depth in the hole.

Table 1. The results of ESR dating of the younger members of the Valles Rhyolites.

Sample	Unit	*D* (mGy/y)	*ED*(Al) (Gy)	*Age*(Al) (ka)	*ED*(Ti) (Gy)	*Age*(Ti) (ka)
$90\text{-}1^{L.C}$	BSR	4.80	150±20	32±4.0	210±20	45±4.0
$90\text{-}3^{C}$	BSR	4.80	130±20	27±4.0	150±20	31±3.0
$90\text{-}4^{A}$	EC	4.80	100±10	21±2.0	120±6.0	25±2.0
$90\text{-}5^{A}$	EC	4.95	160±30	32±6.0	210±20	43±3.0
$90\text{-}6^{A}$	SMR	6.48	790±400	120±60	1300±200	200±30
$90\text{-}7^{A}$	BBO	5.38	200±30	37±6.0	240±10	45±2.0
$90\text{-}11^{B}$	EC	4.80	200±30	42±6.0	190±20	40±4.0
$BVC1^{V.C}$	BSR	4.80	80±10	17±3.0	140±8.0	29±2.0
$UVC1^{V.C}$	VC-1 Tuff	5.10	50±6.0	9.7±1.0	160±8.0	32±1.0
$MVC1^{V.C}$	VC-1 Tuff	5.02	8.4±6.0	1.7±4.0	97±10	19±2.0

Sample localities are shown in Fig. 1, L.C denotes that the sample was collected at the La Cueva site. A, B, C, and V.C denote the points A, B, C, and VC-1 Corehole, respectively.

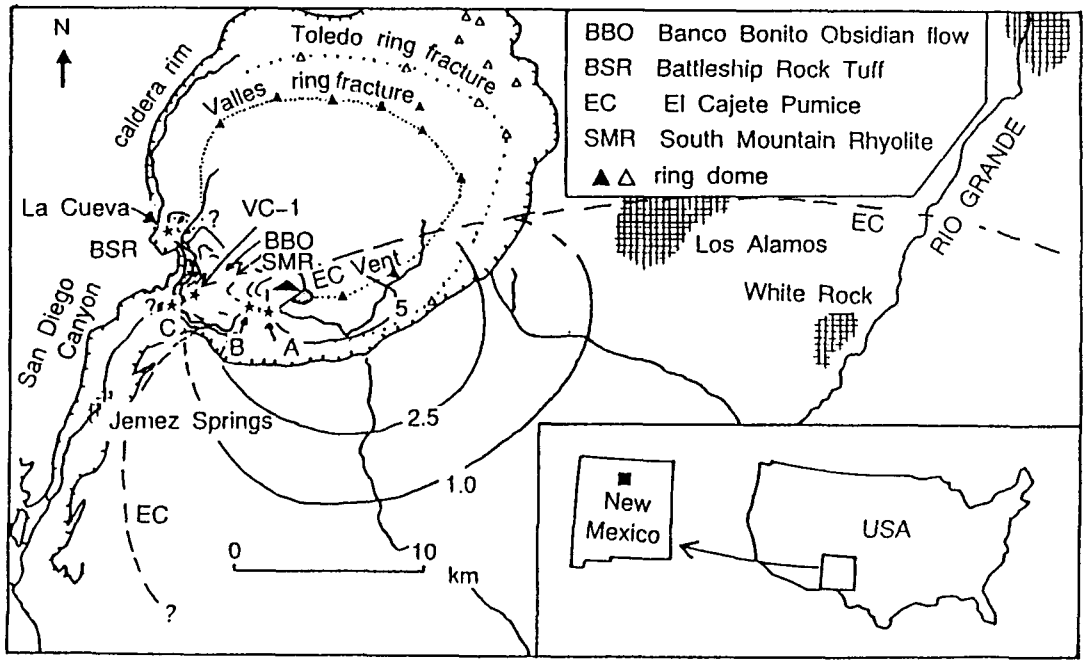

Fig. 1. Sample localities, partially modified from Self *et al.*, 1988.

DISCUSSION

The ESR ages are much younger than those obtained by fission track (130-170 ka), by U-Th disequilibration series (150 ka), and by ^{39}Ar-^{40}Ar (200-1300 ka) methods (Self *et al.*, 1988; 1991). The ESR (Ti-center) ages are possibly equivalent to a ^{14}C age of >42 ka obtained on charcoal from the El Cajete Member (Bailey *et al.*, 1969). Because of the wide variations in age indicated by different methods, some of them must yield erroneous results. For example, the U-Th data reported by Self *et al.* (1988) are incorrectly interpreted. No age can be obtained from their data. The age range of 200-1300 ka obtained by ^{39}Ar-^{40}Ar analyses of biotite phenocrysts in the Banco Bonito member (Self *et al.*, 1991) suggests that a serious excess-Ar effect produces apparent ages much older than the true eruption dates. Goff has obtained conventional K-Ar dates of 0.50 Ma (biotito) and 0.55 (plagioclase) from the Banco Bonito Member, 3.46 Ma (plagioclase) from the El Cajete Member, and 24.3 Ma (plagioclase) from the Battleship Rock Member (all unpublished data) which suggest an excess-Ar problem or presence of xenocrystic phases in these three units. The fission track ages have a large error of 0.1 ka because the rocks are so young. Thus, it is possible that the youngest Valles Rhyolites are much younger than previously thought. If the ESR ages are correct, the stratigraphy and volcanology of the post-0.5 Ma units of the Valles caldera will need revision yet again (*i.e.*, Self *et al.*, 1991)

The second possibility is that ESR method did not work for these samples because the centers were thermally unstable at the ambient temperature. However, this can be eliminated because the characteristic decay times defined as $\tau_0 = 1/I_0 x \lambda$ (Toyoda and Ikeya, submitted), for Al and Ti centers are calculated to be $1x10^6$ years and $1.6x10^{12}$ years, respectively, by using the parameters obtained by annealing experiments described above. The present yearly ambient temperature at ground level of the sampling points is around 10°C. Even if the temperature of the sampling points had been around 30°C, both the Al center and Ti center should have been stable for very long periods of time.

The last possibility is that a recent thermal event such as 10-40 ka event proposed by Harrison *et al.* (1986) partially reset the ESR signals. This postulated event is interpreted from thermal gradient analysis of well logs at the Fenton Hill Site southwest of the caldera. This event may be the equivalent to the renewed hot spring activity that occurred southwest of the caldera at 5 ka (Goff and Shevenell, 1987). However, this event has not produced obvious hydrothermal alteration at any of the outcrops shown in Fig.1. If this thermal event had reduced the ESR intensities to one-third of their values, corrected ESR ages would correlate with some ages obtained by other methods. Thermal resetting has affected the ESR ages of the three samples obtained from the core hole because the ages systematically decrease with depth. Although we see no evidence to support a young thermal event, other than the VC-1 ages, our ESR results correlate with the postulated thermal event of Harrison *et al.* (1986).

CONCLUSION

The cooling history of the Valles caldera was studied by the ESR method using Al and Ti centers in quartz grains which were separated from the youngest units of the Valles Rhyolite. The ESR apparent ages are much younger than fission track ages and ^{39}Ar-^{40}Ar ages. Three possibilities are suggested, the first is that the ESR ages are real, the second is that ESR method did not work for these samples, and the third is that at about 10-40 ka, the signal intensity was partially reduced by a thermal event such as proposed by Harrison *et al.* (1986). Research on the first and second possibilities is continuing. The third possibility might explain the difference between ESR ages and those by other methods (fission track and ^{39}Ar-^{40}Ar). ESR dating has produced new insights regarding the history of the youngest valles caldera rhyolites.

ACKNOWLEDGEMENTS

We thank Dr. N. Kimura at Scientific and Industrial Research at Osaka University for the γ-ray irradiations. This manuscript was reviewed by Dr. G. Wolde Gabriel, Los Alamos National Laboratory (LANL). Quartz separations were performed by C. Mooney and instrumental neutron activation analyses of the samples were obtained from Dr. S. Garcia (LANL). This work was supported in part by a Grant-in-Aid for Encouragement of young scientists (No.03854034) from the Ministry of Education and Culture and in part by Inoue Foundation for Science. The last author was funded by the U.S.Department of Energy/Office of Basic Energy Sciences.

REFERENCES

Bailey R.A., Smith R.A., Smith R.L. and Ross C.S. (1969) Stratigraphic nomenclature of volcanic rocks in the Jemez Mountains, New Mexico. *U.S. Geol. Surv. Bull.*, **1274-P**, 1-19.

Fukuchi T. (1989) ESR dating of fault movement and frictional heating by faulting. Ph. D.Thesis, University of Tsukuba, Japan.

Gardner J.N., Goff F., Garcia S. and Hagan R.C. (1986) Stratigraphic relations and lithologic variations in the Jemez volcanic field, New Mexico. *J. Geophys. Res.*, **91(B10)**, 1763-1778.

Goff F. and Shevenell L. (1987) Travertine deposits of Soda Dam, New Mexico, and their implications for the age and evolution of the Valles caldera hydrothermal system. *Geol. Soc. Amer. Bull.*, **99**, 292-302.

Goff F., Rowley J., Gardner J.N., Hawkins W., Goff S., Charles R., Wachs D., Maassen L. and Heiken G. (1986) Initial results from VC-1, First continential Scientific Drilling Program core hole in Valles caldera, New Mexico. *J. Geophys. Res.*, **91(B2)**, 1742-1752.

Grün R. (1989) Electron Spin Resonance (ESR) Dating. *Quat. Int.*, **1**, 65-109.

Harrison T.M., Morgan P. and Blackwell D.D. (1986) Constraints on the Age of Heating at the Fenton Hill Site, Valles caldera, New Mexico. *J. Geophys. Res.*, **91(B2)**, 1899-1908.

Ikeya M., Miki T. and Tanaka K. (1982) Dating of fault by ESR on intrafault materials. *Science*, **215**, 1392-1393.

Ikeya M. (1983) ESR studies of geothermal boring cores at Hachobara power station. *Jpn. J. Appl. Phys.*, **22**, L763-769.

Ikeya M. and Toyoda S. (1991) Thermal Effect in Metamorphic Rock around an Intrusion Zone with ESR Studies. *Appl. Mag. Res.*, **2**, 69-81.

Imai N., Shimokawa K. and Hirota M. (1985) ESR dating of volcanic ash. *Nature*, **314**, 81-83.

Harrison T.M., Morgan P. and Blackwell D.D. (1986) Constraints on the Age of Heating at the Fenton Hill Site, Valles caldera, New Mexico. *J. Geophys. Res.*, **91(B2)**, 1899-1908.

Self S., Kircher D.E. and Wolff J.A. (1988) The El Cajete Series, Valles Caldera, New Mexico. *J. Geophys. Res.*, **93(B6)**, 6113-6127.

Self S., Wolff J.A., Spell T.L., Skuba C.E. and Morrissey M.M. (1991) Revisions to the stratigraphy and volcanology of the post-0.5 Ma units and the volcanic section of VC-1 core hole, Valles caldera, New Mexico. *J. Geophys. Res.*, **96(B3)**, 4107-4116.

Shimokawa K. and Imai N. (1987) Simultaneous determination of alteration and eruption ages of volcanic rocks by electron spin resonance. *Geochim. Cosmochim. Acta.*, **51**, 115-119.

Smith R.L., Bailey R.A. and Ross C.S. (1970) Geologic map of the Jemez Mountains, New Mexico, scale 1: 250,000. *U.S. Geol. Surv. Inv. Map*, **ID571**.

Spell T.L., Harrison T.M. and Wolff J.A. (1990) $^{40}Ar/^{39}Ar$ dating of the Bandelier Tuff and San Diego Canyon; Ignimbrites, Jemez Mountains, New Mexico: Temporal constraints on magmatic evolution. *J. Volcanol. Geotherm. Res.*, **43**, 175-193.

Toyoda S. and Ikeya M. (in press) Thermal stabilities of paramagnetic defect and impurity centers in quartz: Basis of ESR dating geothermometry. *Geochem. J.*

Yokoyama Y., Falgueres C. and Quaegebeur J.P. (1985) ESR dating of sediment baked by lava flows: comparison of paleodoses for Al and Ti centers. *ESR Dating and Dosimetry*, Ionics, Tokyo, 197-204.

Acknowledgements

First of all, I wish to express my sincere gratitude to my promoter, Professor Motoji Ikeya who introduced me to this field of research and continuously guided to me. I also express my gratitude to Professor Ito (Okayama University) for his kind guidance and helps in high pressure synthesis. I am very grateful to Dr. Chihiro Yamanaka for many invaluable suggestions and advice in discussion.

I am indebted to Associate Professor Itsuo Katakuse for his a lot of encouragements. I acknowledge Dr. Shin Toyoda, Dr. Sumiko Tsukamoto (Ikeda), Dr. Fraser Goff (Los Alamos National Laboratory) and Mr. Syunji Takaki for their diligent cooperation and invaluable discussions.

I am grateful to Dr. Masahiro Furusawa, Dr. Hiroshi Ishii, Mr. Hideki Tobe, Mr. Makoto Hirai, Mr. Kohji Hosokawa, Mr. Hiroshi Furuta, Mr. Hideo Kohno and Mr. Hideki Sasaoka for their helpful suggestions and cooperation. I also acknowledge all other members of Ikeya Laboratory, Department of Earth and Space Science, Faculty of Science, Osaka University for their various supports and encouragements.

The γ-ray irradiations were made at the Institute of Scientific and industrial Research, Osaka University.

At last, I should express sincere gratitude to all of my friends, Mr. Makoto Hirai, Mrs. Sayuri Iga, Mr. Hiroyuki Miyamaru, Mrs. Chizuko Mizushima, Mrs. Junko Morikawa and especially Mrs. Weihua Du, and a lot of other people, for their sincere encouragements on my study. If they were not in my life, I have never finish this work.

A decade has passed since I entered Osaka University. Happiness and sadness have come and gone. I will and can never forget these ten years forever. I will do my best and overcome difficulties. I appreciate my Osaka University for filling up my youth with pleasures leading to success and failure.

This work is partially supported by the grant for Fellowships of the Japan Society for the Promotion of Science for Japanese Junior Scientists (DC1 No. 1455 of 1993) and Grant in Aids for Scientific Studies for Ministry of Education.

List of Publications

1 K. Ogoh, S. Toyoda, S. Ikeda, M. Ikeya and F. Goff
Cooling History of the Valles Caldera, New Mexico Using ESR Dating Method
Applied Radiation and Isotopes **44** (1993) 233-237.

2 K. Ogoh, S. Ikeda and M. Ikeya
Confirmation and Recalculation of Dose-rate Data for TL and ESR Dating
Advances in ESR Applications **9** (1993) 22-28.

3 K. Ogoh, C. Yamanaka, S. Toyoda, M. Ikeya and E. Ito
ESR Studies on Radiation Induced Defects in High Pressure Phase SiO_2
Nuclear Instruments and Methods in Physics Research **B 91** (1994) 331-333.

4 K. Ogoh, C. Yamanaka, M. Ikeya and E. Ito
Hyperfine Interaction of Electron at Oxygen Vacancy with Nearest and Next Nearest ^{29}Si in High-Pressure-Phase SiO_2: Stishovite
Journal of the Physical Society of Japan Letters **64** (1995) 4109-4112.

5 K. Ogoh, C. Yamanaka, M. Ikeya and E. Ito
Two-Center Model for Radiation Induced Aluminum Hole Center in Stishovite
Journal of Physics and Chemistry of Solids **57** (1996) 85-87.

6 K. Ogoh, S. Ikeda and M. Ikeya
Comments on Revised Dose-rate Data for Thermoluminescence / ESR Dating (Liritzis and Kokkoris)
Nuclear Geophysics **9**, No. 6 (1995) in print.

7 K. Ogoh, S. Takaki, C. Yamanaka, M. Ikeya and E. Ito
Thermoluminescence and Electron Spin Resonance of Atomic Hydrogens in Coesite and Stishovite, High Pressure Phases of SiO_2
Journal of the Physical Society of Japan **65**, No.3, (1996) in print.

8 K. Ogoh, C. Yamanaka, M. Ikeya and E. Ito
Oxygen Hole Centers in Coesite
Applied Magnetic Resonance (1996) in print.

和文

1　山中千博・小河一敏・池谷元伺
隕石衝突クレーターのＥＳＲ年代測定
月刊「IONICS（アイオニクス）」第２０巻第２号　１９９４年２月　p. 33-36

2　小河一敏
SiO_2高圧相のESR―隕石衝突クレーターの年代測定法の開発
大阪大学低温センター便り　No. 89　１９９５年１月　p. 6-10

3　小河一敏・山中千博・伊藤英司
スティショバイト：SiO_2高圧相のE'センターの構造解析
ESR応用計測第１１巻　１９９５年９月　p. 4-7

4　小河一敏
ESRで観たSiO_2高圧相の放射線誘起格子欠陥
月刊「IONICS（アイオニクス）」第２２巻第２号掲載予定　１９９６年２月